TURUN
YLIOPISTO
UNIVERSITY
OF TURKU

MOLECULAR INSIGHTS ON PERTUSSIS TOXIN: STRUCTURE, FUNCTION, AND INHIBITION

Moona Sakari

TURUN YLIOPISTON JULKAISUJA – ANNALES UNIVERSITATIS TURKUENSIS
SARJA – SER. D OSA – TOM. 1791 | MEDICA – ODONTOLOGICA | TURKU 2024

TURUN
YLIOPISTO
UNIVERSITY
OF TURKU

MOLECULAR INSIGHTS ON PERTUSSIS TOXIN: STRUCTURE, FUNCTION, AND INHIBITION

Moona Sakari

TURUN YLIOPISTON JULKAISUJA – ANNALES UNIVERSITATIS TURKUENSIS
SARJA – SER. D OSA – TOM. 1791 | MEDICA – ODONTOLOGICA | TURKU 2024

University of Turku

Faculty of Medicine
Institute of Biomedicine
Medical Microbiology and Immunology
Turku Doctoral Programme of Molecular Medicine (TuDMM)

Supervised by

Docent Arto Pulliainen, PhD
Institute of Biomedicine
University of Turku
Turku, Finland

Reviewed by

Associate Professor Herwig Schüler, PhD
Department of Chemistry
Lund University
Lund, Sweden

Emeritus Professor Mikael Skurnik, PhD
Department of Bacteriology and Immunology
University of Helsinki
Helsinki, Finland

Opponent

Professor Christian Hedberg, PhD
Department of Chemistry
Umeå University
Umeå, Sweden

The originality of this publication has been checked in accordance with the University of Turku quality assurance system using the Turnitin OriginalityCheck service.

ISBN 978-951-29-9688-9 (PRINT)
ISBN 978-951-29-9689-6 (PDF)
ISSN 0355-9483 (Print)
ISSN 2343-3213 (Online)
Painosalama, Turku, Finland 2024

To my family and friends

UNIVERSITY OF TURKU
Faculty of Medicine
Institute of Biomedicine
Medical Microbiology and Immunology
MOONA SAKARI: Molecular Insights on Pertussis Toxin: Structure, Function, and Inhibition
Doctoral Dissertation, 185 pp.
Turku Doctoral Programme of Molecular Medicine (TuDMM)
April 2024

ABSTRACT

The rise of antibiotic-resistant pathogenic bacteria and the increasing understanding of the beneficial role of the bacterial microbiota, disrupted by antibiotics, prompt the development of new anti-bacterial therapies. One such approach targets bacterial virulence factors such as exotoxins, which are often the disease-causing virulence factor, making them appealing drug development targets. Detailed molecular understanding of exotoxins is crucial for efficient drug development efforts.

This study focuses on pertussis toxin (PT), a major virulence factor of *Bordetella pertussis*, the causative agent of whooping cough. PT, an ADP-ribosyltransferase (ART) toxin, disrupts cellular signaling by transferring ADP-ribose from nicotinamide adenine dinucleotide (NAD+) to inhibitory α-subunits of G proteins of the host cell, leading to variety of systemic pathologies. The aim of the study was to identify small molecules inhibiting the ART activity of PT, and to obtain atomic resolution structural insights of the binding poses of the inhibitors as well as of the ART activity of PT.

An *in vitro* high-throughput multiwell assay to screen small molecules inhibiting the ART activity of PT was developed. Two compounds, effective at low micromolar levels *in vitro*, with one also potent in living cells, were identified. No binding poses for the compounds were obtained with X-ray crystallography. However, crystal structures of PT in complex with NAD+, its hydrolysis products ADP-ribose and nicotinamide, NAD+ analog PJ34 (ART inhibitor), and a novel NAD+ analog formed upon crystallization with 3-aminobenzamide (ART inhibitor) and NAD+, were obtained. These structures provide novel insights into pre- and post-NAD+ hydrolysis steps of the ART activity of PT and provide a rational basis to develop ART inhibitors as well as the biocatalytic use of PT to produce the novel NAD+ analog for biochemical and structural experiments with NAD+ binding proteins.

In conclusion, this study identified small molecules inhibiting the ART activity of PT and obtained atomic resolution structural insights of the ART activity, as well as binding poses of the small molecules in PT, known to inhibit other ARTs. These findings could aid in the rational drug design approaches and development of PT-specific small-molecule inhibitors.

KEYWORDS:whooping cough, pertussis toxin, ADP-ribosyltransferase, inhibitor, drug development

TURUN YLIOPISTO
Lääketieteellinen tiedekunta
Biolääketieteen laitos
Lääketieteellinen mikrobiologia ja immunologia
MOONA SAKARI: Pertussistoksiini molekyylitasolla: rakenne, toiminta ja toiminnan kohdennettu esto
Väitöskirja, 185 s.
Molekyylilääketieteen tohtoriohjelma (TuDMM)
Huhtikuu 2024

TIIVISTELMÄ

Antibioottiresistentit bakteerit sekä ymmärrys antibioottien haitallisesta vaikutuksesta suotuisaan mikrobistoon korostavat tarvetta kehittää vaihtoehtoisia hoitomuotoja bakteeritaudeille. Yksi keino on bakteerien virulenssitekijöiden, kuten eksotoksiinien, kohdentaminen. Eksotoksiineilla on usein keskeinen osuus taudin aiheuttamisessa, mikä tekee niistä hyviä lääkekehityskohteita. Eksotoksiinien yksityiskohtainen ymmärtäminen on tärkeää uusien hoitomuotojen kehittämisessä.

Tämä tutkimus keskittyy pertussistoksiiniin (PT), joka on hinkuyskää aiheuttavan *Bordetella pertussis* -bakteerin tärkeä virulenssitekijä. PT on ADP-ribosyylitransferaasi (ART), joka häiritsee soluviestintää siirtämällä ADP-riboosin nikotiiniadeniinidinukleotidilta (NAD+) isäntäsolun G-proteiinin inhibitoriseen α-alayksikköön, johtaen moniin systeemisiin häiriöihin. Tavoitteena oli löytää pienmolekyylisiä yhdisteitä, jotka estävät PT:n ART-toimintaa, ja tutkia atomitasolla PT:n rakennetta yhdisteiden sitoutumisen sekä ART-toiminnan kannalta.

Tässä työssä kehitettiin erittäin tehokas PT:n toimintaa estävien pienmolekyylisten yhdisteiden *in vitro* -seulontamenetelmä, jolla löydettiin kaksi PT:n aktiivisuutta estävää pienmolekyylistä yhdistettä. Ne osoittautuivat tehokkaiksi matalina pitoisuuksina *in vitro*, ja toinen on tehokas myös elävissä soluissa. Näille yhdisteille ei saatu kiderakennetta, mutta rakenteet saatiin PT:lle yhdessä NAD+, sen hydrolyysituotteiden ADP-riboosin ja nikotiininamidin, NAD+ analogi PJ34:n (ART-inhibiittori) sekä uuden NAD+ analogin kanssa, joka muodostui kiteytettäessä 3-aminobentsamidia (ART-inhibiittori) ja NAD+:ia. Nämä rakenteet antavat uutta tietoa PT:n ART-toiminnasta NAD+-hydrolyysin eri vaiheissa ja luovat pohjaa PT:n ART-toimintaa estävien yhdisteiden rationaaliselle lääkesuunnittelulle sekä PT:n käytölle biokatalyyttisena alustana uuden NAD+ analogin tuottamiseen biokemiallisiin ja rakenteellisiin kokeisiin NAD+:ia sitovien proteiinien kanssa.

Yhteenvetona tämä väitöstyö löysi pienmolekyylisiä yhdisteitä, jotka estävät PT:n toimintaa ja tarjoaa atomitason rakenteellista tietoa PT:n ART-toiminnasta sekä sitoutumisesta tunnettujen ART-entsyymejä inhiboivien pienmolekyylisten yhdisteiden kanssa. Tämä tieto voi auttaa sekä rationaalisen lääkesuunnittelun menetelmien että PT:lle suunnattuja pienimolekyylisten yhdisteiden kehittämisessä.

AVAINSANAT: hinkuyskä, pertussistoksiini, ADP-ribosyylitransferaasi, inhibiittori, lääkehehitys

Table of Contents

Abbreviations

3-AB	3-aminobenzamide
ADP	adenosine diphosphate
Ag	antigen
ART	ADP-ribosyltransferase
ARTD	ADP-ribosyl-transferases diphtheria toxin-like
ARTT	ADP-ribosylating turn-to-turn
ATP	adenosine trihosphate
BaAD	benzamide amino adenine dinucleotide
BAD	benzamide adenine dinucleotide
BonT	Botulinum neurotoxin
BSA	bovine serum albumin
c/IgG	chimeric immunoglobulin G
C3bot	*Clostridium botulinum* C3-like ADP-ribosyltransferase toxin
C3Stau2	*Staphylococcus aureus* C3-like ADP-ribosyltransferase toxin
cAMP	cyclic adenosine monophosphate
carba-NAD+	carbanicotinamide adenine dinucleotide
CDT	cytolethal distending toxin
CNF1	cytotoxic necrotizing factor 1
CT	cholera toxin
CyaA	bifunctional hemolysin/adenylyl cyclase
Da	Dalton
DMEM	Dulbecco´s modified Eagle´s media
DMSO	dimethyl sulfoxide
DNA	deoxyribonucleic acid
DSF	differential scanning fluorimetry
DT	diphtheria toxin
DTT	dithiothreitol
*Ec*Plt	*E. coli* pertussis-like toxin
ER	endoplasmic reticulum
ETA	exotoxin A
EThcD	electron-transfer/higher-energy collision dissociation

FBS	fetal bovine serum
Fc	fragment crystallizable
FDA	U.S. Food and Drug Administration
GDP	guanosine diphosphate
GMP	good manufacturing practice
GPCR	G protein-coupled receptor
GST	glutathione-S-transferase
Gαi	inhibitory G protein alpha subunit
h/IgG	human immunoglobulin G
h1, h2, …	helix 1, helix2, …
HCD	higher energy collisional dissociation
HEK293T	human embryonic kidney 293 cells containing SV40 T-antigen
HEPES	4-(2-hydroxyethyl)-1-piperazineethanesulfonic acid
HPLC	high performance liquid chromatography
HRP	horseradish peroxidase
HRV 3C	human rhinovirus 3C
H-Y-E	histidine-tyrosine-glutamic acid
Ia	Iota toxin enzymatic component
IC_{50}	half maxmal inhibitory concentration
IgG	immunoglobulin G
kDa	kilodalton
LB medium	lysogeny broth medium
LC-ESI-MS/MS	liquid chromatography electrospray ionization tandem mass spectrometry
LIC	ligase independent cloning
LT	*E. coli* heat labile enterotoxin
MD	molecular docking
MDS	molecular dynamics simulation
MHC II	major histocompatibility complex II
MS	mass spectrometry
NAD+	nicotinamide adenine dinucleotide
NADase	NAD+ glycohydrolase
NCI	National Cancer Institute
NMR	nuclear magnetic resonance
OD_{600}	optical density measured at a wavelength of 600 nm in 1 cm light path
PARP	poly-ADP-ribose polymerase
PBS	phosphate buffered saline
PCR	polymerase chain reaction
PDB	Protein data bank

Pi	inorganic phosphate
PN	phosphate-nicotinamide
PT	pertussis toxin
PTS1	pertussis toxin S1 subunit
RMS	root mean square
RMSD	root-mean-square deviation
RMSF	root mean square fluctuations
RNA	ribonucleic acid
R-S-E	arginine-serine-glutamic acid
RT	room temperature
s1, s2, …	strand 1, strand 2, …
SAR	structure-activity relationship
SDS-PAGE	sodium dodecyl sulfate polyacrylamide gel electrophoresis
SEC	size exclusion chromatography
SEC-MALS	size-exclusion chromatography coupled to multi-angle light scattering
S_N1	unimolecular nucleophilic substitution
S_N2	bimolecular nucleophilic substitution
STS	serine-threonine-serine
Stx1, Stx2	Shiga toxin 1, Shiga toxin 2
TBST	tris-buffered saline with Tween 20
TcdA	*Clostridium difficile* toxin A,
TcdB	*Clostridium difficile* toxin B
TCEP	tris(2-carboxyethyl)phosphine
TCR	T cell receptor
Tm	melting temperature
TNT	tuberculosis necrotizing toxin
TSST-1	toxic shock syndrome toxin 1
TT	tetanus toxin

List of Original Publications

This dissertation is based on the following original publications, which are referred to in the text by their Roman numerals:

I Ashok Y*, **Miettinen M***, Oliveira DKH, Tamirat MZ, Näreoja K, Tiwari A, Hottiger MO, Johnson MS, Lehtiö L, Pulliainen AT. Discovery of Compounds Inhibiting the ADP-Ribosyltransferase Activity of Pertussis Toxin. *ACS Infectious Diseases,* 2020; 6: 588-602. *Equal contribution

II **Sakari M**, Tran MT, Rossjohn J, Pulliainen AT, Beddoe T, Littler DR. Crystal structures of pertussis toxin with NAD+ and analogs provide structural insights into the mechanism of its cytosolic ADP-ribosylation activity. *Journal of Biological Chemistry*, 2022; 298: 101892.

III **Sakari M**, Bhadane R, Azevedo R, Malakoutikhah M, Masoumi A, Littler, R, Härmä H, Kopra K, Pulliainen AT. ADP-ribosyltransferase-catalyzed formation of a non-hydrolyzable NAD+ analog. *Manuscript.*

1 Introduction

Approximately 7 %, *i.e.,* 1513 of 22239 validly described bacterial species are known to be human pathogens, *i.e.,* disease causing bacteria (Bartlett et al., 2022). Pathogenic bacteria have special adaptations and mechanisms to overcome the natural defences of the human body and gain an advantage in the host-pathogen encounter. These factors can be highly diverse in regards of their composition, structure, size, biochemical properties, and mode of action. They include host cell-binding adhesins facilitating colonization, toxins and effector proteins killing or changing cell signaling of the mammalian cells, and specialized secretion systems that deliver these factors from the bacteria to the extracellular space or directly into the cytoplasm of the host cell. Bacterial toxins can be further divided to endotoxins and exotoxins. Exotoxins are generated and actively secreted by the bacteria, while endotoxins, *e.g.,* lipopolysaccharides are the main component of the outer membrane of the cell wall of Gram-negative bacteria. Endotoxins can cause severe inflammation in the infected host, and while usually the inflammation process is considered beneficial to the host in fighting the infection, sometimes the reaction is severe enough to cause endotoxic shock. Exotoxins are protein toxins secreted or release-upon-lysis by the bacteria, both Gram-positive and Gram-negative, aiding their colonization in the host. This study focuses on bacterial exotoxins, particularly those with intracellular effector functions, with specific attention to pertussis toxin.

Pertussis toxin (PT) is one of the many toxins of the bacteria *Bordetella pertussis*, the causative agent of whooping cough, highly contagious respiratory disease that is especially of concern in infants lacking vaccine-induced protection. Currently there is no effective treatment to whooping cough, although antibiotic treatment is used to prevent further transmissions. Pertussis toxin is thought to have a major role in the disease pathogenesis via suppression and modulation of host immune and inflammatory responses, and by targeting this toxin with novel therapeutics, it might be possible to prevent and alleviate the symptoms caused by the toxin and by the bacteria.

The aim of this study is to elucidate the structural and mechanistic aspects of the adenosine diphosphate (ADP)-ribosyltransferase activity of pertussis toxin and to specifically target this activity with small molecule inhibitors.

2 Review of the Literature

2.1 Drug discovery

2.1.1 Target identification and validation

Drug discovery and development pipeline is the complex multiphase process through which potential new medicines are discovered. It involves a wide range of various scientific disciplines, including biology, chemistry, medicine, and pharmacology, and it can take over a decade to finish. The initial phase of drug discovery pipeline is the target identification and validation. A drug target is a molecular structure that is inherently linked to a specific disease state, and when modulated with a particular drug compound, leads to the desired therapeutic effect in the disease state. Accomplishment of this requires comprehensive understanding of the molecular mechanisms behind the disease that is being targeted. Often this initial research takes place in academic settings and involves collecting data to develop a hypothesis suggesting that modulating a certain protein or pathway could lead to a beneficial therapeutic outcome in a particular disease state. Potential drug targets can be identified in different ways, for example by experimental methods in the lab, reviewing published literature, patent records or clinical data and going through open-access databases (data mining) for population genetics or transcriptomic, proteomic and metabolomic data of healthy or diseased individuals.

There are multiple different target identification strategies, which can be divided into two main categories: target deconvolution and target discovery. Target deconvolution strategy begins with a drug that shows effectiveness, and the target is then retrospectively identified in response to an observed phenotypic response. Techniques such as affinity chromatography, expression cloning, microarrays and biochemical suppression can be employed for target deconvolution (Moffat et al., 2017). Target discovery identifies the target first, and then (for example) compound libraries are screened with relevant system-based assays to find a drug that interacts with the target and generates the desired effect. Target-based drug discovery can utilize various approaches, such as crystallography, computational modelling, biochemistry, binding kinetics, molecular pharmacology, genomics, and mutational

studies to reveal how a drug interacts with the target of interest, enabling the determination of structure-activity relationships (SARs) and development of future therapies for the specific target of interest (Croston, 2017).

Ideal drug targets have a proven function in the disease pathophysiology. They can be genes, proteins, RNA, or anything involved in disease pathogenesis. They should have a more prominent effect in the disease in question compared to physiological conditions or other disease states. Availability of existing 3D-structure (*i.e.,* crystal structure, NMR structure), suitable assays for screening, and existing target or disease-specific biomarkers are also beneficial qualities of potential targets. Additionally, existing phenotypic data can help in the early evaluation of potential side effects.

The next step after target identification is to validate the key role of the chosen target in the disease using (ideally a combination) of physiologically relevant *in vitro*, *ex vivo*, and *in vivo* models mimicking the desired target in disease patients. Target validation aims to ensure proof-of-concept, *i.e.,* demonstrate that it is feasible and has therapeutic potential. Early target validation is important in order to focus the efforts on projects having potential to succeed, even though the ultimate validation of the target will only come later through clinical trials (Vamathevan et al., 2019).

2.1.2 Hit-to-lead and lead optimization

Once a promising drug target has been identified and validated, the next step is to identify a "hit" compound that interacts with the target of interest to produce desired biological effects. This hit discovery process includes synthesis and isolation of chemical compounds designed to interact with or block specified targets, or the use of existing compound collections or libraries, assay development to screen the selection of compounds, and the screening itself. A numerous screening approaches, such as virtual screening, high-throughput screening, or phenotypic screening, can be used to find a hit with desired type of activity. Structure-based drug design, fragment-based drug design or ligand-based drug design methods can also be used to identify the potential candidates (Kashyap et al., 2018; McCarthy et al., 2021).

In order to find hits and subsequently select potential compounds for further development, it is necessary to use screening assays that are both pharmacologically relevant and reproducible. The hit-to-lead selection process involves refining the screening criteria with desirable properties to select the most promising molecules from the identified hits for further development. This step also involves the utilization of secondary assays to study hit performance, such as off-target effects, dose-response, as well as physicochemical properties, such as solubility and

stability, and absorption, distribution, metabolism, and excretion characteristics. Secondary assays should also include counter-screens to confirm the activity witnessed with the primary assay and eliminate the false positives or non-specific inhibitors, biologically active compounds reacting with various cellular targets that are also known as pan-assay interference compounds, giving false signals in initial assays. To address the issue, there are software tools that can filter pan-assay interference compounds from screening libraries (Baell & Holloway, 2010). Early-phase preclinical pharmacokinetic and safety assessment of the potential lead compounds is also performed. These studies usually include both *in vitro* and *in vivo* models. Already at this stage the formulation and administration method (*e.g.*, oral, or intravenous), as well as feasibility of large-scale synthesis and manufacturing process according to good manufacturing practice (GMP) of the final drug should be thought of.

After hit-to-lead efforts, the most promising hit series are selected to advance into the lead optimization stage of drug discovery. This stage involves the use of advanced organic chemistry synthesis methods or biotechnological methods to optimize the lead compounds with detailed chemical modifications. These modifications are made to retain advantageous properties while optimizing and modifying the structure of each compound to improve target specificity and selectivity, along with optimized pharmacodynamic, pharmacokinetic and toxicological properties (Vamathevan et al. 2019). Computational *in silico* methods may also be employed for rational design of the modifications, particularly if the structure of the drug target is known.

In addition to eliciting the desired functional response of the target molecule, an ideal lead molecule should possess characteristics such as efficient absorption into the bloodstream, effective distribution to the site of action (*i.e.,* tissue), efficient metabolism, and elimination, *i.e.,* effective excretion from the body, and most importantly, should pass the early-phase safety studies such as cytotoxicity and genotoxicity tests. Once a lead compound is optimized and has been analyzed by all available *in vitro* assays and *in vivo* models with acceptable results, it can undergo scale-up and formulation to develop a drug that can be manufactured and administered in a clinical setting.

2.1.3 Candidate selection and preclinical testing

Preclinical development covers the activities that link drug discovery in the laboratory to initiation of human clinical trials (Steinmetz & Spack, 2009). Further *in vitro* and *in vivo* studies are needed to provide more information on absorption, distribution, metabolism, and excretion properties, potential benefits and risks, dosing and toxicity levels, and mechanism of action. In addition, before the drug can

be investigated in humans, mandatory regulatory non-clinical toxicological testing is required to assess and manage potential risks. Also, best formulation needs to be selected, as well as route of administration, frequency, and duration of exposure needs to be determined and the best scale-up procedure in a GMP-compatible environment developed. After preclinical testing, the findings are assessed, and a decision is made on whether the drug should be tested in people in clinical trials.

2.1.4 Clinical development

Following regulatory and ethics committee approvals, the drug can enter the clinical trials and the first clinical study (Phase I) can be initiated. Phase I is generally conducted on a small group of healthy volunteers. Safety and dosage range of the drug is studied. During phase I studies information is gathered on drug interaction with the human body, dosage-dependent side effects. Studies also provide early information on the effectiveness and explore the optimal administration methods to minimize risks and maximize possible benefits. Approximately 70 % of drugs move to the next phase (U.S. Food and Drug Administration, 2018).

Phase II trials expand the number of participants to include several hundred individuals affected by the targeted disease or condition. During Phase II, the potential therapeutic benefits and potential side effects of the candidate drug are evaluated. Approximately 33% of drugs continue to the next phase (U.S. Food and Drug Administration, 2018).

Phase III consist of several hundreds to several thousands of people who have the disease or condition under investigation. Efficacy and monitoring of adverse reactions are studied in a real-life clinical setting with control group receiving a standard treatment and study group receiving the candidate drug. As this phase last longer than the previous and the study-group is bigger, results are more likely to reveal long-term or uncommon side effects. If the drug candidate proves to be successful in Phase III clinical trials, a new drug application can be submitted to regulatory authorities. Approximately 25-30% of drugs move to the next phase (U.S. Food and Drug Administration, 2018).

Phase IV, also known as post-marketing safety surveillance, includes several thousand people with the disease or condition, and the safety and real-world efficacy of the drug is evaluated in an observational, non-interventional trial. In this stage, with the drug being used by a broad patient population, new rare or long-term side effects may be revealed. Safety surveillance through a spontaneous adverse events monitoring system continues for as long as the product is in the market and only that reveals the true safety profile of a drug.

Each phase can take up to multiple years, and drug discovery pipelines easily take over a decade to finish, and it can fail at any of the phases. The cost of pre-

launch research and development costs for a new drug are immense, evaluated to range from $161 million to $4.54 billion (2019 US$) (Schlander et al., 2021; Wouters et al., 2020).

It is also possible to reposition a drug. In this case the drug has already been approved by the authorities to treat some other disease. Since the preclinical and safety assessments in humans have already been conducted, it enables a faster, cheaper, and more efficient translation into the clinic. Repurposing an established drug for a new condition or disease is not without a risk and a drug development phase is still required. However, repositioning an already approved drug can reduce the drug development process from 10-17 years to 3–12 years (Wooller et al., 2017).

2.2 Bacterial toxins

2.2.1 Bacterial exotoxins

Bacterial exotoxins are a ubiquitous group of proteins that have a significant, and sometimes the primary, role as the disease-causing virulence factor in diseases such as whooping cough, cholera, diphtheria, tetanus, botulism, anthrax, and toxic shock syndrome (Sakari et al. 2022). They are typically classified into three different types based on their effector mechanisms: Type I toxins, superantigens; Type II toxins, membrane-disrupting toxins; and Type III toxins, intracellular-targeting toxins (Figure 1) (Sakari et al. 2022).

Superantigens, such as Staphylococcal and Streptococcal superantigens, bind to specific sites on the T cell receptor (TCR) and the major histocompatibility complex (MHC) molecule, resulting in the activation of a large number of T-cells leading to a major systemic release of cytokines (Spaulding et al., 2013). Membrane-disrupting toxins can be pore-forming toxins such as *Staphylococcus aureus* α-toxin, lipid-modifying enzymes like *S. aureus* β-hemolysin, and detergent-like peptides such as phenol soluble modulins of *S. aureus* (Oliveira et al., 2018). Intracellular targeting toxins have a variety of cytosolic effector functions, mainly involving a modification of specific host cell protein through posttranslational modifications, such as ADP-ribosylation, glycosylation, and ubiquitylation, or noncovalent interactions that inhibit or activate host cell functions to the benefit of the pathogen, for example allowing intracellular replication, host cell remodelling and intercellular spread, or disrupt host cell immune functions to increase their survival (Sakari et al., 2022). Toxins can consist of a single protein, or they can be organized as oligomeric protein complexes. Many of the type III bacterial toxins consist of two components, A and B domains with distinct structure-function properties and are called AB toxins. The A domain, also called an effector domain, is often an enzyme facilitating covalent

and non-covalent modifications or a factor that functions through protein-protein interactions within the cell, while the B domain contains two functional subdomains: a receptor-binding domain defining the cell tropism of the toxins and a translocation domain delivering the A domain across the plasma membrane or endosome lipid bilayer (Henkel et al. 2010). In most cases, the translocation of the A domain is hypothesized to happen via a pore or channel formed by the B domain (Henkel et al. 2010). Sometimes the B domain is a single subunit forming AB-type structure (*e.g.*, diphtheria and botulinum toxins) or it can be in an oligomeric form, forming *e.g.*, AB5-type of structure-function organization (*e.g.*, Shiga, pertussis, and cholera toxins) with the A domain. The A and B domains may be linked by a disulfide bond or associated by non-covalent interactions (Henkel et al. 2010).

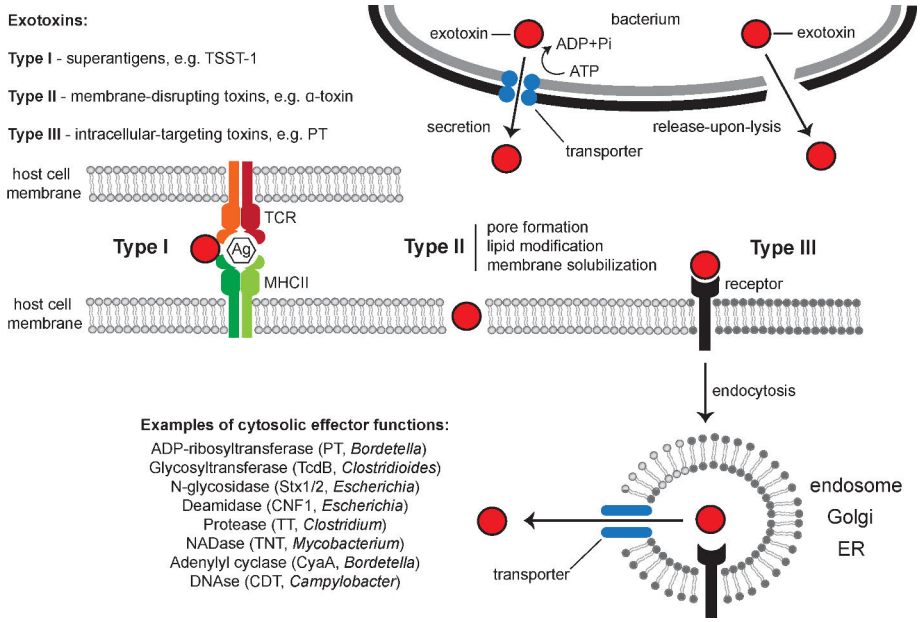

Figure 1. Classification of bacterial exotoxins based on their effector mechanism. Exotoxins are secreted by the bacteria or released upon bacterial lysis. They bind to the host cell surface and exert their effects on host cell surface or are endocytosed inside the cell, where they undergo a maturation process, often involving retrograde trafficking from endosomes to the Golgi and endoplasmic reticulum (ER), followed by the release of effector subunits into the cytosol, where they exert their action. Exotoxins are grouped into three types based on their mechanisms: type I - superantigens, type II - membrane-disrupting toxins, and type III - intracellular-targeting toxins, with some overlap occurring. Abbreviations: ADP - adenosine diphosphate, ATP – adenosine triphosphate, Pi – inorganic phosphate, TCR - T cell receptor, MHCII - major histocompatibility complex class II, Ag - antigen, TSST-1 - toxic shock syndrome toxin, PT - pertussis toxin, TcdB – *Clostridium difficile* toxin B, Stx1,2 - Shiga toxins 1 and 2, CNF1 - cytotoxic necrotizing factor 1, TT - tetanus toxin, TNT - tuberculosis necrotizing toxin, CyaA - bifunctional hemolysin/adenylyl cyclase, CDT - cytolethal distending toxin. Figure is from (Sakari et al. 2022), licensed under CC-BY 4.0 (https://creativecommons.org/licenses/by/4.0/).

2.2.2 ADP-ribosyltyransferase toxins

One important family of bacterial intracellular-targeting toxins with enzymatic activity are the bacterial ADP-ribosyltransferase (ART) toxins that are covalently modifying host macromolecules, commonly proteins, by transferring an ADP-ribose moiety from nicotinamide adenine dinucleotide (NAD+) onto a specific amino acid side chains of target molecules to generate an ADP-ribosylated substrate via *N*-, *O*-, or *S*-glycosidic linkages and a free nicotinamide (Figure 2) (Cohen & Chang, 2018). In addition to proteins, DNA, RNA, or antibiotics can also serve as a target (Baysarowich et al., 2008; Lyons et al., 2016; Nakano et al., 2013; Rominski et al., 2017). ART-toxins are found in different types of bacterial pathogens and each toxin produces a unique pathology by modifying one or more specific host components, which perturb important physiological processes in the infected host, such as protein synthesis, signal transduction, and cytoskeleton formation and dynamics (Lüscher et al., 2018). Examples of well-known bacterial ARTs are pertussis toxin (PT) from *B. pertussis*, cholera toxin (CT) from *Vibrio cholerae* and diphtheria toxin (DT) from *Corynebacterium diphtheria* (Holbourn et al., 2006; Locht & Antoine, 1995). They have a major or causative role in the severe infectious diseases such as whooping cough, cholera, and diphtheria, respectively.

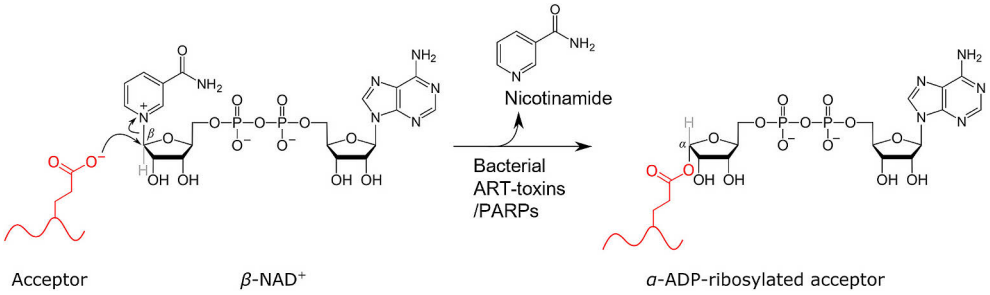

Figure 2. A simplified scheme of the ADP-ribosylation reaction, involving the enzyme-catalyzed transfer of the ADP-ribosyl moiety from β-NAD^+ to a protein amino acid residue (in red) acting as an acceptor of the ADP-ribose. The attachment involves an inversion of bond configuration from β to α at the ADP-ribose C1" atom and a simultaneous release of nicotinamide. Abbreviations: ADP – adenosine diphosphate, ART – ADP-ribosyltransferase, PARP – poly-ADP-ribose polymerase, NAD+ - nicotinamide adenine dinucleotide. Figure is adapted from (Suskiewicz et al., 2021), licensed under CC BY 4.0. (http://creativecommons.org/licenses/by/4.0).

2.2.2.1 Conservation in ART-toxins

While overall sequence homology among all members of the ART toxin family is generally low, the bacterial ARTs [and ARTs in general, *e.g.,* poly-ADP-ribose polymerases, (PARPs)/ ADP-ribosyl-transferases diphtheria toxin-like (ARTDs)]

can be divided into two main classes based on their conservation of three significant residues in the ART-fold, *i.e.,* the NAD+ binding fold: the R-S-E class, related to cholera toxin (cholera toxin group, CT-group); and the H-Y-E class, related to diphtheria toxin (diphtheria toxin group, DT-group) (Yoshida & Tsuge, 2021). The CT group can be further subdivided into the CT-like, C2-like, and C3-like ARTs. Some toxins do not belong to either of these main R-S-E or H-Y-E classes.

Well known toxins from the CT-group include, in addition to CT, the heat-labile enterotoxin from *Escherichia coli* (LT) (Duan et al., 2019) and PT from *B. pertussis* (Carbonetti, 2015; Krueger & Barbieri, 1995). They are two-chain proteins with the ART activity containing subunit A, and a non-toxic host receptor-binding component B. A long loop anchoring the A subunit into the B pentamer during toxin delivery is a structurally distinguishing feature of this group (Mikolčević et al., 2021). C2-like toxins, including for example iota toxin from *Clostridium perfringens* and certhrax from *Bacillus cereus*, are AB toxins containing B domains that are structural duplicates of the A domain (Sakurai et al., 2009; Visschedyk et al., 2012). C3-like toxins are A subunit-only toxins, and examples are *S. aureus* C3stau2, *Clostridium botulinum* C3bot and *Pseudomonas aeruginosa* exotoxin S (Aktories et al., 1989; Barbieri & Sun, 2004; Evans et al., 2003)

The DT group contains, in addition to diphtheria toxin, exotoxin A (ETA) from *P. aeruginosa* and cholix toxin from *V. cholerae*. The DT group of toxins are AB toxins comprising three structural domains of equal size: the catalytic (C) domain constitutes subunit A, while the translocation or transmembrane (T) domain, together with the receptor-binding (R) domain, constitutes subunit B (Mikolčević et al., 2021, Gillet & Barbier, 2015). All members of the DT-group ADP-ribosylate the specific post-translationally modified histidine, diphthamide, which is only found in eukaryotic elongation factor 2 (Gupta et al., 2008; Jørgensen et al., 2006; Mateyak & Kinzy, 2013). CT-group toxins, on the other hand, have a broad amino acid targeting and modify several amino acids such as arginine, cysteine and threonine, as well as glutamine, asparagine and lysine (by iota toxin, PT, *Photorhabdus luminescens* C3 and C5 toxins, C3 toxin and *E.coli* pertussis-like toxin (*Ec*Plt), respectively) (Lang et al., 2010; Littler et al., 2017; Pollard et al., 2018; Tamamura et al., 2017; Tsuge et al., 2008; Tsurumura et al., 2013; Young et al., 2014). While the R-S-E ART family as a whole targets multiple different amino acids, each member still modifies only one amino acid on a single protein target (Cohen & Chang 2018).

All the ART domains have a similar core structure of six strands followed by a helix, with the conserved R-S-E and H-Y-E residues located on these strands (Aravind et al., 2015; Cohen & Chang, 2018; Hottiger et al., 2010) (Figure 3). First strand from the N-terminus contains the arginine or histidine, second strand contains the serine or tyrosine, and the fifth strand contains the catalytic glutamate (Yoshida

& Tsuge, 2021). The conserved core structure also forms a cleft, where NAD+ binds in a bent conformation that creates strain in the pyridinium N-glycosidic bond of the molecule, thus lowering the amount of energy required to cleave the glycosidic bond (Cohen & Chang, 2018). In both R-S-E and H-Y-E arts, each of the conserved amino acids interacts with NAD+. In the R-S-E ARTs, the arginine has electrostatic interactions with the diphosphate backbone of NAD+, while the serine forms hydrogen bonds with the nicotinamide ribose, and the glutamate is thought to stabilize the oxocarbenium intermediate (Cohen & Chang, 2018). In H-Y-E ARTs, the histidine forms hydrogen bonds with the 2-OH of the adenosine ribose and the NH_2 of the nicotinamide amide, the tyrosine π-stacks with the nicotinamide ring, and the glutamate serves a similar stabilizing role as it does in R-S-E ARTs (Cohen & Chang, 2018).

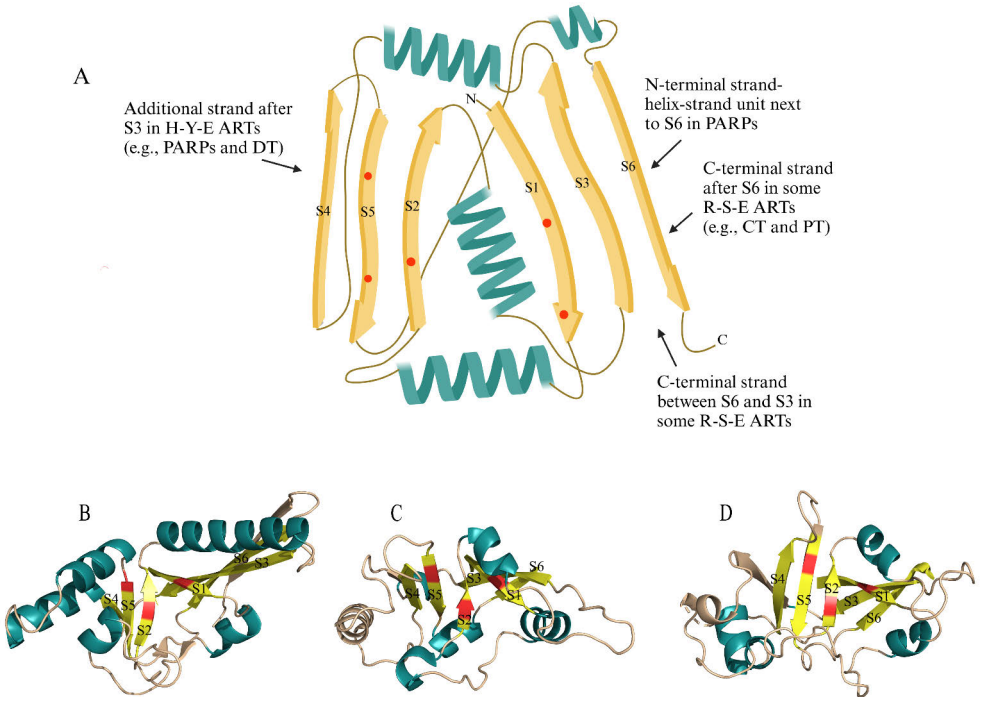

Figure 3. **A.** A schematic of a simplified topology of the ART fold showing specific structural features associated with different ART families (based on Aravind et al. 2015). Positions of conserved active site residues are shown in red, strands (S1-6) in yellow, and helices in teal. Figure was created with www.biorender.com. **B-D.** Cartoon structures of the ART fold of members of CT- and DT-group toxins. Conserved strands are shown in yellow, core fold helices in deep teal. Additional non-conserved strands are shown in wheat color. Conserved strands of the core are labeled based on panel A. Active site residues are shown in red. B. Pertussis toxin (PT) (Protein Data Bank (PDB): 1PRT); C. Pseudomonas exotoxin A (ETA) (PDB: 1IKQ) and D. Diphtheria toxin (DT) (PDB: 1DTP). Abbreviations: ART -ADP-ribosyltransferase, PARP – poly-ADP-polymerase. Structures generated by PyMOL (Version 2.5.5, Shrödinger, LCC).

The three residues forming these evolutionarily conserved characteristic triads are located in different more or less conserved motifs in ART toxins: i) The motif that contains an aromatic amino acid, followed by either the histidine or the arginine crucial for NAD+ binding and maintaining the structure of the active site cleft (the arom-His⁄Arg motif), ii) the aromatic-hydrophobic-serine-threonine-serine motif (STS motif) that stabilizes the NAD+ binding, found in bacterial CT-like ARTs, while in bacterial DT-like ARTs, this motif is either partially (Y-X-T/S) or completely (Y-F/X-A/X) (X for any amino acid) lost, iii) acceptor loop, also called ADP-ribosylating turn-to-turn (ARTT) loop, containing the Q/EXE motif with the catalytic glutamate, that is found in the bacterial CT-like ARTs (Hottiger et al., 2010) (Figure 4). In C3-like toxins the acceptor loop also features an aromatic residue (Phe, Trp, or Tyr), which identified to be important for substrate recognition (X-X-φ-X-X-Q/EXE, where the symbol φ refers to aromatic residue) (Yoshida & Tsuge, 2021). The first glutamate or glutamine in Q/EXE is important for both substrate recognition and target residue specificity, and the last glutamate is the catalytic glutamate (Han & Tainer, 2002; Sun et al., 2004; Toda et al., 2015; Tsuge et al., 2003, 2008; Tsurumura et al., 2013). In the acceptor loop of H-Y-E ARTs only the catalytic glutamate is conserved, not the turn-to-turn motif. They also contain a donor loop lacking from R-S-E ARTs, which has a role in protein substrate recognition and is important in NAD+ binding and catalysis (Jørgensen, Wang, et al., 2008). C3 group of toxins also contain a phosphate-nicotinamide (PN) loop. It is located immediately after the STS motif. It interacts with the target and binds N-phosphate and is suggested to lock the nicotinamide in place during the reaction (Fieldhouse et al., 2010; Fieldhouse & Merrill, 2008; Ménétrey et al., 2008). In addition, C3-group toxins lack the active site loop present in many DT- and CT-like toxins [*e.g.*, DT, LT, and PT], which may act in recognizing ADP-ribose acceptor substrates such as EF-2, and G-proteins (Han & Tainer, 2002). Instead of this loop, they have an α-helix that packs more tightly against the NAD+ cleft, leading to a more compact binding site as compared to many DT- and CT-like toxins (Holbourn et al., 2006).

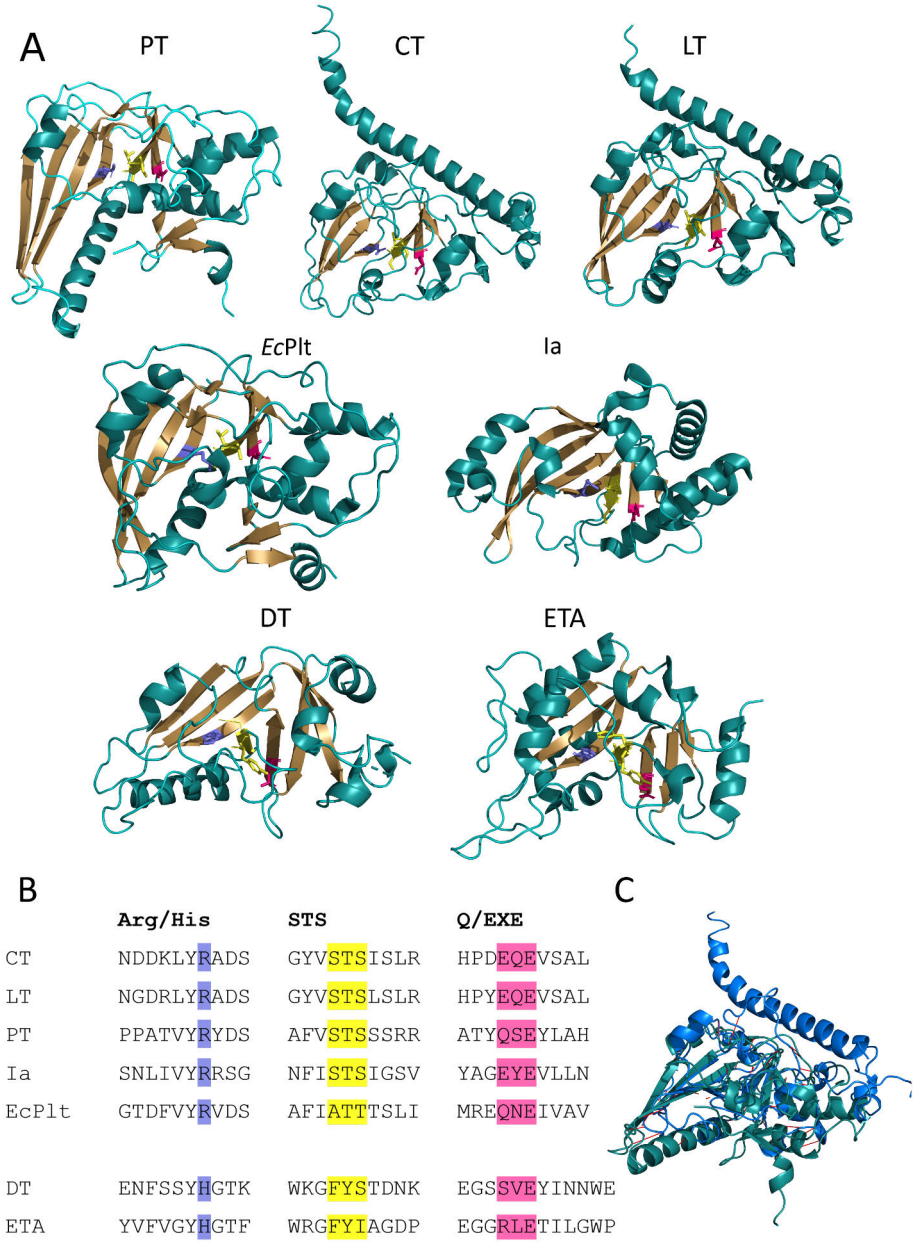

Figure 4. **A**. Cartoons of the A domains of cholera-like, C3-like and diphtheria-like toxins. Strands are shown in sand color, helices in deepteal, Arg/His motif in slate, the STS motif in yellow and the catalytic glutamate in pink. **B.** Sequence alignment of the ART toxins highlighting the conserved residues that make up each of the motifs. **C**. Superimposition of the A domains of pertussis toxin (deepteal) and cholera toxin (blue). Abbreviations: PT – pertussis toxin, CT – cholera toxin, LT – *E. coli* heat-labile enterotoxin, EcPlt – *E. coli* pertussis-like toxin, Ia - iota toxin enzymatic component, DT – diphtheria toxim, ETA – exotoxin A. Structures generated with PyMOL (Version 2.5.5, Schrödinger, LCC).

2.2.2.2 ART toxin reaction mechanism

The conservation of the NAD+ -binding site and common key catalytic residues suggest that the catalytic mechanism is likely common among all members of the ART family, but the reaction details of ADP-ribosylation have long been under a debate. Bimolecular nucleophilic substitution (S_N2) reaction mechanism has been initially suggested (Locht & Antoine, 1995; Soman et al., 1986; Wilson et al., 1990; Wilson & Collier, 1992), but recently there has been mounting evidence favoring unimolecular nucleophilic substitution (S_N1) mechanism (Beattie et al., 1996; Bell & Eisenberg, 1996; Davies et al., 2016; Jørgensen et al., 2005; Scheuring & Schramm, 1997a; Tsuge et al., 2003, 2008; Yoshida & Tsuge, 2021; Zhou et al., 2004), especially for the ADP-ribosylation happening to arginine and asparagine side chains and DNA by the R-S-E class of ARTs. In the both reactions mechanisms suggested, the nucleophilic attack occurs at the anomeric carbon of the nicotinamide ribose, resulting in the cleavage of N-glycosidic bond, which separates the ADP-ribose moiety from the nicotinamide ring (Holbourn et al. 2006).

The S_N2 reaction (Figure 5) is a nucleophilic substitution reaction where a bond is broken, and another is formed in a concerted manner. It is a bimolecular mechanism, meaning that both reacting species are involved in the rate-determining step. The reaction predominantly takes place at an aliphatic sp3 carbon center with an electronegative stable leaving group (electrophile, forms a bond by accepting a pair of electrons) attached to it. In the reaction, the nucleophile (electropositive group, forms bonds by donating a pair of electrons) attacks the substrate at 180° to the leaving group, breaking the carbon-leaving group bond and forming the carbon-nucleophile bond. In the process, the leaving group is displaced from the opposite side, resulting in the formation of a product with inversed tetrahedral geometry in regards of the central atom. S_N1 is the other major type of nucleophilic substitution reaction, and in it the rate-determining step is unimolecular. The reaction occurs in two steps, where first a carbocation (*e.g.,* oxocarbenium) intermediate is formed by the separation of a leaving group, which is then followed by nucleophilic attack (Figure 5). As carbocation is planar, the attack of nucleophile may occur from either side to give a racemic product. However, as biochemical enzyme-catalyzed reactions, including enzymatic S_N1, are generally stereo- and regio-specific, they almost always result in a single isomeric product, not a racemic mixture of products, and some reactions are not necessarily "pure" S_N1 or S_N2, but actually lie somewhere in between as a continuum of more or less tightly associated ion pair mechanisms (Soderberg, 2019).

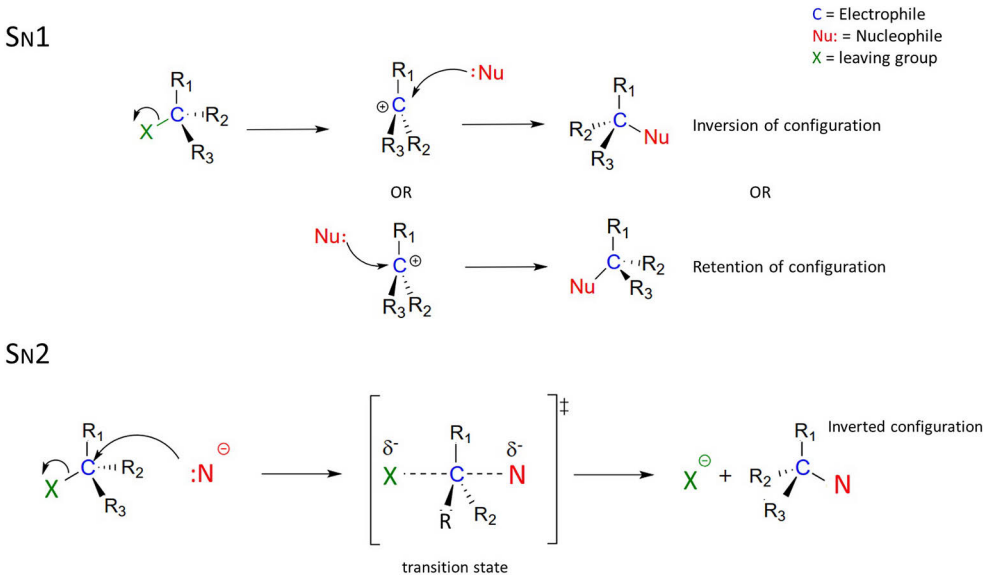

Figure 5. Simplified schematic of S_N1 and S_N2 reaction mechanisms. Both reactions are nucleophilic substitutions, involving a nucleophile replacing a leaving group. S_N1 is a unimolecular reaction, where reaction occurs in two steps, where first a carbocation intermediate is formed by the separation of a leaving group, which is then followed by nucleophilic attack that can happen from either side of the molecule. S_N2 is a bimolecular reaction, where the nucleophile attacks the substrate at 180° to the leaving group, breaking the carbon-leaving group bond and forming the carbon-nucleophile bond, leading to a formation of bimolecular transition state. S_N2 mechanism results in an inversion of the configuration in the product in regards of the central carbon atom. R denotes any atom attached to the central carbon, $\delta-$ or $\delta+$ denotes to a partial charge. Figure adapted from (Soderberg, 2019) licensed under CC BY 4.0. (http://creativecommons.org/licenses/by/4.0)

In the ART toxins, if the ADP-ribosylation reaction proceeds via S_N2 reaction, the attacking nucleophile is the substrate arginine, diphthamide, asparagine or cysteine, depending on the toxin involved, or a water in NAD+ hydrolysis reaction. In the S_N2 mechanism, exemplified by a mechanism proposed for pertussis toxin by Locht and Antoine (Locht & Antoine, 1995), the conserved catalytic glutamate (Glu129) would exert its action on the 2′-OH group of the NAD+ ribose, thereby tending to ionize the nicotinamide ribose diol and labilizing the nicotinamide-ribosyl bond, thus inducing the formation of a pentacoordinate oxocarbenium transition state, however, without a formation of a true oxocarbenium intermediate (as is characteristic for S_N2 type reaction, a non-oxocarbenium ion, nucleophile-associated transition state) (Locht & Antoine, 1995). In PT and other CT-group of toxins containing the catalytic (less conserved) histidine (H35 in PT), it could act to increase the nucleophilicity of the acceptor substrate, cysteine 351 in the G protein or the water molecule in the case of PT, to attack the anomeric carbon of the ribose ring and completely cleave the weakened the pyridine-ribosyl bond (*N*-glycosidic

bond) of NAD+ and yield the products of the reaction. In DT group, the oxocarbenium like transition state is proposed to form due to the conformation of the NAD+, which exposes the anomeric carbon of the ribose ring to the solvent (Tsurumura et al., 2013). Similarly, in DT-group of toxins the catalytic glutamate would attack the anomeric carbon. However, as they do not contain the catalytic type of histidine, there would likely be important differences (Locht & Antoine 1995). To summarize the S_N2 mechanism, the nucleophile, formed at the pre-transition state, attacks the C1′–N1′ glycosidic bond to dissociate nicotinamide and complete nucleophilic substitution reaction in a concerted manner involving an oxocarbenium transition state, but without formation of isolated oxocarbenium intermediate.

In contrast to S_N2, the S_N1 reaction includes the formation of an isolated positively charged oxocarbenium ion intermediate. In the CT group of toxins, the reaction is nowadays thought to happen via the S_N1 alleviated-strain mechanism, first developed for Iota toxin (Tsurumura et al. 2013), but likely widely applicable throughout the CT group and even DT group ARTs, given high core structure similarity and the structural similarity of the strained conformations of NAD+ in the active site (Tsuge et al., 2008). The reaction is described to happen in three steps. Mechanism described for iota toxin is used as an example to describe the suggested mechanism (Tsurumura et al., 2013) (Figure 6). First, the conserved catalytic glutamate of the toxin (E380 in Iota toxin enzymatic component Ia) hydrogen bonds with the 2′-OH group of the N-ribose, and the universally conserved arginine (R295) in CT toxins (histidine in DT toxins) creates phosphate electrostatic interactions holding the NAD+ in a highly folded conformation that favors oxocarbenium ion formation. The formed positively charged oxocarbenium ion is in a strained conformation and a rotation of *N*-ribose via both O3-NP and NP-NO5 alleviates the strain forming a second cationic intermediate, which also might help in reducing the nucleophile-electrophile distance. In Ia, after cleavage of the nicotinamide, the oxocarbenium cation may be stabilized via Y251 (Tsurumura et al. 2013). Next, the electrophile and nucleophile would still need to migrate by an unknown mechanism that further reduces the distance between them (Tsurumura et al. 2013). Finally, the nucleophile (R177 of actin, in case of Ia), which associates with the first glutamine or glutamate (E378 in Ia) from Q/EXE motif, attacks NC1 of *N*-ribose, leading to α-selective ADP-ribosylation of the target protein. This mechanism has been witnessed for arginine and asparagine, but the mechanisms underlying the specificities of other amino acids (*e.g.*, cysteine modified by PT) remain unresolved, but as stated above, this mechanism is likely applicable also in these cases. ADP-ribosylation reaction is evidenced to proceed via S_N1 mechanism also in DT group of toxins, and a similar strain-alleviation model may also explain the reaction mechanism, as a model in which the nucleophile needs migrate toward the *N*-ribose has been proposed (Jørgensen et al., 2005).

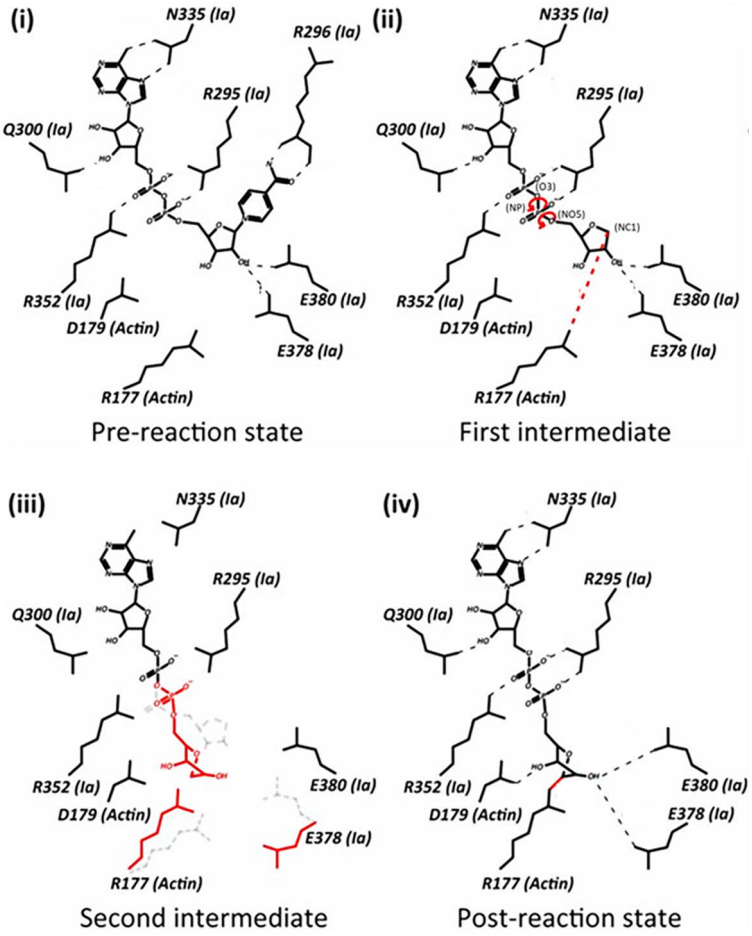

Figure 6. Schematic illustrating the S_N1 mechanism of ADP ribosylation in Ia: (i) the pre-reaction state of NAD+-Ia-Actin; (ii) cleavage of nicotinamide via an S_N1 reaction triggered by strain in the nicotinamide mononucleotide portion, leading to the formation of the first oxocarbenium cation intermediate with a strained conformation; (iii) induction of the second cationic intermediate by relieving the strained conformation, mainly through O3-NP and NP-NO5 rotation. Subsequently, *N*-ribose and R177 of actin migrate closer to each other, facilitated by a yet unknown mechanism, and NC1 nucleophilicly attacks R177; (iv) Ia-ADP-ribose-actin as the postreaction state. Abbreviations: Ia – iota toxin enzymatic component, NAD+ - nicotinamide adenine dinucleotide. Figure adapted from (Tsurumura et al., 2013).

2.3 Targeting bacterial toxins as a therapeutic strategy

Anti-virulence therapeutic strategies are designed to interfere with bacterial virulence factors, leading to bacterial disarmament and clearance without killing the bacteria. Such approaches are believed to impose less evolutionary pressure for the development of resistance compared to conventional antibiotics. Additionally, anti-

virulence-targeted drugs have the potential to minimize the collateral damage to the beneficial microbiota by selectively targeting the pathogen. These drugs can be used as prophylactic and therapeutic treatments, or in combination with antibiotics. Decades of basic research using *in vitro* assays, cell and tissue culture models, and animal experimentation have provided a deep understanding of bacterial virulence factors (Diard & Hardt, 2017), which is driving the development of new targeted anti-virulence therapies. These strategies include, for example, preventing bacterial adhesion to host tissue, modulating virulence gene expression, interfering with bacterial quorum sensing, and targeting specific toxins. It is especially beneficial to target toxins that are the primary cause or play a major role in the development of the disease. Examples of such toxins causing globally significant infectious diseases include pertussis toxin from *B. pertussis*, the causative agent of whooping cough; the diarrhoea-causing toxins of *Clostridium difficile* and Shiga toxin from *E. coli*; and the anthrax toxin from *Bacillus anthracis*, the causative agent of anthrax (Hedge et al., 2008; Moayeri et al., 2015; O'Brien et al., 1979).

Various drug modalities can be employed in targeting the bacterial exotoxins, such as monoclonal antibodies, antibody fragments, antibody mimetics, human antimicrobial peptides, receptor analogs, neutralizing scaffolds, dominant-negative mutants, and small molecules (Sakari et al., 2022). Each of these modalities have certain benefits as well as challenges (Table 1.). For example, monoclonal antibodies have advantages such as high specificity, long half-life in circulation, and good tolerability, but have low tissue and cell penetration. In addition to acting as exotoxin-neutralizing binders, they also may execute beneficial fragment crystallizable (Fc)-mediated functions, such as complementary interactions and phagocytosis of exotoxin-antibody complexes (Sakari et al 2022). Antibody fragments and antibody mimetics, on the other hand, are smaller and have better tissue penetration, but they have a short serum half-life when compared to antibodies. Receptor analogs and neutralizing scaffolds are an extremely diverse group of exotoxin-targeted drug leads and candidates, and have generally a good tolerability, especially if they are based on host natural components. Dominant-negative mutants can neutralize membrane-disrupting toxins, but development requires structural knowledge and screening. Small molecules have distinct advantages as exotoxin-targeted drugs. Due to their small size, small molecules penetrate tissues efficiently and may also enter the cell, allowing them to effectively target cytosolic functions. Most small molecules can be formulated for oral administration, allowing easy way of systemic distribution via absorption into the bloodstream. Additionally, chemical synthesis makes small molecule production cost-effective compared to other modalities like monoclonal antibodies. Due to their small molecular weight and simple chemical structures, small molecules often exhibit greater predictability in their pharmacokinetics and pharmacodynamics.

Table 1. Summary of the key advantages and disadvantages associated with the different exotoxin-targeted drug modalities.[a]. Table is from (Sakari et al. 2022), licensed under CC BY 4.0. (http://creativecommons.org/licenses/by/4.0)

MODALITIES	ADVANTAGES	DISADVANTAGES
Monoclonal antibodies	high target scope high diversity high specificity high affinity high stability good tolerability long half-life targets immune system to exotoxin	low tissue penetration low cell permeability demanding production high end product price limited routes for administration
Antibody fragments	high target scope high diversity high specificity high affinity high stability good tolerability high tissue penetration ease of production	short half-life low cell permeability limited routes for administration
Antibody mimetics	high target scope high diversity high specificity high affinity high stability good tolerability high tissue penetration ease of production	short half-life low cell permeability limited routes for administration
Receptor analogs and neutralizing scaffolds	high target scope high diversity high affinity good tolerability ease of production multiple routes for administration	low specificity (off-target effects) low cell permeability
Dominant negative mutants	high specificity high affinity	low target scope low diversity short half-life low cell permeability limited routes for administration
Small molecules	high target scope high diversity high tissue penetration high cell permeability ease of production multiple routes for administration	short half-life low specificity (off-target effects)

[a]Note that especially the category "*Receptor analogs and neutralizing scaffolds"* is a highly diverse group and as such the advantages and disadvantages can vary greatly and need to be assessed case by case. Certain fundamental features of the modalities can also be engineered, such as increasing the half-life of antibody fragments.

Small molecules can be designed to interact with biological targets, mainly proteins, using high-resolution structure-based rational drug design approaches. They can have varying modes of action, such as binding to and inhibiting enzyme active sites, targeting allosteric sites that have influence on enzyme dynamics or conformational changes, or preventing interactions. Screening of bioactive hit compounds can be

done efficiently with high-throughput screening (HTS) of small-molecular weight compounds or fragment libraries utilizing biochemical or cell-based assays. To date, most of the preclinical research targeting bacterial toxins has had the primary focus on monoclonal antibodies, antibody fragments, receptor analogs, and neutralizing scaffolds, and all the toxin-targeted drugs currently approved by the U.S. Food and Drug Administration (FDA) are monoclonal antibodies (Sakari et al., 2022) (Table 2). This is in striking contrast to the drug development pipelines for other pathologies, where small molecules dominate the research. For them, approximately two-thirds of approved medications are small molecules, either synthetised or from natural sources (Markossian et al., 2018).

There are multiple points in the functional pathway of bacterial exotoxins that can be targeted, including expression (transcription, translation, protein folding), secretion, cell surface binding, intracellular maturation, and cytosolic effector functions (Sakari et al. 2022). Affecting the production of bacterial toxins prior to their secretion or release-upon-lysis is possible with for example small molecules that prevent the transcription, translation or proper protein folding of the bacterial toxin, exemplified by the research identifying inhibitors of staphylococcal transcription factor AgrA, preventing it from binding to promoters of exotoxin-encoding genes, thus blocking transcription (Greenberg et al., 2018), and the work identifying antivirulence drug leads targeting the Sec-pathway responsible for the secretion of most bacterial proteins (Jin et al., 2016). As exotoxin binding to the specific cell receptor is a specific step required for their function, and as some toxins (*e.g.*, superantigens, membrane disrupting toxins) perform their function at this cellular localization, preventing the toxin interaction with cell membrane components is one effective way of countering bacterial toxins. This step is targeted by many exotoxin-targeted drug modalities, including all FDA-approved drugs and most clinical trial drug candidates (Sakari et al., 2022). Intracellular-targeting toxins have complex maturation processes, and they may rely on auto-processing or oligomerization to deliver their enzymatic cargo into the cytosol. Monoclonal antibodies, antibody fragments, and small molecules can interfere with these intracellular maturation processes. The final step to interfere with the toxin function is the step where the toxin's effector domain has been released into the cytosol from the endosome or Golgi/ endoplasmic reticulum (ER) compartment or gained access to the cytosol straight from the plasma membrane. At present, the developmental pipelines for small molecules targeting bacterial toxins, are solely concentrated on compounds that interfere with the cytosolic effector functions (Sakari et al. 2022). Small molecules are often able to enter the cell due to their small size, thus allowing effective targeting of the cytosolic processes, unlike the other modalities, which have poorer tissue penetration and cell entering capabilities due to their size.

Table 2. Exotoxin-targeted drugs that are either already FDA-approved or that have entered clinical trials. Clinical trial data based on ClinicalTrials.gov database as literature searches, as of 29 August 2023 (https://www.clinicaltrials.gov). Ebselen trials have been conducted in diseases other than C. difficile infections, *e.g.*, diabetes phase III trial NCT00762671. Table is from (Sakari et al. 2022).

mAb	Format	Pathogen	Target	State	Trial ID
Raxibacumab (Abthrax®)	h(human)/IgG1	*B. anthracis*	Anthrax toxin	FDA 2012 Phase IV	NCT00639678 NCT02016963 NCT02339155 NCT02177721
Obiltoxaximab (Anthim®)	c(chimeric)/ IgG1	*B. anthracis*	Anthrax toxin	FDA 2016 Phase IV	NCT00138411 NCT00829582 NCT01932242 NCT01929226 NCT01453907 NCT01932437 NCT01952444 NCT03088111
Bezlotoxumab (Zinplava®)	h/IgG1	*C. difficile*	Toxin B (TcdB)	FDA 2016 Phase IV	NCT01241552 NCT01513239 NCT04626947 NCT03880539 NCT03937999 NCT03756454 NCT04415918 NCT03182907 NCT03829475 NCT04317963 NCT04075422 NCT04725123
ASN100	2 x h/IgG1	*S. aureus*	α-toxin, 5 leukocidins	Phase II (terminated)	NCT02940626 NCT01357213
MEDI4893 (Suvratoxu-mab)	h/IgG1	*S. aureus*	α-toxin	Phase III	NCT05331885 NCT02296320 NCT01769417
AR-301 (Tosatoxuma)	h/IgG1	*S. aureus*	α-toxin	Phase III	NCT01589185 NCT03816956
Shigamabs	2 x c/IgG1	*E. coli*	Shiga toxin (Stx1-2)	Phase II	NCT01252199
TMA-15 (Urtoxazumab)	hIgG1	*E. coli*	Stx2	Phase I	not availabe
XOMA 3Ab	c/IgG1 2 x h/IgG1	*C. botulinum*	Botulinum neurotoxin A (BoNT/A)	Phase I	NCT01357213
NTM-1632	3 x c/IgG1	*C. botulinum*	BoNT/B	Phase I	NCT02779140
NTM-1634	4 x h/IgG1	*C. botulinum*	BoNT/C-D	Phase I	NCT03046550
NTM-1633	3 x c/IgG1	*C. botulinum*	BoNT/E	Phase I	NCT03603665
S315	h/IgG1	*C. diphteriae*	Diphtheria toxin	Phase I	NCT04075175

Receptor analog	Format	Pathogen	Target	State	Trial ID
SYNSORB-Pk	Polyvalent carbohydrate conjugate	*E. coli*	Stx1-2	Phase III (failed)	NCT00004465
Neuralizing scaffold	**Format**	**Pathogen**	**Target**	**Current state**	**Trial ID**
Tolevamer	Styrene sulfonate polymer	*C. difficile*	TcdA-B	Phase III (failed)	NCT00106509 NCT00196794 NCT00382304 NCT00466635 NCT00034294
CAL02	Liposome	*S. pneumoniae*	pneumolysin	Phase II	NCT05776004 NCT02583373
Small molecule	**Format**	**Pathogen**	**Target**	**Current state**	**Trial ID**
Ebselen	Organo-selenium compound	*C. difficile*	TcdA-B	Pre-clinical (Phase III)	NCT01452607 NCT00762671 NCT04677972

Naturally, host cell components, particularly host cell proteins involved in the functional pathway of exotoxins, can also be targeted. For example, small molecules that affect endosomal maturation, retrograde trafficking, intracellular activatory proteolytic processing, and intracellular chaperone-assisted activatory folding of exotoxins have been identified (Ernst et al., 2021; Gillespie et al., 2013; Hartmann et al., 2018; Secher et al., 2015; Stechmann et al., 2010; Tam et al., 2018). However, by targeting bacterial toxins instead of host proteins, off-target effects resulting from interference with normal host cell functions when targeting a host protein or process may potentially be avoided.

2.4 Pertussis toxin

2.4.1 Role of pertussis toxin in disease

Pertussis *i.e.*, whooping cough is a globally distributed highly contagious acute respiratory disease (Diavatopoulos et al., 2005; Kilgore et al., 2016) caused by the *B. pertussis*, a pathogenic Gram-negative coccobacillus of the genus *Bordetella*. It is transmitted directly from human to human, probably via aerosolized respiratory droplets (De Greeff et al., 2010; Kilgore et al., 2016) and is known to affect all ages: infants, children, and adults. Classic pertussis is a cough illness that can last for weeks and is characterized by paroxysms of repeated coughs that end with a gasping "whoop", (Decker & Edwards, 2021) and can lead to possible secondary complications such as vomiting, rib fractures and pneumothorax. Life threatening

complications, especially in newborns and infants, include leukocytosis, pulmonary hypertension, pneumonia, encephalopathy, seizures, and apnea (Cherry, 2016; Decker & Edwards, 2021).

B. pertussis binds to ciliated cells and proliferates within the upper and lower respiratory tract (Andreasen & Carbonetti, 2008), where several virulence factors *e.g.*, pertussis toxin, adenylate cyclase toxin, tracheal cytotoxin, filamentous hemagglutinin, fimbriae and pertactin are released, and their coordinated interplay results to pertussis disease. (Locht et al., 2001; Melvin et al., 2014). PT is considered to be the main virulence factor, as its activity has been linked to more severe disease, especially in infants, and reports on PT-deficient strains causing infection are scarce (Bouchez et al., 2009), a finding that strongly suggests important role for PT in the infection and disease formation in humans. Significant amount of evidence supporting the role of PT in the disease pathogenesis have been gained mainly from animal model studies, where *e.g.,* the systemic administration of PT has been shown to induce leukocytosis in animals (Bradford WL et al., 1956; Elahi et al., 2005; Hinds et al., 1996; Morse & Morse, 1976; Pauza et al., 1997; Samore & Siber, 1992) and pulmonary hypertension in a neonatal mouse model of pertussis (Scanlon et al., 2017; Scanlon et al., 2022). In addition, several animal models have provided evidence that indicate a role for PT in the development and characteristics of pertussis cough (Hall et al., 1994; Jiang et al., 2021; Parton et al., 1994; Warfel et al., 2012), although administration of purified PT does not elicit cough, indicating that PT does not have a direct effect in the cough pathology (Hewitt & Canning, 2010; Toyota et al., 1980). Additionally, studies show that PT has a fundamental role in the immune evasion of *B. pertussis*, *e.g.,* by delaying neutrophil recruitment onto the infection site and interfering with induction of adaptive immune responses (Andreasen & Carbonetti, 2008; Carbonetti et al., 2003, 2004, 2007; Connelly et al., 2012; Kirimanjeswara et al., 2005; Klimova et al., 2022; Spangrude et al., 1985). In addition, PT is shown to cause disruption of tight junctions between airway epithelial cells, which contributes to pulmonary edema development (Scanlon et al., 2019) (Figure 7).

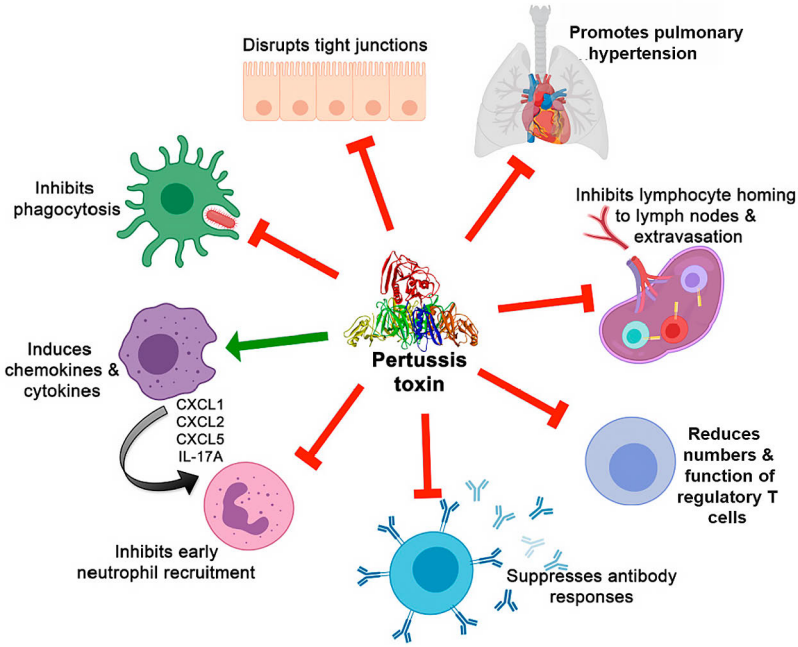

Figure 7. Schematic depicting some the aspects of pertussis toxin pathogenesis. PT disrupts the tight junctions of epithelial cells, contributing to pulmonary edema and promotes pulmonary hypertension (by yet incompletely understood mechanism). PT is also known to interfere with immune responses by *e.g.,* affecting the regulatory T cells, supressing antibody responses, inhibiting neutrophil recruitment and phagocytosis and inducing chemokines and cytokines. Figure is adapted from (Scanlon et al., 2019.), licensed under CC BY 4.0. (http://creativecommons.org/licenses/by/4.0)

2.4.2 Treatment of pertussis

In a non-immunized individual, pertussis has three stages: catarrhal, paroxysmal, and convalescent. The catarrhal stage shows cold-like symptoms, not necessarily prompting diagnosis. After about 7-10 days, the paroxysmal stage begins with distinct coughing fits, sometimes with the characterizing "whoop", raising suspicion of pertussis. This stage lasts up to 10 weeks, peaking around 2-3 weeks. The convalescent stage is marked by a gradual resolution of these fits. Following diagnosis, pertussis is treated with macrolide antibiotics - primarily azithromycin, clarithromycin, and erythromycin. If administered early (catarrhal and early paroxysmal stages), the antibiotics can reduce the severity, duration, and the risk of complications, particularly in infants (Carlsson et al., 2015, Winter et al., 2015, Tiwari et al. 2015, Heininger et al. 1993, Tiwari et al., 2005). However, the late diagnosis due to the cold-like symptoms in the catarrhal stage often limits antibiotic treatment efficacy. Nevertheless, antibiotics help reduce disease spread and can act prophylactically for close contacts of the infected individual (Cherry 2018, Terry et

al. 2015). In addition to antibiotic treatments, symptomatic treatment of the cough with *e.g.*, antihistamines, anti-inflammatory steroids, and bronchodilators has been proposed, but they have not yielded significant beneficial effect in clinical trial (Wang et al., 2014).

While antibiotics eliminate *B. pertussis* bacteria, they do not alleviate symptoms arising from the damaged tissues caused by the bacteria or by pertussis toxin (and other toxins) already secreted by the bacteria (Altunaiji et al., 2007; Carbonetti, 2016). It has been witnessed that due to toxins the symptoms last for weeks to months after the organism has disappeared (Locht, 2023). Symptoms persist until toxins are cleared and the cellular damage in the lungs heal. Additionally, while antibiotic resistance is not a major concern for pertussis, macrolide resistant strains have been reported (Guillot et al., 2012; Ivaska et al., 2022; Z. Wang et al., 2014; Yang et al., 2015).

As there is no effective treatment to pertussis, disease prevention has an important role. The pertussis whole cell vaccine became widely available in the 1940s and after the widespread introduction of the vaccine, the incidence of pertussis has decreased more than 75 % compared with the pre-vaccine era (Hall et al., 2021). Due to the side effects caused by the whole cell vaccine, the use of an acellular vaccine containing pertussis toxin, pertactin, filamentous hemagglutinin and fimbriae 2 or 3 has become more common vaccination strategy in industrialized countries since the late 1990s and early 2000s (Barkoff & He 2019), with the whole cell pertussis vaccine still in use mainly in the developing countries. Both vaccine types have the disadvantage of vaccine offering protection only for 5-10 years, with acellular protection waning faster (Sheridan et al., 2012; Tartof et al., 2013; Witt et al., 2012). Despite the universal vaccination strategies in use, pertussis continues to be a disease associated with a significant burden even in developed countries with cyclical epidemic peaks every 3-5 years (Mooi et al., 2000) and with larger epidemics reported in multiple developed countries (Campbell et al., 2012; Sealey et al., 2015; Van der Maas et al., 2013; Winter et al., 2012, 2014). In addition, seroprevalence studies have shown that the disease is also under-reported, and the actual circulation is higher in many countries (Barkoff et al., 2015). A model from 2014 estimated that there were 24.1 million pertussis cases and 160,700 deaths from pertussis in children younger 5 years that year (Yeung et al., 2017).

The resurgence of pertussis despite high vaccination rates prompts questions on the factors contributing to this increase. In part the increase has been attributed to improved diagnostics, better surveillance, and reporting (Kilgore et al., 2016). Waning adult immunity, especially after receiving acellular pertussis vaccine and molecular changes in the pathogenic *B. pertussis* strains over time (Barkoff & He, 2019) that might reduce the effectiveness of vaccines against these evolved strains (Van der Maas et al., 2013; Wirsing Von König et al., 2002), as well as incomplete

vaccine coverage due to *e.g.,* vaccine refusal (Phadke et al., 2016) are also thought to contribute to the increase. In addition, the acellular pertussis vaccines, while protecting against severe symptoms, do not prevent infection or transmission of the bacteria, based on experimentation in a baboon model (Warfel et al., 2014), contributing to the pertussis circulation in the population.

Considering the above-mentioned reasons, efforts to address pertussis resurgence should involve improving vaccine formulations and optimizing vaccination campaigns, but also exploring alternative ways to treat the disease. As pertussis toxin has a major role in whooping cough and mediates the severity of the disease (Carbonetti et al., 2007; Scanlon et al., 2019), there is a therapeutic promise to target pertussis toxin with novel pharmacological strategies in order to attenuate the symptoms and to protect against severe pertussis disease. This could be especially beneficial for young children not yet having the vaccine-induced protection against whooping cough. Young children are often diagnosed at the early stages of infection, allowing for timely intervention against pertussis toxin-induced pathology. Exposed family members could also benefit from prophylactic pertussis toxin inhibitors, possibly combined with macrolide antibiotics.

2.4.3 Cell binding, entry, and intracellular processing

Pertussis toxin is a bacterial AB5-type protein exotoxin, where the A component of PT (subunit S1) contains an enzymatic ART-domain, and the B component is the receptor-binding portion containing the rest of the subunits (S2-S5). The B-pentamer and S1-subunit assemble in the periplasm of the bacteria via non-covalent bonds to form a PT holotoxin, which is secreted by a type IV secretion system (Llosa et al., 2009; Stein et al., 1994; Weiss et al., 1993). The B-pentamer binds to the cell surface via sialylated sugars attached to proteins, which are found on most mammalian cell plasma membranes, enabling PT to intoxicate a wide range of different cells. (Armstrong et al., 1988; Hausman & Burns, 1993; Witvliet et al., 1989). A specific receptor has not been identified so far.

Following PT holotoxin binding to host cell surface, it is endocytosed and subsequently follows a retrograde trafficking route to the trans-Golgi network and ER (Plaut & Carbonetti, 2008) (Figure 8). In the ER, the interaction between S1 subunit and B pentamer is destabilized by binding of ATP to PT, contributing to the dissociation of the S1 subunit (Hazes et al., 1996; Plaut et al., 2016). The released S1 is in its unfolded conformation, which favors its transport from the ER into the cytosol via the ER-associated degradation pathway (Banerjee et al., 2016; Pande et al., 2006). This pathway is a cellular pathway targeting misfolded proteins from the ER to the cytosol, where they undergo ubiquitination and subsequent degradation by the proteasome system (Pande et al., 2006). As PTS1 does not contain any lysine

residues needed for ubiquitination, it can take advantage of this transport pathway while simultaneously evading subsequent degradation (Worthington & Carbonetti, 2007). Members of the heat shock family and peptidyl-prolyl cis-trans isomerases, protein folding helper enzymes, are indicated to be involved in this ER-to-cytosol transport, as experimental data shows that inhibiting the action of these chaperones reduces the number of PTS1 molecules in the cytosol, as well as reduced ADP-ribosylation of Gαi (Ernst et al., 2018a; Ernst et al., 2021; Kellner et al., 2019). Similar findings are reported for other ADP-ribosylating toxins such as C2, iota and cytolethal distending toxin (Ernst et al., 2015, 2016; Ernst et al., 2018b; Ernst et al., 2017a; Ernst et al., 2017b; Kaiser et al., 2011, 2012).

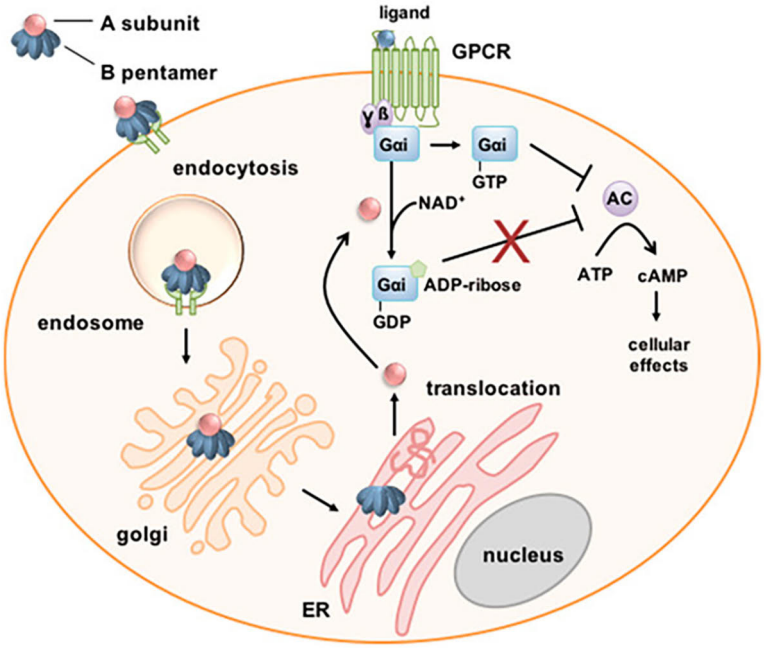

Figure 8. Schematic of the cellular uptake and mode of action of PT. PT binds to the cell surface via its B-subunit (B pentamer) and is endocytosed. It undergoes a retrograde transport to the trans-Golgi network and endoplasmic reticulum (ER), where the A-subunit PTS1 dissociates from the B-subunit and is translocated via the ER-associated degradation pathway into the cytosol, where PTS ADP-ribosylates inhibitory α-subunits (Gαi) of the heterotrimeric G protein, preventing it from interacting with G protein-coupled receptors (GPCR) on the cell membrane and subsequently preventing it from inhibiting adenylate cyclase (AC), resulting in increased and disturbed cyclic adenosine monophosphate (cAMP) signaling. Other abbreviations: GDP - guanosine diphosphate, GTP - guanosine triphosphate, ADP – adenosine diphosphate, NAD+ - nicotinamide adenine dinucleotide. Figure is from (Ernst 2022), licensed under CC BY 4.0. (http://creativecommons.org/licenses/by/4.0).

In the cytosol, the S1 toxin subunit catalyzes the transfer of ADP-ribose from the co-substrate NAD+ onto a specific C-terminal cysteine of the inhibitory α-subunits of heterotrimeric signal-transducing G proteins (Gαi/Gαo) (Bokoch et al., 1983; Hsia et al., 1985; Katada & Ui, 1982; West et al., 1985). This ADP-ribosylation creates a steric hindrance that prevents Gαi protein from interacting with G protein–coupled receptor, thus locking the α-subunits into an inactive state [guanosine diphosphate (GDP)-bound form], rendering it unable to negatively regulate the membrane-bound adenylate cyclase. This leads to increased intracellular cyclic adenosine monophosphate (cAMP) levels, which subsequently leads to disturbed cellular signaling, resulting systemic pathologies. The disturbed cAMP-signaling causes various effects depending on the cell type (Scanlon et al., 2019), and the presence of PT-binding sialoglycoproteins on multiple different cell types might explain range of different effects observed following PT intoxication.

In early stages of infection, PT activity leads to delayed recruitment of neutrophils, monocytes and lymphocytes to the respiratory tract and leads to decreased amounts of pro-inflammatory chemokines and cytokines and increased bacterial burden in a mouse infection model (Andreasen & Carbonetti, 2008; Kirimanjeswara et al., 2005; Spangrude et al., 1985).

2.4.4 Cellular effects of pertussis toxin

The role of PT in the pathogenesis of whooping cough has been extensively studied with various *in vitro* methods and *in vivo* in murine and, more recently, non-human primate models. Data has also been collected from infected individuals. Pertussis toxin is known to play a role in several biological activities, primarily through its ADP-ribosyltransferase activity towards Gαi, resulting in the loss of inhibition of AC activity and increase of the intracellular concentration of cAMP. This accumulation of cAMP disturbs many cellular processes, as cAMP is an important second messenger that regulates several intracellular signaling pathways. Accumulation of cAMP is considered to be the cause of majority of the systemic pathological events caused by *B. pertussis* infection (Locht et al. 2011), and depending on the target cell, it can result in a variety of biological activities, such as induction of morphological changes of the cell, lipolysis, stimulation of pancreatic islet cells, exocrine secretion, histamine sensitization, leukocytosis, inhibition of chemotaxis and inhibition of lymphocyte and neutrophil migration (Carbonetti, 2015; de Gouw et al., 2011; Katada & Ui, 1980; Locht & Antoine, 1995; Morse & Morse, 1976; Müller-Wieland et al., 1991; Munoz et al., 1981; Spangrude et al., 1985). Of note, *B. pertussis* contains another toxin, adenylate cyclase toxin that catalyzes the formation of unregulated cAMP levels to even greater extent than what

PT activity does. However, they are thought to act in a different disease stages and possibly affect different cell types.

Besides increased cAMP levels, PT-mediated ADP-ribosylation may also have cAMP-independent effects on various cellular mechanisms, including expression of αi and αo subunits and expression of regulators of G-protein signaling-proteins, regulation of signaling events related to cell cycle, growth, and proliferation such as regulation of kinase pathways and tuberin phosphorylation (Clark et al., 2003; Wu & Wong, 2005a, 2005b; Yung et al., 2008). Additionally, some cAMP-independent effects might be mediated by the βγ-complex, as its binding to the G-protein complex depends on the binding of the α-subunit (Leaney & Tinker, 2000; Tomura et al., 1997).

Furthermore, some of the activities attributed to PT, such as hemagglutination, platelet aggregation, glucose oxidation in adipocytes, and T-cell mitogenicity and regulation, are independent of the ADP-ribosyltransferase reaction, but depend on receptor-binding properties of PT (Banga et al., 1987; Gray et al., 1989; Lobet et al., 1993; Loosmore et al., 1993; Schneider et al., 2007; Sindt et al., 1994; Strnad & Carchman, 1987; Tamura et al., 1983; Thom & Casnellie, 1989). PT has been also described to have other B-oligomer mediated effects on cellular processes, including those involving tyrosine kinases, nuclear factor-κB, Toll-like receptor 4, and Rac (Garcia et al., 2001; Lee et al., 2010; H. Li & Wong, 2001; Nishida et al., 2010; Poltorak et al., 1998; Z. Y. Wang et al., 2006). However, the actual extent of the role of these B-oligomer mediated effects in the pathogenesis of whooping cough is unclear.

2.4.5 Structure of pertussis toxin

PT is a complex 105-kDa exotoxin arranged in an AB5 structure that comprises six different subunits, named S1 through S5 (Figure 9). S1 is the enzymatically active subunit, catalyzing the ADP-ribosylation of Gαi/Gαo. It also has NAD+ glycohydrolase (NADase) activity in the absence of G proteins, catalyzing the cleavage of NAD+ into ADP-ribose and nicotinamide. The receptor-binding B-oligomer is composed of S2, S3, S4, S4 and S5.

The crystal structure of PT has been solved as an uncomplexed structure (APO structure), in complex with soluble oligosaccharide and in complex with ATP (Hazes et al., 1996; Stein et al., 1994a; Stein et al., 1994b). The crystal structure reveals that the S1 subunit shares structural homology with other ADP-ribosylating bacterial toxins (Littler et al., 2017; Sixma et al., 1991; Song et al., 2013), with some differences in the carboxy-terminal end that might explain its unique activation mechanism (Stein et al., 1994). The cell-binding heteropentameric B-subunit has structural resemblance to the symmetrical B-pentamers of the cholera toxin and

Shiga toxin families, even though there is almost no sequence homology between the B subunits of these toxins (Stein et al., 1994).

In the secreted form of PT, the large pyramid-shaped enzymatic S1-subunit sits on a pseudo-pentameric disc–like arrangement of structurally similar glycan-binding subunits S2:S4:S3:S4:S5 (Stein et al., 1994a; Stein et al., 1994b; Tamura et al., 1982). The holotoxin comprises 952 residues overall. Each of the B-subunits contains a similar fold of about 100 residues that interact with approximate five-fold symmetry to form a pseudo-pentameric domain in the center of the B-oligomer (Stein et al., 1994a). This central domain contains a barrel formed by five -helices surrounded by a ring of 30 antiparallel β-strands from the B-oligomer subunits. S1 is anchored via its carboxyl terminus that extends into the pore of a central barrel. S2 and S3 subunit contain an amino-terminal extension of approximately 100 residues as compared to S4 and S5 subunits, forming additional domains at the periphery of the B-oligomer (Stein et al. 1994a).

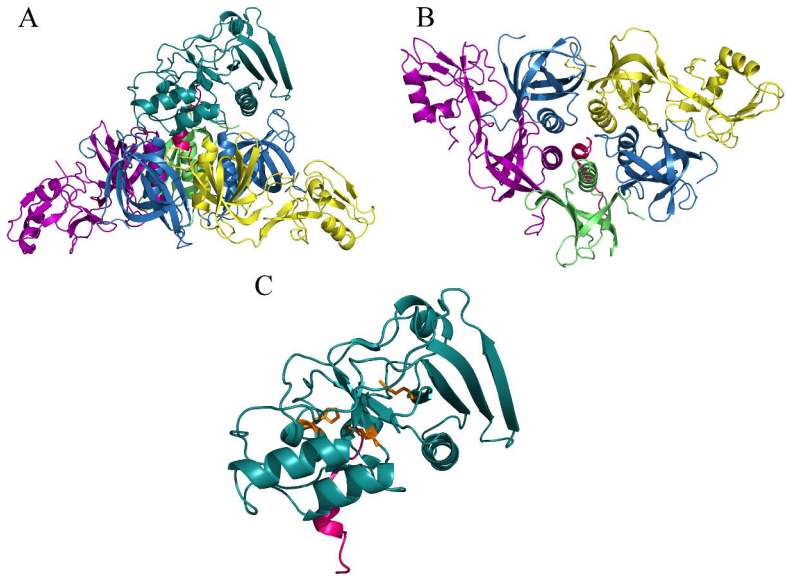

Figure 9. The structure of pertussis toxin (PDB: 1PRT). **A**. A sideview of S1 subunit (deepteal, with hotpink C-terminus) positioned on top of the B-oligomer (subunit coloring: S2 = purple, S3 = yellow, S4 = skyblue, and S5 = lime). **B.** A bottom view of the triangular shaped B-oligomer with 5 α-helices in the centre, surrounding a pore where the C-terminal end of S1 anchors. **C**. Representation of the S1 subunit active site residues R9, E129 and H35 in a stick mode (orange). Generated with PyMOL (version 2.5.5, Schrödinger, LCC).

2.4.5.1 S1 subunit

The S1 subunit fold is similar to the catalytic subunits of LT, *Ec*Plt, DT, ETA (Allured et al., 1986; Choe et al., 1992; Littler et al., 2017; Sixma et al., 1991; Stein et al., 1994; Zhang et al., 1995) and most of the secondary structures of S1 can be superimposed with those of the A subunit of LT (Stein et al., 1994) and CT (Figure 3). S1 subunit has a complicated topology with many short stretches of secondary structure, containing in total seven α-helices and twelve β-strands. Some of the sheets and helices are longer in PT compared to LT, and there are significant differences in connecting loops. Structural data together with functional analysis indicate that the N-terminal part of the S1 subunit contains the residues required for the catalytic activity and that they reside within the first 175 amino acids of S1, while residues 176-235 form an area that has no structural homologue in LT (Krueger & Barbieri, 1994; Locht & Antoine, 1995). It is not essential for the catalytic activity of S1 *in vitro,* demonstrated with carboxy-terminal deletion mutants (Barbieri & Cortina, 1988; Burns DL et al., 1987; Pizza et al., 1988). The S1 subunit contains a single intramolecular disulfide bond between the two conserved cysteines (C41 and C201) in the secreted oxidized state, which holds the C-terminus (residues 180-235) of the S1 subunit in the NAD+-binding site, preventing the enzymatic ART activity (Stein et al., 1994). In the reducing environment of the cytoplasm, this disulfide bond is reduced, and the inhibitory effect of the C-terminus is released, making the subunit enzymatically active (Moss et al., 1983). Residues 195-204 are required for optimal ADP-ribosylation of trimeric G proteins (Krueger & Barbieri, 1994). Amino acids 205-219 appear to link the catalytic region of the S1 subunit and the carboxyl-terminal B-oligomer-binding region of S1, while hydrophobic amino acids 220 to 235 also seem to be important for association of the S1 subunit with the B-oligomer. (Krueger & Barbieri, 1994; Stein et al., 1994). The carboxyl terminus enters a pore in the center of the B-oligomer with a short helix and ends within the pore (Stein et al., 1994).

2.4.5.2 Active site

The active site of PT shares structural homology with the active site of other known bacterial ADP-ribosylating bacterial toxins (for example LT, CT, ETA and DT, *Ec*Plt), even though they do not have high degree of sequence identity (~5-20%) (Allured et al., 1986; Choe et al., 1992; Littler et al., 2017; Sixma et al., 1991; Stein et al., 1994; Zhang et al., 1995). The common core fold of approximately 100 residues consists of two antiparallel β-sheets and two α-helices, where the NAD+-binding cleft is formed at the interface of the two β-sheets (Bell & Eisenberg, 1996). The active site residues of PT can be superimposed with a root mean square (RMS) difference of 1.0A for LT, 1.5A for exotoxin A and 1.6A for diphtheria toxin (Stein

et al., 1994). Based on sequence alignments and systematic analyses, only two residues are conserved in all of these toxins. These are Y8 and E129 in PT (Y6 and E112 of LT and CT, Y8 and E118 in *Ec*Plt, Y20 and E148 of DT, and Y439 and E553 in ETA). The glutamic acid has been shown to be essential for enzymatic activity in these toxins (Antoine et al., 1993; Barbieri et al., 1989; Burnette et al., 1988; Cieplak et al., 1990; S. A. Cockle, 1989; Locht et al., 1989; Pizza et al., 1988).

The crystal structure of PTS1 reveals, that the negatively charged carboxyl group of catalytic E129 is within hydrogen-bonding distance of H35, S52 and Q127, and various experiments have shown also these to be involved in the ADP-ribosylation of Gαi (Antoine et al., 1993; Antoine & Locht, 1994; Locht et al., 1989; Locht & Antoine, 1995; Stein et al., 1994; Xu et al., 1994). The carboxyl group of E129 is likely interacting with the positive charge on the ribosyl ring of NAD+ at the transition state. Mutations of H35 are associated with reduced ADP-ribosyltransferase activity and even more effect on the NAD+-glycohydrolase activity, indicating a role for H35 during catalysis, likely by enhancing the nucleophilicity of the thiol of cysteine residue in G protein by ionization (Antoine & Locht, 1994; Scheuring & Schramm, 1997a; Xu et al., 1994). This conserved histidine can be found in LT and CT (H44 in both), while DT-group of ARTs do not contain this type of catalytic histidine. S52 substitutions have been seen to reduce the catalytic activity, but it is suggested to be involved in maintaining the conformation of the active site, rather than a direct role in the catalysis (Antoine & Locht, 1994; Locht & Antoine, 1995). S52 is part of the STS motif and the characterizing serine in R-S-E group of toxins, hydrogen bonding with several positions in the nicotinamide ribose. A matching serine in CT and LT is S61. Q127 is, with E129, a part of the conserved Q/EXE-motif in R-S-E/CT-group of ARTs (Q110 in CT and LT, Q116 in *Ec*Plt). Additionally, R9, W26 and C41 are also involved in the NAD+ binding based on kinetic studies with S1 analogs with amino acid substitutions (Burnette et al., 1988; Cortina & Barbieri, 1989; Locht et al., 1989, 1990). R9 is the characterizing arginine residue in R-S-E ARTs, creating electrostatic interactions with the diphosphate backbone of NAD+, and mutating it abolishes the ART activity (Brown et al., 1991; Burnette et al., 1988). Homologous arginine residue in LT and CT is R7. In addition, W26 deletion or substitutions by site-directed mutagenesis have showed a dramatic decrease in the enzyme activity, indicating a role in catalysis or NAD+ binding. Neither CT or LT contain aromatic amino acid in the equivalent position, but an analogous tryptophan is present in similar position in the NAD+-binding site of DT and ETA (W50 and W466 respectively (Barbieri & Cortina, 1988; Lobban et al., 1991; Locht et al., 1989)(Allured et al., 1986; Beattie et al., 1996; Choe et al., 1992; Chung & Collier, 1977; Kandel et al., 1974; Sixma et al., 1991; Stein et al., 1994; Wilson & Collier, 1992). In DT, W50 is thought to play only an indirect role in NAD+ binding, possibly

functioning as an anchor stabilizing the loop (containing Y54 and Y65) that packs against the nicotinamide mononucleotide ribose moiety of NAD+ (Wilson et al., 1994). W26 might have a similar role in pertussis toxin.

In a docking model of the transition state complex of Pertussis toxin and NAD+, the nicotinamide ring makes contact with residues S52, T53, S54, Q127, E129, and Y130 (Scheuring et al., 1998). In the docked model, R9 and H35 are in contact with the pyrophosphate moiety of NAD+, while W26 makes contacts with the adenylyl ribose ring of NAD+. The fluorescence from W26 is quenched upon NAD+ binding, confirming the role in the NAD+ binding (Cortina & Barbieri, 1989).

In regards of the Gαi interaction with the active site, the shape of the active site and a docking model of the ternary pertussis toxin-NAD-Gαi transition-state complex performed with Gαi peptide, containing 10 C-terminal amino acids, suggest that Gαi binds roughly parallel to NAD+ (Scheuring et al., 1998). In that geometry the position of C351 of Gαi was seen in the correct position for nucleophilic attack, and the rest of the peptide was positioned to avoid steric clashes (Scheuring et al., 1998).

3 Aims

Whooping cough, caused by *Bordetella pertussis*, remains a global concern despite vaccination. It can be especially severe in infants and young children, with antibiotics often ineffective due to late diagnosis, and while they eliminate the bacteria, they cannot eradicate bacterial toxins already present within the tissues. Coupled with vaccination offering limited protection and not preventing further transmission, these facts highlight the need for alternative therapeutic options.

Pertussis toxin (PT), a key virulence factor in whooping cough, disrupts cellular functions via ADP-ribosylation of the Gαi protein inside the host cell, causing various pathological effects during the disease. Thus, targeting the ADP-ribosyltransferase (ART) activity of PT with small molecular weight compounds could alleviate the symptoms in whooping cough.

The overall aim of the study was to identify small molecular weight compounds that inhibit the ART activity of PT, and to obtain atomic resolution structural insights of the binding poses of the inhibitors as well as of the ART activity of PT.

The specific research objectives were:

1. To develop a high-throughput multiwell assay to screen small molecular weight compounds that inhibit the ART activity of PT.
2. To screen and validate small molecular weight inhibitors targeting the ART activity of PT *in vitro* and *in vivo.*
3. To structurally characterize the mechanisms of inhibition of the ART activity of PT by the identified small molecular weight compounds.
4. To structurally characterize the mechanism of the ART activity of PT.

4 Materials and Methods

4.1 Expression and purification of pertussis toxin S1 and Gαi proteins (I-III)

4.1.1 Expression plasmids (I-III)

In studies I and III, the plasmids used for recombinant pertussis toxin and Gαi proteins were generated using synthetic DNA fragments (Eurofins Genomics and GenScript, respectively). Vectors for pertussis toxin wildtype (wt) and C41S, C41G mutants were cloned with NdeI and BamHI into pET15b (Novagen) allowing expression of an N-terminally HIS-tagged pertussis toxin S1 subunit (denoted as PtxS1 from here onwards). Expression vector for pertussis toxin Q127D/E129D mutant was generated by linearizing the pET15b-PtxS1 wildtype plasmid with polymerase chain reaction (PCR) using oligonucleotide primers containing mutagenic nucleotides (Eurofins genomics). The PCR product was gel-isolated, religated, and transformed to acquire the mutant plasmid. Synthetic fragment for recombinant Gαi proteins was cloned into pNIC-Bsa4 (Structural Genomics Consortium) using the ligation independent cloning (LIC) method allowing expression of an N-terminally poly-histidine (HIS)-tagged Gαi. Expression vector for Cys351Ala Gαi was generated by using the Gαi-encoding plasmid as a template in PCR using oligonucleotide primers containing mutagenic nucleotides and LIC-cloning overhangs (Eurofins genomics). The PCR product was cloned into pNIC-Bsa4 using the LIC method allowing expression of an N-terminally HIS-tagged Gαi-Cys351Ala mutant similar to Gαi-wt. All expression plasmids were verified by sequencing.

In study II, the PtxS1 construct consisting of residues D35-R256, and the human GNAI3 construct, consisting of residues V34-Y354, were both synthesized and cloned into a pET28-derived vector, yielding proteins fused to a HIS-tag through a human rhinovirus 3C (HRV 3C) cleavage site. Single-site mutants were generated by using high-fidelity PCR reaction combined with subsequent DpnI digestion of the parental vector. All constructs were confirmed by sequencing.

Available commercial kits were used for plasmid extraction and purification (NucleoSpin Gel and PCR Clean-up, NucleoSpin Plasmid, Duren, Germany). Other

enzymes and reagents were purchased from New England Biolabs (Ipswitch, MA, USA) and Thermo Fisher Scientific (Vilnius, Lithuania).

4.1.2 Protein expression and purification (I-III)

Detailed information of all protein expressions and purifications are in the original publications (I, II and III). Briefly, the proteins were expressed in *E. coli* BL21-(DE3) (Novagen) using either Terrific Broth autoinduction medium (Formedium, AIMTB0205) supplemented with 0.8 % (w/v) glycerol or Luria Bertani (LB) media and appropriate antibiotics. Bacteria were grown at 37°C until the cell density reached the target level (OD_{600}=1 for autoinduction and 0.6-0.8 for LB media), after which the temperature was decreased to 18 °C, and for LB media cultures the cells were induced with 0.2 mM of isopropyl β-D-1-thiogalactopyranoside. After 18-24 hours the cells were harvested by centrifugation. Cells were resuspended in lysis buffer, lysed by adding 1 mg/ml lysozyme and sonication. Lysates were clarified by centrifugation, after which the proteins were separated from the lysate by immobilized metal ion affinity chromatography for histidine-tagged proteins (HisTrap and nickel-nitrilotriacetic acid columns) and eluted with 400-500 mM imidazole. In study II, if necessary, the HIS-tag was cut with glutathione S-transferase-fused HRV 3C protease, which was followed by removal of the protease by passing over agarose resin with a flow, followed by subsequent gel filtration. Proteins were further purified with size exclusion chromatography (SEC) with Superdex S75 16/60 (GE Healthcare Life Sciences). Protein purity was checked with sodium dodecyl sulfate polyacrylamide gel electrophoresis (SDS-PAGE), SEC fractions were pooled, and the concentration was determined with the Bradford method (Bradford, 1976). Proteins were stored at -80°C.

4.2 Multiangle light scattering (I)

Size-exclusion chromatography coupled to multi-angle light scattering (SEC-MALS) was used to determine the oligomerization state of PtxS1 and the complex formation of PtxS1 and Gαi. SEC-MALS buffer [100 mM 4-(2-hydroxyethyl)-1-piperazineethanesulfonic acid (HEPES) (pH 7.5), 500 mM NaCl, 10% (w/v) glycerol, and 0.5 mM tris(2-carboxyethyl)phosphine (TCEP)] was used for all experiments. The buffer was passed through a 0.1 μm filter to remove small particles and had a flow rate of 0.150 ml per minute. A Shimadzu autosampler coupled high performance liquid chromatography (HPLC) machine was used to inject 100 μg of protein samples into a Superdex 200 10/300 increase column (GE Healthcare). MALS data were collected with a miniDAWN TREOS detector from Wyatt technology and analyzed with Astra software. To investigate complex formation, 100 μg of PtxS1 and 100 μg of Gαi were incubated on ice for 2 hours before being injected into the column.

4.3 Differential scanning fluorimetry (DSF) (I, III)

Differential scanning fluorimetry (DSF), also known as thermal shift assay, was used to study the thermal stability (folding) of proteins, protein-inhibitor interactions, and protein-protein interactions. To study the thermal stability of recombinant Gαi, Gαi mutant, PtxS1 and PtxS1 mutants alone or in the presence of inhibitors NSC228155 or NSC29193, DSF was performed using a CFX96 Real-Time PCR detection system (Bio-Rad). The proteins were at a concentration of 0.2-0.25 mg/ml in 20 mM HEPES (pH 7.5), 500 mM NaCl, 10% (w/v) glycerol, and 0.5 mM TCEP or in phosphate buffered saline (PBS; 2 mM NaH_2PO_4, 8 mM Na_2HPO_4, 137 mM NaCl, pH 7.2). Inhibitor concentrations ranging from 50 µM to 1 mM were used in the assay. The samples were incubated with 5 × SYPRO Orange (Thermo Scientific) for 5-10 minutes and then heated from 20 to 90 °C with 0.5 °C or 1 °C increments (1 min/1 °C) and analyzed on a the CFX96 RealTime PCR detection system (Bio-Rad) or 2500 Real-Time PCR system (Applied Biosystems). Data was analyzed with the Boltzmann sigmoidal equation using GraphPad (GraphPad software, Inc.).

4.4 *In vitro* NAD+ consumption assay (I, III)

4.4.1 Basic reaction setup and validation (I, III)

The NAD+ consumption assay was performed in triplicates, using an F-bottom 96-well black plate (Greiner BioOne, 655209). In study I, the optimized reaction conditions (60% NAD+ consumption) consisted of 125 nM PtxS1 and 500 nM NAD+ with or without 1 µM Gαi in 50 mM sodium phosphate (pH 7.0). 0.1% dimethyl sulfoxide (DMSO) was used in the reactions. DMSO tolerance was assessed with an additional test using the optimized conditions and varying the concentrations of DMSO from 0.1% to 5%. In study III, modified conditions of 1, 5, or 10 µM of wt or mutant PtxS1 with or without 10 µM NAD+ (Sigma-Aldrich, N3014) in a reaction buffer [100 mM HEPES (pH 7.5), 500 mM NaCl, 10% (w/v) glycerol, 2 mM DTT] were used. The reactions were carried out at room temperature (RT, 22 °C) with shaking at 300 rpm for 60 minutes, in a total reaction volume of 50 µl. The reactions were stopped by adding 20 µl of 20% acetophenone (diluted in ethanol) and 20 µl of 2 M KOH and incubated at RT for 10 min. 90 µl of formic acid was added and further incubated for 20 min. In study I, the plates were read using Tecan infinity M1000 pro, with excitation and emission wavelengths set at 372 nm and 444 nm, respectively. The maximum signal was defined as the NAD+ buffer control, and the minimum signal was obtained from the recombinant PtxS1 catalyzed reaction in the presence of recombinant Gαi. The raw fluorescence values were corrected by subtracting the blank containing buffer. Statistical analyses were performed using a two-tailed Student's t-

test with two sample equal variance on typically 8 parallel values. In study III, the plates were read using VICTOR Nivo Multimode Plate Reader (PerkinElmer, Waltham, MA, USA), with excitation and emission wavelengths set at 355 and 450 nm, respectively. Maximum signal was defined as the NAD+ buffer control, and the minimum signal was the wt recombinant PtxS1-catalyzed reaction. Data are displayed as means and the standard error of the mean.

To validate the repeatability of the NAD+ consumption assay, five control plates were tested, with the same experimental conditions and protein batches. Three plates were prepared on the first day, while the second and third days had one plate each. Each plate included 40 wells for maximum and minimum signals individually, along with buffer blanks. The coefficient of variation (CV%) was calculated separately for the minimum and maximum signals using the formula (Standard deviation/average) × 100. Assay parameters such as signal-to-noise (S/N), signal-to-background (S/B), and screening window coefficient (Z') were calculated as previously described (Putt & Hergenrother, 2004; Venkannagari et al., 2013).

4.4.2 Small molecule library screening (I)

In the small molecule library screening, each plate consisted of a buffer blank, a control reaction (minimum signal with recombinant PtxS1-wt), and a maximum signal (NAD+ and recombinant Gαi). Both the maximum and minimum signals contained 0.1% DMSO. To account for the inherent fluorescence of compounds, separate controls with NAD+, Gαi, and compounds were prepared. Compounds were tested at a concentration of 10 μM, and compounds displaying more than 50% inhibition were considered as hits. The high scaffold diversity compound library for screening was obtained from the National Cancer Institute (NCI) Developmental Therapeutics program repository (NCI diversity set III).

4.4.3 Small molecule IC_{50} measurements (I)

For IC_{50} measurements, the NAD+ consumption assay incubation time was adjusted to ensure that the substrate conversion did not exceed 30% to minimize the effect of reduction in substrate concentration while maintaining a robust signal. Compounds were tested over a concentration range of 100-0.01 μM in a half-log dilution series. Each plate included a buffer blank, a positive control with PtxS1-wt added, representing 100% consumption activity, and a negative control without enzyme, representing 0% consumption activity. Control values were included two half-log units below and above the inhibitor concentration series for reactions with 0% and 100% activity, respectively. The IC_{50} values were determined by fitting the data to a log (inhibitor) versus response-variable slope using GraphPad (GraphPad Software,

Inc). Chemical structures were drawn using either MarvinSketch 5.11.3 (chemAxon) or ChemDraw 18.0 (PerkinElmer).

4.5 *In vitro* ADP-ribosylation assays (I-III)

4.5.1 *In vitro* ADP-ribosylation assay with western blot read-out (I, II, III)

The ADP-ribosyltransferase activity of recombinant PtxS1 wt and mutant toxins against the target protein Gαi was studied using *in vitro* ADP-ribosylation assays with western blot readouts. Several reaction setups were employed in studies I-III.

The enzyme excess reactions generally contained 10 μM recombinant PtxS1 proteins, 10 μM biotinylated NAD+ (Trevigen, 4670-500-01), or 10 μM NAD+ (Sigma, N3014) and either 4 μM recombinant Gαi proteins or membrane fraction of HEK293T cells (30 μg of total protein) as the substrate in 100 mM HEPES (pH 7.5), 500 mM NaCl, and 10% (w/v) glycerol. The membrane fraction preparation is described elsewhere (Pulliainen et al., 2012). The ADP-ribosylation reactions were carried out at RT for 3 h with shaking at 300 rpm.

Substrate excess conditions generally included 20-100 nM recombinant PtxS1 proteins and 500-1000 nM recombinant Gαi in 50 mM sodium phosphate (pH 7.0) or in various HEPES-based buffers [50-100 mM HEPES (pH 7.0-7.5), 140-500 mM NaCl, 0-20 mM DTT] with 1-2 μM biotinylated NAD+ (Trevigen, 4670-500-01). The ADP-ribosylation reactions were carried out at RT for 3 h with shaking at 300 rpm. These conditions were also utilized for validating hits from chemical library screening and assessing the inhibitory effect of specific compounds.

For validating hits from chemical library screening, the substrate-excess condition was used with 10 μM of the indicated compound (and 0.1% DMSO in control reaction). For validating the inhibitory effect of PJ34 and 3-aminobenzamie (3-AB), a range of concentrations (200, 1000, 2500, 5000, and 7500 μM) of the indicated compound (and H_2O in control reaction) was used. Inhibitory compounds were incubated for 5 min with S1 prior to adding the rest of the reaction components. Additionally, study II had conditions where 1 μM of recombinant Gαi substrate was incubated with 20 nM recombinant PtxS1 and 50 μM Biotin-NAD6-Biotin-17-NAD+ (BPS Biosciences #80610) and a short incubation of 5 min at 37 °C.

A titration series was used in study III to study the auto-ADP-ribosylation activity of PtxS1 wt and mutants as well as their ART activity against Gαi. 0.3, 1, and 10 μM PtxS1 were co-incubated with 10 μM biotinylated NAD+ (Trevigen, 4670-500-01) with or without 1 μM recombinant Gαi substrate in 100 mM HEPES (pH 7.5), 500 mM NaCl, and 10% glycerol. Reactions were carried out at RT for 40 minutes or 24 hours for long reactions. In addition, reactions with pertussis holotoxin (BIOTREND, LL-

179A) instead of recombinant PtxS1 were used, where 0.2 or 1 µg of the holotoxin was first co-incubated with 20 mM DTT for 30 min at RT, followed by biotinylated NAD+ (Trevigen, 4670-500-01) and recombinant Gαi substrate for 40 min, RT, 300 rpm.

In all the cases, reactions were stopped by adding Laemmli loading dye and heating to 90-100 °C for 3-10 minutes. Sample proteins were separated by SDS-PAGE and transferred to nitrocellulose membranes. Subsequently, specific antibodies were used to detect the modified proteins.

4.5.2 *In vitro* ADP-ribosylation assay with nickel-plate readout (I)

Alternative *in vitro* ADP-ribosylation assay with nickel-plate readout was also used to analyze the enzymatic activity of recombinant PtxS1 with recombinant Gαi and inhibitors NSC288155 and NSC29193. 500 nM PtxS1, 2 µM Gαi, and 200 µM inhibitors in 50 mM HEPES (pH 7.5), 100 mM NaCl, 4 mM $MgCl_2$, and 0.2 mM TCEP were used. Triplicate reactions were started by adding an NAD+-mixture with final concentrations of 24.5 µM NAD+ and 0.5 µM biotinylated NAD+ (Sigma, N3014 and Trevigen, 4670-500-01, respectively). Reactions were incubated for 30 min at RT in constant shaking and transferred to white nickel-coated 96-well plates (Pierce, 15242), incubated for 60 min at RT, stopped with 7 M guanidine hydrochloride, washed thrice with Tris-buffered saline [10 mM Tris-HCl (pH 7.5), 150 mM NaCl] containing 0.05% Tween 20 (TBST), and blocked with 1% (w/v) bovine serum albumin (BSA) in TBST for 40 min at RT. Streptavidin-conjugated horseradish peroxidase (GE Healthcare, RPN1231VS) in TBST-BSA was added (1:5000) for 60 min and after four TBST washes the chemiluminescence was detected by using chemiluminescent substrate (Advansta, WesternBright Quantum) and subsequent detection of chemiluminescence with Hidex Sense microplate reader (Hidex).

4.6 Cell-based assays (I)

4.6.1 Cell lines and cell cultures (I)

Human embryonic kidney 293 cells containing the SV40 T-antigen (HEK293T) were recovered from the local cell line repository of the Institute of Biomedicine, University of Turku, Finland (liquid N2 storage - a cryovial of the stock culture). Propagation of HEK293T cells was done with Dulbecco´s modified Eagle´s media (DMEM) supplemented with 10 % heat-inactivated fetal bovine serum (FBS) and penicillin-streptomycin. Cells were cultured under the incubator conditions (+37 °C in humidified atmosphere with 5% CO2). Only verified mycoplasma-negative cells were used for the experiments.

4.6.2 *In vivo* ADP-ribosylation assay (I)

HEK293T cells were cultured in DMEM supplemented with 10% heat inactivated FBS and were seeded at a density of 500,000 cells per well in 6-well plates with 3 ml of media per well in the late afternoon. The next morning, compounds NSC228155 and NSC29193 at concentrations of 0.1, 1, and 5 μM in a fresh medium was added to the cells. All reactions, including controls without the inhibitors, contained 0.05% DMSO. After 30 minutes of incubation at 37°C under normal cell culturing conditions, pertussis holotoxin (List Biological Laboratories Inc., 179A) was added to the cells at concentrations of 10 or 100 ng/ml. Cells were then incubated for an additional 2 hours, placed on ice, washed twice with PBS, and collected into lysis buffer (70 ul) [50 mM Tris-HCl (pH 7.5), 400 mM NaCl, 0.1% sodium deoxycholate, 1% NP-40, 75 μM tannic acid (poly-ADP-ribose glycohydrolase inhibitor), 40 μM PJ34 (PARP inhibitor) supplemented with Pierce Protease and Phosphatase Inhibitor Mini Tablets (40 μl/ml of 5x stock solution - one tablet/2 ml]. The lysate was kept on ice for 30 min, then centrifuged for 15 min, 4 °C, 16,100g. The protein concentration was measured from the supernatants with Bradford protein assay, and the samples were scaled for protein content. Laemmli loading dye was added to 1× and the samples were heated for 10 min at 95 °C. 30 μg of total protein per lane was separated with SDS-PAGE and transferred to nitrocellulose membranes. Subsequently, specific antibodies were used to detect the modified proteins. For the compound NSC29193 concentrations up to 50 μM with varying lengths of pre-incubation prior to holotoxin addition and additional incubations after holotoxin addition were also tested with otherwise similar processing.

4.6.3 MTT cell viability assay (I)

HEK293T cells were seeded on 96-well plates at a density of 20,000 cells per well in 100 μL of DMEM with 10% FBS in the late afternoon. The following morning, inhibitor NSC228155 was added to the cells in triplicate at varying concentrations ranging from 0.1 μM to 60 μM, with the final concentration of DMSO being 0.6% in all of the wells. The cells were then incubated for 2.5 hours at 37°C under normal cell culturing conditions, after which the cell viability was investigated using the CellTiter 96 Non-Radioactive Cell Proliferation Assay (MTT) (Promega, G4002) according to the manufacturer's instructions. The MTT dye solution was incubated with cells for 1 h at 37 °C under normal cell culturing conditions. The IC_{50} value for NSC228155 cytotoxicity was calculated using GraphPad (GraphPad software, Inc.) with data displayed as means and the standard error of the mean. Data were normalized based on the negative control, *i.e.*, cells treated with 0.6% DMSO (100% viability) and positive control *i.e.*, cells killed with 200 μM H_2O_2 (0% viability) and expressed as percentage of these controls. Normalized response was compared to the

common logarithm of the concentration of the inhibitor (μM) and the IC_{50} calculated using a variable slope. Statistical analyses were conducted using two tailed Student's t-test (two sample equal variance).

4.6.4 Microscopy (I)

HEK293T cells were seeded onto glass coverslips coated with collagen at a concentration of 50 μg/ml (Gibco, A1048301) in 24-well plates in DMEM supplemented with 10% FBS, at a density of 100,000 cells per well in the late afternoon, and incubated overnight at 37°C. The next morning, the cells were treated with fresh media containing NSC228155 at a concentration of 5 μM (0.05% DMSO in all reactions, including control reactions). After 30 minutes of incubation under normal cell culture conditions, Alexa Fluor 594-conjugated Cholera Toxin Subunit B (Thermo Fisher Scientific, C34777) was added to the cells at a concentration of 1 μg/ml, and the incubation was continued for 2 hours. The cells were then fixed with 4% paraformaldehyde in PBS for 10 minutes at RT, washed three times with PBS, and permeabilized with 0.1% Triton X-100 in PBS for 5 minutes at RT, followed by a single wash with PBS. The DNA was stained with 4',6-diamidino-2-phenylindole (300 nM) (Santa Cruz Biotechnology, sc-3598) for 5 minutes at RT, after which the cells were washed three times with PBS, and mounted onto microscope slides with MOWIOL 4-88 (Sigma, 475904) containing 2.5% 1,4-diazobicyclo[2,2,2]-octane antifade (Sigma, 8.03456). The cells were imaged with a Zeiss AxioImager M1 microscope and a Zeiss AxioCam MRm monochrome camera using an EC Plan-Neofluar 40x/1.30 Oil M27 objective, driven by Zen 2 pro software.

4.7 SDS-PAGE and western blotting (I-III)

Western blotting was used to analyze the abundance of proteins as well as the ADP-ribosylation of recombinant proteins in the *in vitro* reaction samples and endogenous proteins in cell lysates. The proteins were denatured by heating samples to 90-100 °C for 3-10 minutes in Laemmli loading buffer. SDS-PAGE was used to separate the equally loaded protein samples. After SDS-PAGE, samples were transferred to nitrocellulose membranes with wet-transfer system (Bio-Rad), which was followed by blocking. Membranes were incubated in primary antibodies diluted in TBST containing 5% (w/v) non-fat milk or 2% (w/v) BSA. All primary antibody incubations were for 24–48 h at 4 °C in rotation, followed by washing thrice with TBST containing either 5% (w/v) non-fat milk or 2% (w/v) BSA for 10 min each time. Horseradish peroxidase (HRP)-conjugated anti-rabbit or anti-mouse IgG was used as a secondary antibody. All secondary incubations were done in the same buffer as the related primary antibody for 3 h at 4 °C in rotation. Alternatively, direct

HRP-conjugated antibodies were used, with 1% (w/v) casein blocking buffer and incubation for 2-3 h at 4 °C in rotation. HRP-conjugated antibody incubations were followed by three 10 min washes with TBST. All membranes were subsequently developed with WesternBrightECL (Advansta) and imaged on ImageQuant LAS 4000 (GE Healthcare) or ChemiDocXRS+ (Bio-Rad) and saved as 16-bit TIFF files. The specific primary and direct conjugated antibodies used in studies I-III are listed in Table 3. Mouse IgG kappa binding protein conjugated to HRP (1:2500) (sc-516102, Santa Cruz Biotechnology) and goat anti-mouse IgG-HRP antibody (1:5000) (SouthernBiotech, 1010-05) were used to detect the mouse primary antibodies. Goat anti-rabbit IgG-HRP (1:2500) (sc-2004, Santa Cruz Biotechnology) or goat anti-rabbit IgG-HRP (1:5000) (SouthernBiotech, 4010-05) were used to detect the rabbit primary antibodies.

Table 3. Primary and direct conjugated antibodies used in western blotting.

PRIMARY ANTIBODIES					
Target	**Species, Type**	**Cat. No.**	**Company**	**Dilution**	**Study**
GAPDH	Mouse, monoclonal	ab9484	Abcam	1:1000	I
Gαi	Mouse, monoclonal	sc-136478	Santa Cruz Biotechnology	1:500	I
PTS1	Mouse, monoclonal	99/512	National Institute for Biological Standards and Controls	1:200	I, III
Poly-ADP-ribose	Rabbit, polyclonal	ALX-210-890A	Enzo Life Sciences	1:1000	I
PARP1	Mouse, monoclonal	sc-8007	Santa Cruz Biotechnology	1:300	I
Mono-ADP-ribose	Rabbit, polyclonal	N/A	Hottiger-laboratory	1:1000	I
HIS-tag (in recombinant PtxS1 and/or Gαi)	Mouse, monoclonal	MAB050	R&D Systems	1:1000	I, II, III
Poly/Mono-ADP Ribose	Rabbit, monoclonal	83732S	Cell Signaling technology	1:1000	III
DIRECT CONJUGATED ANTIBODIES					
Target	**Type**	**Cat. No.**	**Company**	**Dilution**	**Study**
Biotin	HRP-conjugated Strepatavidin	RPN1231VS	GE Healthcare	1:5000	I, II, III
Biotin	HRP-conjugated Strepatavidin	NEL750001EA	PerkinElmer	1:7000	I
Biotin	StrepTactin-HRP	161-0381	Bio-RAD		II
HIS-tag (in recombinant PtxS1 and/or Gαi)	HRP-conjugated anti-HIS antibody	34460	Qiagen	1:5000	I

4.8 Densitometry (I, II)

Pixel intensities of the selected western blot TIFF-files were quantified using ImageJ 1.44 (National Institutes of Health, USA) To quantify the effect of inhibitor NSC228155 on the pertussis holotoxin-catalyzed ADP-ribosylation of Gαi in living human cells, the pixel intensities of the anti-mono-ADP ribose signal were normalized based on the anti-GAPDH loading control. To quantify the inhibitory effect of PJ34 and 3-AB on recombinant S1-catalyzed ADP-ribosylation of recombinant Gαi, the pixel intensities of the streptavidin-HRP signal were normalized based on the control sample, *i.e.*, the sample without inhibitor added. Student's t test with two-sample equal variance was used to determine the p-values.

4.9 Mass spectrometry analysis of ADP-ribose conjugates (III)

4.9.1 Sample preparation

Wt recombinant PtxS1 (10 μM) was incubated alone or in combination with NAD+ (10 μM, Sigma, #N1511) or NAD+ (10 μM) and recombinant Gαi (10 μM) for 3 hours at RT, 300 rpm, in a reaction buffer containing 100 mM HEPES (pH 7.5), 500 mM NaCl, 10% glycerol, 2 mM DTT. Similar control reactions were also performed for 10 μM Gαi and 10 μM NAD+ alone. After the incubation, reactions were subjected to denaturation and cysteine reduction by incubating them in 3 M urea (Sigma, #U4884) and 0.01 M of DTT (Sigma, #43819) for 1 h at 25°C. Then, samples were alkylated with 0.05 M of iodocetamide (Sigma, #I6125) at RT for 1 h in the dark. A 10K Amicon® Ultra Centrifugal Filter (Merck, #UFC501008) was used to exchange the buffer to 25 mM ammonium bicarbonate (Sigma, #09830). Proteins were digested with addition of trypsin (1:30 (w:w) trypsin to protein, Promega #V5117) overnight at 37ºC. The 10K Amicon® Ultra Centrifugal Filter was used to remove undigested proteins. The eluted peptides were dried in a vacuum centrifuge system (Savant Speedvac Concentrator SVC-100) and resuspended in 20 μL of 0.1% formic acid (Merck, #5.43804.0250) in 3% acetonitrile (Merck, #1.00029.1000). Peptide samples were stored at -20 °C prior to mass spectrometry analysis.

4.9.2 HPLC-ESI-MS/MS

The liquid chromatography electrospray ionization tandem mass spectrometry (LC-ESI-MS/MS) was achieved by nanoflow Easy-nLC1200 high performance (HPLC) liquid chromatograph system (Thermo Fisher Scientific) coupled to an Orbitrap

Fusion™ Lumos™ Mass Spectrometer. Peptides (1 µl) were loaded on a C18 trapping column (100 µm ID x 2 cm) for sample pre-concentration and clean up and subsequently separated inline in a 15 cm C18 column. Both columns were in-house packed with ReproSil-Pur 3 µm 120 Å C18-AQ bulk media (Dr. Maisch HPLC GmbH, Ammerbuch-Entringen, Germany). The mobile phase consisted of water and 0.1% formic acid (solvent A) or 80 % acetonitrile (v/v) with 0.1% formic acid (solvent B). A stepped gradient was used to elute peptides: from 5% to 35% solvent B in 20 min, from 35% to 100% in 5 min and followed by a wash for 5 min at 100% solvent B. The flow rate was 300 nl/min.

In the mass spectrometer, a data-dependent acquisition mode was used with a cycle time set to 3 s. Briefly full-scan MS spectra were acquired from 350 to 2000 m/z at 120,000 resolution, with automatic gain control of 200,000 and maximum injection time of 50 ms. Precursors with 2+ and 6+ charge states and intensities >50,000 were selected for MS/MS. Precursor ions were first subjected to higher-energy collisional dissociation (HCD) fragmentation using the quadrupole mass filter with a 1.6 m/z isolation window, a normalized collision energy of 38%, an orbitrap resolution of 15000, and a maximum injection time of 22 ms. When at least three ADP-ribose fragment ions (m/z 136.06, m/z 250.09, m/z 348.07, or m/z 428.04) were detected, a second HCD fragmentation and electron-transfer/higher-energy collision dissociation (EThcD) fragmentation were triggered for ADP-ribosylated peptide candidates. The MS/MS spectra was acquired with automatic gain control values of 500,000, the maximum injection time of 54 ms and a dynamic exclusion time of 15 s. Normalized collision energy was 30% for the second HCD and a supplemental activation energy was 25 % for EThcD. The number of dependent scans was set to 10.

4.9.3 Mass spectrometry data analysis (I)

The raw MS/MS spectra were analyzed by Proteome Discoverer 2.5 (Thermo Fisher Scientific) connected to the Mascot search engine (Matrix Science, London, UK; version 2.8.2), using the SwissProt Pertussis toxin subunit 1 protein sequence (*Bordetella pertussis*, UniProt SwissProt accession P04977) and human database (UniProt release 2023_01). Mascot search engine was used for peptide identification, and a peptide tolerance of 10 ppm and MS/MS fragment mass tolerance of 0.02 Da were applied. The enzyme specificity was set to trypsin and a maximum of two missed cleavages were allowed. Carbamidomethylation of cysteine was specified as a fixed modification, while variable modifications included oxidation of methionine and ADP-ribosylation of arginine, asparagine, aspartic acid, cysteine, glutamic acid, glutamine, histidine, lysine, serine, threonine, and tyrosine residues. The neutral losses from the ADP-ribose modification equal to 249.09 Da, 347.06 Da and 583.08

Da were used for scoring in HCD fragment ion spectra. ADP-ribose fragment marker ions at m/z 136.0623, 250.0940, 348.0709, and 428.0372 were excluded for scoring in HCD and in EThcD spectra (Gehrig et al., 2021). ADP-ribosylation site localization probabilities were calculated by the Mascot search engine. Peptide spectrum matches featuring site localization probability above 75% and Mascot expectation value below 0.05 were included in the final results. In-house written R scripts were used to extract data from Mascot reports.

4.10 BaAD production reactions

25-400 µM recombinant PtxS1 wt and mutants C41S, C41G and Q127D/E129D were combined with 2-50 mM 3-AB (Princeton Bio, PBMR044728 or Selleckhem, 51132, both dissolved in H_2O) and 2-20 mM NAD+ (Sigma, N3014, dissolved in H_2O) in 100 mM HEPES (pH 7,5), 500 mM NaCl, 10 % glycerol, 2 mM DTT in 10 µl reaction volume. First, PtxS1 and 3-AB were combined and incubated for 30 min at RT. This was followed by the addition of NAD+ and subsequent incubation of 3 h at RT, after which the reactions were stored frozen at -80 °C until further processing for HPLC and HPLC-MS analysis.

Samples were prepared for HPLC by diluting them 4-10-fold with H_2O and incubating them for 15 min at RT, followed by centrifugation (9270 x g, 10 min, RT) with a 10K centrifugal filter (Pall Nanosep® 10K Omega Centrifugal Devices OD010C34) to remove the enzyme. The collected filtrate (10-50 µl) was injected into HPLC using reverse-phase HPLC with two different methods. Method A was done using a C18 column (150 mm × 4.6 mm × 5 µm, Supelco™Analytical) with a flow rate of 1 ml/min and a gradient elution with three solvents: solvent A (0.2 M triethylammonium acetate in H_2O), solvent B (H_2O), and solvent C (acetonitrile). Solvent C was gradually increased from 0 to 30 % over duration of 15 minutes, while solvent A percentage was kept constant at 20%. Method B was done using Agilent 1200 series reverse-phase HPLC using a C18 column (Waters SunFire C18, 150 mm x 2.1 mm x 3.5 µm column, #186002535) with a flowrate of 0.5 mL/min and isocratic elution with a mobile phase of 10 mM $(NH_4)H_2PO_4$ (pH 5.5) and acetonitrile (97.5:2.5). Detection was done at 260 nm using a photo diode array detector. All the individual reaction components (NAD+, Sigma, N3014; 3-AB, Selleckchem, S1132; nicotinamide, Sigma, N0636; ADP-ribose, Sigma, A0752) and the reaction filtrates were analysed with HPLC, and the purity of the resulting peaks were determined by spectral scan analysis.

The peaks with a retention time of approximately 7.25 minutes were collected from HPLC injections with method A and the peaks with ca. 8 min retention time were collected from HPLC injections with method B, dried, and subsequently dissolved in H_2O for HPLC/MS analysis, which was performed using the Waters

Acquity RDa system with a C18 column (30 mm × 4.6 mm × 3.5 µm, 130Å, XBridge BEH) at a flow rate of 0.8 ml/min and a gradient elution with two solvents: solvent A (H_2O + 0.1% formic acid) and solvent B (MeOH + 0.1% formic acid). For method B samples, the elution was started with 95% A and 5% B, shifted to 100% B at 2.2 minutes and kept constant until 4.6 minutes, then returned to the initial ratio by 4.8 minutes and kept constant until 5.0 minutes. Detection was carried out by using ACQUITY RDa Detector in small molecule positive ion mode with full scan and fragmentation.

Similarly, the BaAD content in the centricon-trapped enzymes was analyzed. The proteins were recovered from the centricon filters by adding 100 µL of H_2O. The solutions were heated for 5 min at 75 °C and centrifuged through a 10K centrifugal filter to remove the denatured enzyme, as described above. Filtrate was collected and injected into HPLC (20-100 µl).

4.11 Structure and binding simulations (I-III)

4.11.1 Structure preparation and molecular docking (I, III)

The Schrödinger drug discovery suite (Release 2019-1: Maestro, Schrödinger, LLC, New York, NY, 2019 (Study I); Release 2023-1: Maestro, Schrödinger, LLC, New York, NY, 2023 (Study III)) was utilized for computational modelling, including structure preparation, ligand docking, binding free energy predictions, molecular docking (MD) simulations, and visualizations.

In study I, the crystal structure of pertussis toxin was obtained from the PDB at a resolution of 2.7 Å (PDB_1BCP) (Hazes et al., 1996) and only the catalytic subunit was considered by truncating the protein by removing the residues 222-260 from the coordinate file. The truncated structure was prepared for docking using the protein preparation wizard in Maestro. The protein structure was refined by adding hydrogen atoms, determining protonation states of ionizable groups, and performing energy minimization. A grid was specified for the binding pocket based on the superimposition of the PtxS1 structure with the S1 subunit of the pertussis-like toxin structure from *E. coli* with bound NAD+ [PDB_4Z9D, (Littler et al., 2017)], and the ligands NSC228155 and NSC29193 were prepared for docking using the LigPrep program in Maestro. including possible ionization states at pH 7.0 ± 2.0 and generating four tautomeric states for NSC29193. The ligands were docked to the pertussis S1 structure using extra-precision and standard-precision methods of the Glide-software (Friesner et al., 2004), keeping the protein structure rigid but allowing ligand flexibility. The docking poses were ranked based on the Glide docking score and the free energy of binding calculations was performed using the Maestro Prime/MM-GBSA tool.

In study III, the docking was carried out at the β-NAD+ binding sites, defined by the crystal structures of PtxS1 co-crystallized with β-NAD+ and α-BaAD (obtained in study II). The binding pocket for the APO structure of PtxS1 was defined by truncating the inhibitory C-terminal region occupying the NAD+ binding pocket (Cys41-Cys202 linkage removal). During docking, the protein structure was aligned with the co-crystallized β-NAD+ structure, and a grid box was generated around the β-NAD+ binding site. The ligands were docked to the pertussis S1 structure using the Glide extra-precision mode, employing flexible ligand sampling and the docking poses were ranked based on the Glide docking score, which included Epik state penalties. To calculate the binding free energies for the docked poses of the ligands, the Prime/MM-GBSA tool of Maestro software was used.

4.11.2 Molecular Dynamics Simulation (I, III)

The dynamics of the protein-ligand complexes were studied by performing molecular dynamics simulations (MDS) on the selected binding poses of ligands bound to the S1 structure using the Desmond program in Maestro (Schrödinger Release 2019-1 and 2023-1: Maestro, Schrödinger, LLC, New York, NY, 2019/2023) (Bowers et al., 2006). A simulation system set up was defined with a TIP3P water model in an octahedral box for study I, and single point charge water molecules in an orthorhombic simulation box with periodic boundary conditions for study III, with a 10 Å distance between solute surface atoms and an edge of the box (Jorgensen et al. 1983) and system neutralization was done by adding Na+ ions, with additional Na+/Cl- ions added to reach a 150 mM and 15 mM salt concentrations for study I and III, respectively. Prior to the simulations the systems were relaxed. For study I the relaxation was achieved with the default equilibration protocol in Desmond, followed by a 100 ns production simulation, where the energies were saved every 1.2 ps, whereas coordinates were recorded every 100 ps. For study III, the relaxation was done in two steps: first step with restraints on the solute heavy atoms for 12 ps with Brownian Dynamics in the canonical ensemble (amount of substance, volume and temperature are conserved) at 10 Kelvin using a Berendsen thermostat (Berendsen et al., 1984) followed by 12 ps Langevin dynamics in the isothermal-isobaric ensemble at 300 Kelvin and 1 atm pressure using a Berendsen thermostat and barostat, and the second step for 2 ps without any restraints. After relaxation, the production simulations were carried out in the isothermal-isobaric ensemble for a duration of 500 ns, using a 2 fs time step. The simulations were carried out using the OPLS3e force field (Harder et al., 2016) in study I and OPLS4 force field (Lu et al., 2021) in study III at constant temperature (300 K) and constant pressure (1 atm) regulated by using the Nose-Hoover chain thermostat and Martyna-Tobias-Klein barostat, respectively (Martyna et al., 1992, 1994). Short-range and

long-range interactions were computed with a 9 Å distance cutoff. The resulting trajectories were analyzed in terms of ligand stability (as root mean squared deviation, RMSD) and lifetime of protein–ligand interactions using the Simulation Interactions Diagram application in Desmond.

4.11.3 Alphafold modelling (II)

Alphafold2 modeling (Jumper et al., 2021) was used to study the interaction of S1 and the C-terminal helix of Gαi protein by computationally folding the S1 sequence including C41S, S52E mutations with the C-terminus of different Gαi sequences. Short sequences of Gαi (Gmini) were used for modeling in order to reduce the computational loads. The obtained computational model was overlaid upon the crystallographically obtained nucleotide-bound forms of S1 to provide positioning of the NAD+ within the context of the substrate-docked toxin. The S1 S52E mutation was used to mimic NAD hydroxyls.

5 Results

5.1 Inhibition of pertussis toxin ADP-ribosyltransferase activity

5.1.1 Characterization of recombinant PtxS1 from *E. coli*

The mechanistic details of the ADP-ribosylation reaction catalyzed by PT were investigated by employing a recombinant protein construct of the N-terminally HIS-tagged Pertussis toxin S1 subunit (PtxS1) that was expressed in and purified from *E. coli*. This construct lacked the N-terminal secretion signal sequence and a part of the C-terminus, which typically obstructs the NAD+ binding site (I, Figure 1, and Figure 2A). Following purification via metal affinity and SEC, the protein was found to remain proteolytically stable, as it was observed to migrate in SDS-PAGE according to its theoretical size of 23.4 kDa (I, Figure 2B). Proper folding and monomeric state in solution were confirmed by DSF and SEC-MALS (I, Figure 2C-D), respectively. A similarly designed mutant protein with a double amino acid substitution (Q127D/E129D) was also generated.

The ADP-ribosyltransferase activity of recombinant PtxS1 toward Gαi was confirmed through two separate ADP-ribosylation assays. The potential impact of the C-terminal truncation of the PtxS1 construct on Gαi ADP-ribosylation was assessed, considering that residues 195-294 are necessary for optimal ADP-ribosylation of trimeric G proteins (Krueger & Barbieri, 1994). However, it was not expected to affect NAD+ glycohydrolase activity, based on previous research (Cortina et al., 1991; Locht et al., 1987). In the first assay, HEK293T cell membrane preparations with an endogenous level of Gαi were used in an NAD+-biotin western blot assay, where one major protein corresponding to the theoretical size of endogenous Gαi (40.4 kDa for isoform 1, UniProt_P63096) was witnessed being ADP-ribosylated (I, Figure 2E). In the second assay, a recombinant N-terminally HIS-tagged Gαi, purified from *E. coli*, was used in an NAD+ western blot assay, confirming that the recombinant construct retained its activity toward Gαi, as it was observed to be ADP-ribosylated (I, Figure 2F).

Additionally, the recombinant PtxS1 wt was found to auto-ADP-ribosylate itself (I, Figure 2E), and some degree of auto-modification occurred already during the

expression in *E. coli* (I, Figure 2F). This auto-ADP-ribosylation activity was significantly reduced in the Q127D/E129D mutant, as was the ADP-ribosyltransferase activity towards Gαi (I, Supplementary Figure S2), which was expected as residues Q127 and E129 of PtxS1 are also conserved in several other bacterial ART-toxins with a role of positioning NAD+ and facilitating the transfer of ADP-ribose to a substrate amino acid residue (Littler et al., 2017; Simon et al., 2014).

The specifics of the interaction between PtxS1 and Gαi were studied by employing both wild-type and mutant protein constructs of both proteins in the NAD+-biotin western blot assay. To determine the substrate amino acid specificity of the truncated PtxS1, its ability to modify the C351A mutant of recombinant Gαi was assessed. The results demonstrated that recombinant PtxS1 ADP-ribosylated recombinant Gαi-wt but was unable to ADP-ribosylate the recombinant Gαi mutant (I, Supplementary Figure S3). Importantly, the loss of ADP-ribosylation was not attributed to any changes in the folding of the C351A mutant, as confirmed by DSF analysis. Melting temperature (Tm) of the mutant was of 44.3 ± 0.2 °C, which was comparable to the Tm of Gαi-wt (43.8 ± 0.2 °C). Thus, the specificity of recombinant PtxS1 toward Gαi was consistent with that observed for the pertussis AB5 holotoxin. Additionally, the interaction between recombinant PtxS1 and Gαi proteins in solution was studied by SEC analysis, which showed the presence of only monomeric PtxS1 and Gαi proteins (I, Supplementary Figure S1), suggesting that complex formation during catalysis is likely weak, kiss-and-run type of interaction.

5.1.2 Multiwell-based screening and *in vitro* characterization of inhibitory compounds against PtxS1

In order to screen inhibitors against the enzymatic activity of PtxS1, a multiwell fluorimetric method, previously developed for measuring the activity of poly-ADP-ribose and mono-ADP-ribose synthesizing enzymes (Narwal et al., 2012; Putt & Hergenrother, 2004; Venkannagari et al., 2013) was optimized to PtxS1 and PtxS1-Gαi enzyme-substrate pair. In this endpoint assay, remaining NAD+ at the end of reaction time is converted into a stable fluorophore and the decrease in fluorescence relative to the non-enzyme control reflects the level of enzymatic NAD+ consumption. Co-incubation of recombinant PtxS1 and Gαi with NAD+ for 40 minutes resulted in a significant concentration and time-dependent decrease in fluorescence compared to the non-enzyme control (I, Figure 3A-B), while no decrease in fluoresce signal was witnessed for Q127D/E129D mutant under similar reaction conditions (I, Figure 3A).

As DMSO is a common solvent for small molecule libraries, its effect on the NAD+-consuming activity of recombinant PtxS1 was also assessed. DMSO

concentration up to 0.2% did not significantly impact the activity, but 1% DMSO already had a significant ($p = 10^{-4}$) reducing effect (I, Figure 3C). Thus, the compound screenings were performed in 0.1 % DMSO.

The assay repeatability (well-to-well, plate-to-plate and day-to-day variations) was tested by measuring five independent runs of minimal (NAD+ as incubated in PtxS1- and Gαi-containing buffer) and maximal (NAD+ as incubated in plain buffer) signals. Coefficients of variations (CVs) for these signals were calculated, and the average Z' value, a statistical data quality indicator for bioassays, was determined to be 0.68, indicating that the fluorometric assay is suitable for high-throughput screening. The statistical parameters for the NAD+ quantitation assay can be found in the supplement of the original publication (I, Supp. Table S1).

The screening was started by assessing a set of compounds, including FDA-approved anticancer drugs, known to inhibit the activity of human DT-like ARTs for their ability to inhibit the enzymatic activity of PT. However, none of the compounds were found to inhibit the NAD+-consumption activity of recombinant PtxS1 in the presence of recombinant Gαi (with an arbitrary inhibitory threshold of 50%) in the multiwell fluorimetric assay.

Subsequently, a selected compound library representing high scaffold diversity from the NCI Diversity Set III was screened, resulting in nine compounds that exhibited more than 50% inhibition of the NAD+-consumption activity of PtxS1 in the presence of Gαi (data not shown). In a separate NAD+-biotin western blot assay, strong inhibition of PtxS1-catalyzed Gαi ADP-ribosylation was observed with five out of these nine primary compound hits (Figure 4A-B). As two of these compounds, NSC119875 and NSC44750, were seen to influence the integrity of Gαi and/or PtxS1 proteins (I, Figure 4A), they were excluded from further studies. Dose–response assessment of the three remaining compounds (NSC228155, NSC29193 and NSC149286) was conducted by utilizing the fluorometric NAD+-consumption assay in the presence of recombinant Gαi. NSC228155 and NSC29193 had low micromolar IC_{50}-values of 3.0 and 6.8 μM, respectively, based on the NAD+ consumption assay, while NSC149286 was less potent with an IC_{50}-value of 20 μM and was excluded from further analyses (I, Figure 4C).

An alternative NAD+-biotin assay, utilizing HIS-tagged proteins captured in a 96-well nickel-coated plate, revealed that in addition to inhibiting the PtxS1-catalyzed conjugation of ADP-ribose-biotin onto Gαi, compounds NSC228155 and NSC29193 also inhibited the auto-ADP-ribosylation activity of PtxS1 (I, Figure 4F), indicating that these two compounds interact directly with the recombinant PtxS1.

5.1.3 *In silico* characterization of inhibitory compounds against PtxS1

To further study the potential mechanism of inhibition for NSC29193 and NSC228155, the interaction and binding of the inhibitors to PtxS1 was studied. As efforts to crystallize the PtxS1 subunits in complex with NSC228155 or NSC29193 were not successful, the putative binding modes of the compounds to PtxS1 were studied with docking and MDS methods, (I, Figure 5, Supp. Figure S4-S5) using a model structure of PtxS1 generated with homology modelling of the S1-like protein from *E. coli* bound with NAD+ (Littler et al., 2017).

The top ranked positions of NSC228155, pose 1 (I, Figure 5A) for the lowest free energy of binding and pose 2 (I, Supp. Figure S5A) having the best docking score, featured the aromatic pyridine ring of NSC228155 positioned in a confined region analogous to where the nicotinamide ring of NAD+ would bind to PtxS1, with the double benzoxadiazole ring located near the center of the NAD+-binding pocket. In pose 1, the pyridine ring of the inhibitor was observed to form hydrogen bonds with Y10 via its oxygen, and π–π stacking interactions were seen between the pyridine ring and the nearby Y59, as well as between the benzoxadiazole ring and Y63 (I, Figure 5A). In pose 2 the pyridine backbone hydrogen bond with Y10 was lost, but the pyridine ring made π–π interactions with both Y63 and Y10 and ionic interactions with R9 and R67 (I, Supp. Figure S5A). During the MDS, pose 1 remained stable and retained its position with a RMSD of 0.9 Å, whereas pose 2 displayed instability and occupied different locations within the binding pocket, with an average RMSD of 22 Å for the ligand coordinates based on superimposition with PtxS1 (I, Supp. Figure S4B).

In pose 1 of NSC29193 (I, Figure 5B), it was positioned near to the binding site of nicotinamide ring of NAD+ within PtxS1, forming hydrogen bonds with Y10 and S52, π–cation interactions with R9, π–π stacking with Y63. In pose 2, NSC29193 was positioned near where the adenine ring of NAD+ would bind in S1, stacking against the aromatic ring of W26, hydrogen bonding with T24 and forming ionic interactions with R9 and R13 via electrons of the nitrogen atom on the five-member ring. (I, Supp. Figure S5B). Pose 1 of NSC29193 remained stable throughout the MDS, with an average RMSD of 0.1 and 1.0 Å with respect to the ligand and receptor backbone atoms, maintaining hydrogen bonds and interactions with key residues (I, Supp. Figure S4C). However, pose 2 of NSC29193 experienced disruption at around 20 ns due to the reorientation of W26, a key interaction partner, resulting in the ligand binding to different areas of the binding pocket, with the average 12 Å RMSD of the ligand with respect to the superposed coordinates of the toxin (I, Supp. Figure S4D). Overall, the docking and molecular dynamic simulation analysis provided insight into the plausible binding poses of NSC228155 and NSC29193 within the NAD+-binding pocket of PtxS1.

5.1.4 Inhibitory compounds of pertussis toxin in living human cells

A cell-based assay utilizing pertussis holotoxin and a western blot read-out was optimized to study the inhibitor effectivity in living cells. The optimal dosage of the holotoxin was determined via titration and the resulting ADP-ribosylation of endogenous Gαi using an antibody recognizing mono-ADP-ribose. A concentration dependent mono-ADP-ribosylation of a single protein matching size of endogenous Gαi (40.4 kDa) was detected (I, Figure 6A).

Next, HEK293T cells were preincubated for 30 minutes with either NSC228155 or NSC29193 before the addition of holotoxin and subsequent co-incubation. No inhibitory effect was observed with NSC29193 under multiple analyzed conditions. However, in the presence of NSC22815, a concentration dependent inhibition of the Gαi ADP-ribosylation by the holotoxin was detected (I, Figure 6B). 5 μM NSC228155 resulted in approximately 80% inhibition of ADP-ribosylation of Gαi. Based on densitometric analysis of the anti-mono-ADP-ribose signal, the IC_{50} for the inhibitory effect of NSC228155 was 2.35 μM (I, Figure 6C).

The maximum tolerated dose of the inhibitor NSC228155 in HEK293T cells was determined by titration. Even though partial cell detachment was observed at 50 μM of NSC228155 (data not shown), the 5 μM inhibitory concentration was not seen to cause any evident distress to the cells. No significant poly-ADP-ribosylation of PARP1, which is associated with DNA damage (Miettinen et al., 2019), nor proteolytic processing of PARP1 from its full-length form (approximately 120 kDa) into a shorter form (approximately 90 kDa), which is indicative of cell death (Chaitanya et al., 2010), was detected (I, Figure 6D). Furthermore, no cell death-associated nuclear fragmentation was observed in the cells (I, Supp. Fig. S7). MTT assay was used to determine the cell viability. 3.5-hour incubation with 20 μM or higher NSC228155 concentrations were seen to significantly affect the metabolic activity of HEK293T cells and the IC_{50} of NSC228155 cytotoxicity was determined to be 15.33 μM (I, Figure 6E).

Additionally, NSC228155 was not seen to impact the levels of cell-associated PtxS1 or the proteolytic processing of PtxS1 (I, Supp. Figure S6), suggested to happen in the early stages of pertussis toxin internalization (Finck-Barbançon & Barbieri, 1996). Neither did it alter the cellular localization of the retrograde trafficking marker Alexa594-conjugated cholera toxin B5-oligomer, including its accumulation near the nuclei where the ER is located (I, Supp. Figure S7). These findings indicate that the inhibitor does not interfere with endocytosis or endosomal trafficking.

5.2 Mechanistic and structural insights of pertussis toxin ADP-ribosyltransferase activity

5.2.1 Structural changes and requirements of S1 during binding and hydrolysis of NAD+ and the ADP-ribosylation reaction

By utilizing enzymatically impaired PtxS1 construct (E129D), as wild type S1 hydrolyses NAD+ even in the absence of Gαi protein substrate, a crystal structure of mutant PtxS1 in complex with NAD+ (named $S1_{E129D}$) was obtained. In the presence of 200 mM potassium iodide also the wt PtxS1 remained catalytically inactive and crystal structure of the S1 in an NAD+-bound state was also acquired for the wt protein (named $S1_{NAD}$) (II, Figure 1B-C). Crystal structure was also obtained for the PtxS1 C41S mutant, which has only minor activity, in complex with ADP-ribose and nicotinamide (named $S1_{ADPR/NA}$). The preliminary phases for these structures were obtained by using a previously solved S1 subunit of PT holotoxin [PDB: 1BCP, referred to as $S1_{APO}$, (Hazes et al., 1996)] as a molecular replacement model, followed by iterative processes of manual building and refinement to improve accuracy. The crystal structure data showed four molecules in the crystal unit cell, with the protein backbone being nearly identical in all four molecules, except for a small region spanning amino acids 112 to 129 (corresponding to helix h5 of the holotoxin) (I, Figure 1), where there are multiple alternate conformations and poor electron density maps for some protomers. This type of plastic region is thought to play a role in Gαi protein recognition in related toxins (Ménétrey et al., 2008). These structures obtained made it possible to compare the structural changes occurring during NAD+ binding and hydrolysis (II, Figure 2).

Comparison of the obtained crystal structures with the APO structure (Hazes et al., 1996) revealed that the S1 subunit is undergoing significant structural changes as it transitions from an inhibitory to an active state upon NAD+ binding (II, Figure 2). In the inhibitory state, the C-terminal residues fully occlude the NAD+ binding site, and the reduction of C41 and C201, and the adjacent loss of the C-terminal residues result in significant structural rearrangements that allow the walls of the NAD+-binding cleft to contract inwards, enabling helical rotation of h2 to establish contacts with the *N*-ribose and the nicotinamide part of NAD+. Additionally, the residues within the active-site loop ($_{41}$CQVGSS$_{46}$) undergo significant refolding, closing over the nucleotide-binding site in the $S1_{NAD}$ structure, forming the so-called nucleotide clamp.

The enzymatic core of the ART domain is comprised of approximately 150 amino acids and adopts a U-shaped structure, featuring a concave cleft that forms the NAD+-binding site (Littler et al. 2017), where NAD+ is sandwiched between the

residues of the two β-sheets that are on either side of this cleft. In S1, on one side is the β-sheet with strands s1, s3, s4, and s6 sandwiched between h3 and h1, and on the other side the β-sheet with s2, s5, and s7 β-sheet along with its h2, h4, and h5 helices (II, Figure 2B). With the dissociation of the C-terminal residues (h6), only minor changes occur in the ADP-interacting section of this cleft, while more pronounced changes take place at the nicotinamide end, allowing NAD+ to interact with the $_{52}$STS$_{54}$ motif and engage in a β-sheet-like interaction with Y10. The hydroxyl of Y63 forms hydrogen bonds with the *N*-phosphate of NAD+. The microenvironment around the catalytic E129 undergoes remodelling with the catalytic glutamate surrounded by hydrophobic residues, which matures the active site into a form more resembling that of other ART enzymes (Tsurumura et al., 2013).

The S1$_{ADPR/NA}$ structure (II, Figure 1C), providing insight into the post-NAD+ hydrolysis step, was obtained by incubating the C41S S1 mutant with NAD+ before crystallization and data collection. It revealed that, after cleavage of the glycosidic bond, the reaction products remained mainly in their original positions, with only small movement of h2 and minimal changes within the active site loop, except for the newly liberated *N*-ribose that rotated by approximately 130 degrees along the PN-O5 bond (II, Figure 3A-B), positioning ADP-ribose in a more extended conformation, a position that may allow the stabilization of an oxocarbenium intermediate via polar interactions and permits E129 to form direct hydrogen bond with the 3′-hydroxyl of the ribose, while the 2′-hydroxyl has a bridged water-mediated contact.

5.2.2 Important amino acids for pertussis toxin S1 activity and S1-Gαi interaction

To determine which amino acid residues within PTS1 are important for the catalytic activity, a set of mutants with single amino acid substitutions were generated, targeting residues in and around the active site of the S1 (II, Figure 3A-B). The activity of these PtxS1 mutants towards recombinant Gαi was analyzed using the NAD+-biotin western blot-assay. The results were consistent with earlier findings (Antoine et al., 1993; Barbieri et al., 1989; Brown et al., 1991; Burnette et al., 1988; Cieplak et al., 1990; S. A. Cockle, 1989; Locht et al., 1989, 1990; Pizza et al., 1988), with the E129D mutant being inactive while the C41S mutant has catalytic activity corresponding to that of the wt PtxS1 (II, Figure 3D). Given the role that conserved glutamine or glutamate residues (Q/E), such as Q127 in PT, often play in catalysis of ART enzymes (Domenighini & Rappuoli, 1996), the Q127D mutant was also tested for ADP-ribosylation activity. A reduction of approximately 50 % in Gαi modification was observed, suggesting that Q127 has a role, but not an essential one, in facilitating catalysis. When tyrosine residues Y59 and Y63, which are located near

the catalytic site, were substituted with alanine, a significant reduction in activity was also detected (II, Figure 3D).

Specifics of PtxS1 interaction with Gαi were studied with wt and mutant PtxS1 and Gαi proteins. Already previous findings showed that mutating cysteine 351 to alanine abolishes the activity (I, Supp. Figure S3). Obliteration of the modification was evidenced also by swapping the position of the wt Gαi C351 and G352, indicating that the position of the target amino acid four amino acids from the C-terminal end of Gαi is vital for the modification to happen. Elimination of the last C-terminal residue Y354 reduced activity ~5-fold based on pixel intensity analysis, but did not abolish it. However, eliminating the β-branched alanine residue in the Gαi mutant (L353A) had little effect on its suitability to function as a substrate (II, Figure 3D).

To determine which regions of S1 play a role in the interaction with Gαi protein substrate, bulky mutations V62Y and S54Q were inserted into PtxS1, which could potentially disrupt protein-protein interactions. However, the enzymatic activity was unaffected by both mutations (II, Figure 3D), suggesting that these amino acids are unlikely to be involved in the protein-protein interaction with Gαi. Alphafold2 modeling of the crystal structure $S1_{NAD}$ (II, Figure 1B) complexed with G protein substrate revealed several possible docking modes for the C-terminal helix of Gαi (II, Figure 3E and Supp. Figure S3A). One of the more plausible predictions showed S1 interacting with Gαi that is in a helical structure comparable to its GPCR-bound form (II, Supp. Figure S3). In this model, the conserved hydrophobic residues within the C-terminus of Gαi ($_{344}$IKNNLKECGLF$_{354}$) directly interacted with S1 residues Y59 and Y63, located near the NAD-binding site.

5.2.3 Structural flexibility of S1 subunit leads to induced fit-inhibitor interactions and in the formation of novel NAD+ analog

Two compounds, 3-Amino benzamide (3-AB) and N-(5,6-dihydro-6-oxo-2-phenanthridinyl)-2 (dimethylamino)acetamide (PJ34), which were already a part of the panel of selected compounds known to inhibit the ART activity PARPs/ARTDs in study I, were used to further study the interaction of broad-specificity mimetics of nicotinamide to S1. In the NAD+-biotin western blot-assay measuring the recombinant PtxS1-catalyzed conjugation of ADP-ribose-biotin onto recombinant Gαi, 3-AB and PJ34 were seen to inhibit the S1-catalyzed Gαi ADP-ribosylation activity at millimolar concentrations (II, Figure 4A and 5A). 3-AB is a near-minimal nicotinamide mimic (II, Figure 4C), while PJ34 belongs to a group of 6(5H)-Phenanthridinones that are tricyclic γ-Lactam compounds known to inhibit PARP enzymes (Banasik et al., 1992) and bacterial ARTs (Jørgensen, Purdy, et al., 2008;

Lyons et al., 2016; Yates et al., 2005). When bound within PARP-1, the benzamide backbone of such molecules acts as a competitive inhibitor occupying their nicotinamide sites.

The binding mode of both of these relatively high millimolar-range inhibitors was further studied by obtaining crystal structures of PtxS1 in complex with the compounds. PJ34 was co-complexed with the PtxS1 C41S mutant and the obtained structure ($S1_{PJ34}$) (II, Figure 5B) shows, that the planar tricyclic ring system of PJ34 is positioned in a way that the second aromatic ring base stacks against R9 of S1 in place of its interaction with the NAD+ phosphates. In contrast, the subsites for the adenine moiety of NAD+ and its two ribose sugars remain unoccupied. The dimethylamino acetamide group of PJ34 projects out of the standard NAD+-binding groove. PJ34 bound state resembles more the APO form of S1 than the more compact active NAD+-bound state.

The inherent flexibility of S1 (II, Supp. Figure S2B), which allows it to bind PARP inhibitors even when they incompletely fill the nucleotide-binding site (induced-fit inhibitor binding) and may result in constant assembly and disassembly of its nicotinamide-binding site, might explain why no crystals were obtained for the S1 in complex with 3-AB. However, a co-complex of PtxS1 together with 3-AB and NAD+ was obtained ($S1_{BaAD}$). In a high 1.0-Å resolution, this structure showed 3-AB occupying the nicotinamide-binding site in S1 (II, Figure 4B). Notably, a covalent bond was witnessed between the anomeric carbon of *N*-ribose and the aniline nitrogen of 3-AB, indicating that a novel NAD+ analog was formed at the catalytic center of S1. The analog was termed benzamide amino adenine dinucleotide (BaAD). The binding mode of BaAD appeared to share elements from both the pre- and post-NAD-hydrolysis states.

5.3 Novel nonhydrolyzable NAD+ analog biocatalysis by the ADP-ribosyltransferase activity of pertussis toxin

5.3.1 Formation mechanism and binding of the novel NAD+ analog BaAD in the catalytic site of S1

The crystal structure of BaAD/PtxS1, resolved at 1.0-Å resolution, revealed an α-configuration for the glycosidic bond between the anomeric 1'-carbon of ribose and the nitrogen of 3-AB (II, Figure 4B; III, Figure 7A-B), contrasting with natural substrate NAD+ as well as carba-NAD+ and BAD, non-hydrolyzable NAD+ analogues (Langelier et al., 2018; Szczepankiewicz et al., 2012), which all have the same β-configuration stereochemistry. Thus, it seems that the formation of α-BaAD by PtxS1 likely involves the canonical stereospecific ADP-ribosyltransferase-

catalyzed reaction scheme producing α-ADP-ribosyl linkages from β-NAD+ (III, Figure 7C) (Ferro & Oppenheimer, 1978; Moss et al., 1979; Oppenheimer, 1978), where the PtxS1/β-NAD+ complex undergoes activation of β-NAD+ to create a short-lived and reactive oxocarbenium ion. Subsequently, the nitrogen atom of the 3-AB amine group, rather than the oxygen atom of a water molecule or the cysteine sulfur atom of Gαi, initiates a nucleophilic attack on the electrophilic ribose 1'-carbon. This nucleophilic attack may occur either via 3-AB bound in the nicotinamide pocket (with 3-AB replacing nicotinamide after oxocarbenium cation formation) or through the free solution form of 3-AB, followed by the insertion of 3-AB remnants into the nicotinamide pocket.

The binding position of α-BaAD in PtxS1 closely resembles that of β-NAD+, especially at the adenine end, phosphate groups, and the nicotinamide end/3-AB remnant, as evidenced by the post β-NAD+ hydrolysis structure with bound α-ADP-ribose and nicotinamide (III, Figure 1A). However, a significant movement of the ribose group can be seen (III, Figure 1A), which results from the additional atom of the 3-AB remnant compared to NAD+, and the tight fit of the of the nicotinamide end/3-AB remnant in the catalytic pocket (III, Figure 1B), which locks the binding position of the nicotinamide end/3-AB remnant in place.

To gain a deeper understanding of the binding properties of α-BaAD, a modeling study was conducted. Docking and binding free energy analyses, using the co-crystallized poses of β-NAD+ and α-BaAD as references, were performed. Comparison with docking scores and binding free energy values obtained for the APO structure (PDB 1PRT, Stein et al., 1994) indicate that significant conformational changes are necessary to accommodate β-NAD+ and its analogs (III, Table 1). These changes can be observed in the structural comparison between PtxS1 pre- and post-NAD+ hydrolysis (II, Figures 1-2; III, Figure 3A). Binding free energy values from modelling and MD-simulations were also calculated for hypothetical β-BaAD configuration, and based on the values, the α-BaAD appears to exhibit better affinity for the NAD+ binding site. Interaction patterns of α-BaAD with PtxS1 are similar to those of β-NAD+ (III, Figure 2), while the interactions of hypothetical β-BaAD with PtxS1 are notably different and weaker. If β-BaAD is ever formed, it has relatively poor affinity to the NAD+ binding site. Experimental data only demonstrated α-BaAD binding to the active site. Additionally, docking, and binding free energies were analyzed for β-carba-NAD+ and β-BAD (III, Table 1). Both analogues showed comparable docking scores and binding free energies with β-NAD+.

5.3.2 Impact of mutations on the catalytic activity of PtxS1

α-BaAD binding was observed only in the active site of the C41S mutant of truncated PtxS1 upon crystallization with NAD+ and 3-AB, indicating that there might be potential differences in the biochemical properties of this mutant compared to the wt PtxS1. C41 is situated within a flexible loop known as the NAD+ loop and the active site loop, which undergoes a conformational change when transitioning from its resting state (APO conformation) to interact with NAD+ when it binds to the active site (III, Figure 3A).To investigate the potential effects of the C41 mutations, MD simulations on the structure of recombinant PtxS1 co-crystallized with β-NAD+ and two *in silico* mutant structures, C41S, and C41G were conducted. The RMSD values were compared over a 500 ns MD simulation and for wt and C41G mutant they were seen to converge early and remain stable throughout the simulation, whereas the C41S mutant exhibited higher RMSD values, indicating increased structural fluctuations (III, Figure 3B). Analysis of root mean square fluctuations (RMSF) to identify the specific amino acid residues responsible for these fluctuations showed higher fluctuations in the active site loop (amino acids 38-49), h3-helix (amino acids 56-80), the flexible loop region (amino acids 112-127), the loop between β8 and β9 (amino acids 150-155), in the C41S mutant compared to the wt and C41G mutant (III, Figure 3C).

The effect of different mutations to PtxS1 activity was also experimentally analyzed. The impact of the mutations on the NADase activity and to Gαi ADP-ribosylation was determined with the fluorometric NAD+-consumption assay and NAD+-biotin western blot-assay, respectively. The C41G mutant exhibited similar NADase and ADP-ribosyltransferase activities as the wt protein, while the C41S and Q127D/E129D mutants showed reduced NADase activity (III, Figure 3D-E), and Q127D/E129D also had a clearly compromised ADP-ribosyltransferase activity (III, Figure 4E). Based on the results, C41S mutation appeared to cause differential effect on PtxS1 activity depending on whether the Gαi substrate protein was present or not.

In addition to the ADP-ribosylation of the substrate protein Gαi, auto-ADP-ribosylation of PtxS1 was observed, being strongly diminished in the Q127D/E129D double mutant, but not significantly affected in the other forms of PtxS1 (III, Figure 3D, Figure 4A). Interestingly, the Q127D/E129D double mutation effect was lost after prolonged *in vitro* incubation, without Gαi (III, Figure 4A). A minimal level of auto-ADP-ribosylation, resulting from the expression in the *E. coli* host, was detected even before the *in vitro* ADP-ribosylation assays (III, Figure 4B). Besides the extensively truncated recombinant forms of PtxS1, auto-ADP-ribosylation was also observed with a reductant-activated pertussis holotoxin (III, Figure 4C-D). Mass spectrometry mapping identified the ADP-ribosylation of three amino acids (C41, T125, Y126) at the NAD+ binding cleft in the wt PtxS1 (III, Figure 4E, Supp. Figure S2).

Importantly, it was also confirmed that the C41S and C41G mutations had a negligible and the Q127D/E129D double mutation only a minor effect on protein folding as evidenced by DSF analysis (III, Figure 3F). Overall, the biochemical data, supported by the modeling exercise, suggest catalytic alterations especially with the C41S mutation, which may explain the detection of α-BaAD in the C41S mutant crystallization experiments.

5.3.3 Experimental confirmation on the formation of a novel NAD+ analog

To support the crystallization data on the formation of BaAD by PtxS1 in the active site, a complementary assay was performed with wt and mutant constructs. An hour-scale incubation of PtxS1 in the presence or absence of different combinations of 3-AB and NAD+ at RT and subsequent analysis of the non-protein bound reaction components by HPLC with gradient elution (method A) using 260 nm UV detector resulted in the detection of distinct peak with ca. 7.25 retention time that was missing from the controls (III, Figure 5C-D). Also, NAD+ hydrolysis could be distinguished from the HPLC traces, as well as the inhibitory effect of 20 mM 3-AB on this activity (III, Figure 5C). The formation was found to be enzyme concentration-dependent and to correlate with the 3-AB levels (III, Figure 5F), as well as be dependent of the ADP-ribosyltransferase activity, as wt, C41S and C41G, but not the transferase-deficient double mutant reaction contained the ca. 7.25 retention time peak (III, Figure 5C-D and Supp. Figure S3). When analyzing the protein-bound reaction components, no peak at ca. 7.25 retention time was detected (III, Figure 5E), suggesting that the ca. 7.25 retention time peak compound is almost fully released into solution after its formation in the NAD+ binding catalytic pocket of PtxS1.

Improved separation of reaction components in HPLC using a C18 matrix with isocratic elution mobile phase (method B) revealed a distinct peak at around 8 minutes retention time, which was not detected in the controls (III, Figure 6A-B). Based on spectral scan analysis, the peak was consisted of one compound (III, Figure 6C). The ca. 8.0 min retention time peak compound was collected from different HPLC runs, pooled and further characterized in LC-MS analysis (III, Figure 6), where compounds with molar masses closely matching the expected neutral molar mass of BaAD (677,12477 g/mol) were witnessed. They were identified as BaAD with three different adducts (+H, -e, +NH4) (III, Figures 6D-G), with molar masses of 677.1120, 677.1285 and 677.1224 g/mol, respectively. In conclusion, the HPLC and mass spectrometry data provide evidence that recombinant PtxS1 catalyzes the formation of BaAD, and a significant portion of the formed BaAD is released into the solution.

6 Discussion

Infection with *B. pertussis* can cause various physiological effects, including leukocytosis, hyper-insulinemia, histamine sensitization, and disease protection, in addition to the typical symptoms of whooping cough. Extensive research over the decades has shown that these activities are all attributed to a single molecule known as pertussis toxin, contrary to previous beliefs of multiple molecular entities. Over the past 50 years, the 3D-structure, molecular mechanisms, and role of pertussis toxin in protective immunity has been elucidated, but a detailed structural understanding of the enzymatic mechanism of pertussis toxin has eluded the field. While the exact role of pertussis toxin in the pertussis disease formation is still a somewhat open question, primarily due to PT binding to and entering a multitude of different cell types, significantly complicating the determination of physiological effects, many functions have been established for it in *in vitro* and *in vivo* animal model studies and it has been shown to have a major role in the disease. Thus, it might be beneficial to target pertussis toxin, and the ART activity it harbours, to treat the disease and alleviate the symptoms of infected individuals. A detailed understanding of the mechanism of action and structural requirements during the ADP-ribosylation reaction may aid in rational drug design approaches and development of PT-specific inhibitors. In this study, the identification of the first two small molecular weight compounds against the ART activity of PTS1 *in vitro* and in living cells is reported alongside with putative binding poses for the inhibitors obtained with docking and molecular dynamic simulations. This study also reports crystal structures of pertussis toxin S1-subunit in complex with NAD+, NAD+ hydrolysis products ADP-ribose and nicotinamide, NAD+ analog PJ34, and a novel NAD+ analog, BaAD, formed upon S1 subunit crystallization with 3-AB and NAD+, thus revealing novel details of pre- and post-NAD+ hydrolysis steps of the ART activity of PT, confirmed by mutagenesis and biochemical experiments.

6.1 Structural and mechanistic understanding of pertussis toxin activity

The mechanistic and structural aspects of pertussis toxin and its ADP-ribosyltransferase activity were studied in this thesis, providing deeper

understanding of the enzymatic function, importance of specific amino acids and the structural changes happening during the ART-reaction. The findings provide useful information for potential applications in drug development and biotechnology.

In the studies, a truncated version of pertussis toxin S1 subunit was utilized. This protein is a minimalized catalytic domain of the pertussis toxin S1 subunit, lacking the N-terminal secretion signal sequence as well as part of the C-terminus, which normally masks the active site and likely requires disulfide bond reduction (C41-C201) and significant movement of the C-terminus for the catalytic activity in the cells (Stein et al., 1994a; Stein et al., 1994b). As such, this construct is continuously active due to the exposed ADP-ribosyltransferase catalytic site, including the NAD+-binding pocket (Stein et al., 1994a; Stein et al., 1994b). Based on previous biochemical work (Cortina et al., 1991; Locht et al., 1987) the C-terminal truncation was not expected to affect the NAD+ glycohydrolase activity, *i.e.* PtxS1-catalyzed reaction between NAD+ and water to yield ADP-ribose and nicotinamide, but it might have negatively affected the ADP-ribosylation of Gαi. ART activity of this truncated recombinant PtxS1 toward Gαi was confirmed by an NAD+ western blot-assay utilizing recombinant PtxS1 and recombinant Gαi. The utilization of the recombinant Gαi also showed that it may serve as a substrate without the G-protein βγ-complex or other cellular constituents. However, while the ART activity was retained, the truncation might have some unstudied effects on reaction rate or in the Gαi binding or recognition. Complex formation during catalysis between the recombinant PtxS1 and Gαi appeared to be weak *i.e.,* transient kiss and-run type of interaction, as no complex formation was seen with SEC analysis. Molecular dissection (Krueger & Barbieri, 1994) has indicated that the C-terminal domain of S1 is involved in G-protein binding, and although previous crystal structure of the pertussis holotoxin (Stein et al., 1994) does not provide indication towards it, the deleted part C-terminus might also provide some additional interactions, which are not present in the truncated construct. In addition, while Gαi can serve as a substrate without the βγ-complex, the complex might still have a role in the interaction, as isolated Gαi have been shown to be poorer substrates than the Gαi in the trimeric αβγ-complex (Casey et al., 1989; Katada et al., 1986). Also, the obtained crystal structures revealed that NAD+ binding into the active site causes structural changes in PtxS1, and this might also stabilize the interaction between S1 and Gαi to some extent. However, this kind of reaction setup was not studied.

The enzymatic activity of PtxS1 was assessed and characterized with both wildtype and mutant variants in a structural and biochemical level. Q127 and E129 of S1 are conserved with several other bacterial ART-toxins (the catalytic Q/EXE motif), where these residues position NAD+, particularly the nicotinamide end, and promote the transfer of ADP-ribose to a substrate amino acid residue (Simon et al., 2014; Stein et al., 1994). As expected, these single amino acid mutants, as well as

Q127D/E129D double mutant were seen to be inactive in the ADP-ribosylation assays, consistent with previous data on similar single amino acid mutations of PTS1 (Antoine et al., 1993; Barbieri et al., 1989; Brown et al., 1991; Burnette et al., 1988; Cieplak et al., 1990; S. Cockle et al., 1989; Locht et al., 1989; Pizza et al., 1988). The crystal structures obtained help in understanding why this E129D mutation inactivates the protein. In the $S1_{E129D}$ structure the interaction between the negative charge of E129 and the *N*-ribose ring of NAD+ is disrupted as it is displaced toward solvent. While obtaining the $S1_{NAD}$ structure, the unexpected inactivating effect of iodide ions displacing the negative charge of E129 was also witnessed. These findings inform that the precise positioning of the glutamate is required for the catalysis. Q127 on the other hand was often seen facing towards the solvent rather than the NAD+-binding site, despite the close proximity to the catalytic E129. Q127 is situated at the base of the flexible loop ($_{112}$GDNAGRILAGALATYQ$_{127}$) (h5 of the holotoxin) showing multiple conformations at the crystals obtained. Similar kind of plastic loop (ARTT loop) has been observed in iota toxin Ia-subunit (Tsurumura et al., 2013) and in C3 toxin (Ménétrey et al., 2008). The ARTT loop and its plasticity has been indicated to have a role in the ART-substrate protein-complex (Tsurumura et al., 2013) and has been thought to mediate Gαi recognition in related toxins (Ménétrey et al., 2008). In Ia the corresponding amino acid (E378) is suggested to be important also for keeping the oxocarbenium cation from reacting with unfavorable water during the transition from the pre-reaction to the post-reaction state (Tsurumura et al., 2013). Similar h5 mutation in *Ec*Plt (I111Y) is seen to be likewise inactivating (Littler et al., 2017).

Mutating C41, which has previously been shown to be involved in NAD+ binding based on kinetic studies (Locht et al., 1990), was seen to have a differential effect on the NADase and ART activity depending on whether Gαi was present or not. The effect was also dependent on the amino acid the cysteine was mutated into (glycine vs. serine). The nature of these amino acid characteristics do not readily themselves explain the differences seen in the activities, as all can be considered of polar nature and are capable of forming hydrogen bonds with NAD+, although in a different manner due to the different affinities and flexibilities of the side chains. MDS conducted to study the effects of C41 mutations showed higher RMSD values especially for the C41S mutant, indicating increased structural fluctuations. While both glycine and serine mutants both had differential interactions with the surrounding amino acids as compared to wt, it might be the different compensating interactions seen with C41G that explain why it retains activity similar to wt toxin while the serine mutant does not. The differential effect witnessed for C41S in the presence or absence of Gαi might indicate that NAD+ hydrolysis in the absence of the substrate protein Gαi and the ART-reaction when Gαi is present could happen via somewhat different reaction mechanisms, supported by the differences observed

in the reaction kinetics and transition state characteristics between NAD+ hydrolysis and ADP-ribosylation catalyzed by PTS1 (Scheuring & Schramm, 1997b). C41 is located in the middle of a flexible loop (NAD+ loop/active site loop) that moves from the APO conformation [PDB 1PRT, (Stein et al., 1994)] on top of NAD+ upon NAD+ binding, as observed from the obtained crystal structures (study II). While DFS did not indicate any changes in the protein folding for C41 mutants, there might be subtle changes in the active site loop folding over NAD+ that affect the NADase activity.

The crystal structures obtained also confirm the previous prediction on that the inactivation of S1 due to mutating the characterizing arginine residue of R-S-E ARTs, R9 in PTS1, to lysine is due to the disruption of the interaction of the guanidinium groups of arginine with both NAD+ phosphates (Brown et al., 1991), as this interaction is witnessed in the crystal structures. W26 has also been indicated in the NAD+ binding (Cortina & Barbieri, 1989) and the crystal structures show it forming π-cation and π-π-stacking interactions with NAD+. The crystal structures also repeat the previous findings in that the negatively charged carboxyl group of E129 is within hydrogen-bonding distance of H35, S52 and Q127, and they stabilize it in the catalytically permissive position. These amino acids have been shown to have a role in the ADP-ribosylation of Gαi (Antoine et al., 1993; Antoine & Locht, 1994; Locht et al., 1989; Locht & Antoine, 1995; Stein et al., 1994; Xu et al., 1994). Mutations of H35 are associated with reduced ART activity and even more effect on the NAD+-glycohydrolase activity, indicating a role for H35 during catalysis, likely by enhancing the nucleophilicity of the thiol of cysteine residue in G protein by ionization (Antoine & Locht, 1994; Scheuring & Schramm, 1997a; Xu et al., 1994). S52 substitutions have been seen to reduce the catalytic activity, but it is suggested to be involved in maintaining the conformation of the active site, rather than a direct role in the catalysis (Antoine & Locht, 1994; Locht & Antoine, 1995). S52, a part of the STS motif and the characterizing serine in R-S-E group of toxins, is seen to form hydrogen bonds with several positions in the nicotinamide ribose.

Other interesting amino acids identified in the study in the active site of PtxS1 are Y59 and Y63. While modeling of the truncated PtxS1 and Gαi interaction with Alphafold resulted in multiple binding modes, one of the most plausible modes showed the two tyrosines (Y59 and Y63) interacting with the hydrophobic amino acids on the Gαi peptide and experimentally mutating either one of these tyrosines to alanine resulted in virtually complete abrogation of the ART activity. Crystal structure ($S1_{NAD}$) shows these residues enclosing upon the nicotinamide group of NAD+ and forming hydrogen bonds with it. These results indicate that Y59 and Y63 might be involved in both NAD+ and Gαi binding during the catalysis. Previous docking model of the ternary pertussis toxin-NAD-Gαi transition-state complex (Scheuring et al., 1998) utilizing a peptide of 10 amino acids from the C-terminus of

Gαi shows it binding to the active site parallel to NAD+ when the position of C351 is in the correct position for nucleophilic attack. This model also indicated a possible interaction of Y59 and Y63 with C-terminal residue of Gαi (Scheuring et al., 1998). Docking done by Scheuring et al. could not utilize neither of the crystal structures that were published from Gαi at the time (Coleman et al., 1994; Mixon et al., 1995), one complexed with nonhydrolyzable GTP analogue and the other with GDP. In the Alphafold2 docking model generated in this thesis study, the preferred model showed S1 engaged with Gαi in a structure resembling the GPCR-bound (GDP-bound to Gαi) form.

6.2 Mechanism of action for the S1 catalyzed ADP-ribosyltransferase reaction

A conserved mechanism of action is suggested for all members of ART family and a common feature in the ART enzymes is a nucleotide clamp (the active site loop folding over NAD+ binding pocket in PtxS1) that proposedly facilitates enzymatic activity by simultaneously fixing the adenine base while inducing a compact and strained conformation in the other end of the molecule near the nicotinamide, *N*-ribose, and *N*-phosphate (Han & Tainer, 2002; Tsuge & Tsurumura, 2015; Tsurumura et al., 2013; Yoshida & Tsuge, 2021). The strained conformation of NAD+ is alleviated through the rotation of the oxocarbenium cation around the phosphate bonds of NAD+, bringing the electrophilic carbon of *N*-ribose into proximity with a nucleophilic residue of the target, enabling a nucleophilic attack and ultimately leading to the transfer of ADP-ribose (Tsuge et al., 2008). This suggested reaction scheme mimics what happens at the catalytic center of S1 in the presence or absence of the Gαi substrate, as the formation of the oxocarbenium cation transition state has been witnessed in S1 in both catalytic conditions prior the nucleophilic attack by the sulfur atom of Gαi cysteine during target ADP-ribosylation or by oxygen atom of the water molecule during NAD+ hydrolysis (Scheuring et al., 1998; Scheuring & Schramm, 1997b, 1997a). In more detail, the reaction would go as follows: first the catalytic Glu129 weakens the *N*-glycosidic bond of NAD+, promoting cleavage and the formation of a highly strained oxocarbenium intermediate. The adenine/phosphate clamp of the enzyme induces strain relief, leading to the rotation of the *N*-phosphate and *N*-ribose and the formation of a second oxocarbenium intermediate. The $S1_{ADPR/NA}$ structure suggests that the strain relief would happen via rotation of the *N*-ribose sugar, as the movement of the *N*-phosphate in S1 is restricted by Y63, in contrast to Iota toxin, where the strain relief is thought to happen through rotation of both the *N*-phosphate and *N*-ribose of the nucleotide prior to the formation of an ADP-ribosylated actin (Tsurumura et al., 2013). In PT this rotation moves the anomeric carbon, reducing

the nucleophile-electrophile distance and stabilizes the charge on the oxocarbenium prior to nucleophilic attack by the G protein substrate.

6.3 Inhibiting pertussis toxin ADP-ribosyltransferase activity

Currently there is no proven treatment available that can effectively alleviate pertussis symptoms. While antibiotic treatment is available and important in preventing further transmissions, it does not reduce the symptoms unless administered in the early stages of infection, which rarely occurs due to a late diagnosis. Antibiotics can only eradicate *B. pertussis*, but they do not alleviate symptoms that arise due to PT (or other toxins) already secreted by the bacteria (Altunaiji et al., 2007; Carbonetti, 2016). In addition, while antibiotic resistance is not a major concern for pertussis, macrolide resistant strains have been reported (Guillot et al., 2012; Z. Wang et al., 2014; Yang et al., 2015). As pertussis toxin has a major role in whooping cough and mediates the severity of the disease, there is a therapeutic promise to target pertussis toxin with novel pharmacological strategies in order to attenuate the symptoms and to protect against severe pertussis disease.

In previous and in recent years, neutralizing inhibitors such as antibodies and peptides that interact or bind pertussis toxin before or during receptor-binding have been studied. Murine based, humanized monoclonal antibodies hu11E6 and hu1B7, have been developed to neutralize pertussis toxin (Acquaye-Seedah et al., 2018; Nguyen et al., 2015, 2020; Sato & Sato, 1990). Antibodies hu11E6 and hu1B7 either fully or to some extent, respectively, prevent pertussis toxin binding to its cell surface receptor. They might also accelerate pertussis toxin clearance via immune complex formation. The antibody hu1B7 recognizes an epitope in the B subunit of PT, spanning the A/B domain interface, and seems to capture pertussis toxin either on or close to the surface of cells, possibly interfering with the transport of the toxin at the early endosome-to-Golgi transfer step (Acquaye-Seedah et al., 2018). On the other hand, hu11E6 is directed against PTS1 (Acquaye-Seedah et al., 2018; Sato et al., 1987). A cocktail of hu1B7/hu11E6 has been shown to have a prophylactic and therapeutic effect in mouse and adult baboon pertussis models, respectively (Acquaye-Seedah et al., 2018; Nguyen et al., 2015). Monotherapy of hu1B7 has also demonstrated a potent prophylactic effect (Nguyen et al., 2020). Based on the humanized antibodies hu1B7 and hu11E6 recognizing two distinct epitopes of PT, a bispecific antibody has also been developed. It combines the specificity of the two antibodies and has shown a synergistic neutralization in a murine model of PT-induced leukocytosis (Wagner et al., 2016).

Recently, human antimicrobial peptides α-defensin-1 and -5, part of the innate immunity, were identified as inhibitors of PT activity (Kling et al., 2021). In the

presence of these defensins, PTS1 enzyme activity was inhibited and the amount of ADP-ribosylated Gαi was significantly reduced in PT-treated cells (Kling et al. 2021). In addition, a novel live cell bioassay (Paramonov et al., 2020) revealed that these defensins were both capable of reducing the high cAMP levels, which are resulting from PT-mediated ADP-ribosylation of Gαi, suggesting that the defensins interfered with PT activity (Kling et al., 2021). Members of the defensin family have been found to inhibit the activity of other bacterial toxins such as diphtheria toxin, *C. difficile* toxins and anthrax lethal toxin (Fischer et al., 2020; Giesemann et al., 2008; Kim et al., 2005; Korbmacher et al., 2020; Kudryashova et al., 2014, 2017). In some of the cases, α-defensins are known to destabilize or cause unfolding of toxins (Kudryashova et al., 2014, 2017), and that might also be the case for pertussis toxin. Another possibility might be blocking of the active site of PTS1 by the α-defensins, leading to decreased enzyme activity (Ernst, 2022).

While antibodies and peptides can be effective in neutralizing the toxin prior to uptake into cells, they have limited capability to cross biological membranes. Inhibitors targeting later stages of toxin uptake and activity, such as translocation into the cytosol or enzyme activity, are needed to inactivate toxin molecules that have already entered cells. Most small molecules can effectively penetrate tissues and cells, which enables them to reach the toxin and render them inactive even if they have already entered the cytosol of the target cell. However, to this point, no such inhibitors targeting pertussis toxin in these later stages existed. One study designed and synthetized transition state analogues of NAD+ to resemble the oxocarbenium ion transition state of bacterial ART toxins (DT, CT, and PT), but they were not shown to be effective in blocking the pertussis toxin action (Zhou et al., 2004). As it is, this thesis study describes the first small molecule weight compounds inhibiting the ART activity of pertussis toxin.

In this study, the small molecular weight inhibitors were identified by utilizing *in vitro* NAD+ consumption assay, a multiwell fluorimetric method previously developed for measuring the activity of poly-ADP-ribose and mono-ADP-ribose synthesizing enzymes (Narwal et al., 2012; Putt & Hergenrother, 2004; Venkannagari et al., 2013). The endpoint assay measures the conversion of NAD+ to a stable fluorophore and the decrease in fluorescence compared to the non-enzyme control indicates the level of NAD+-consuming enzymatic activity. This assay with the PtxS1-Gαi recombinant enzyme-substrate pair was optimized to be high-throughput-compatible and was used to screen a high scaffold diversity compound library in parallel to a panel of selected compounds known to inhibit the ART activity of human diphtheria toxin-like ADP-ribosyltransferases (ARTDs/PARPs). The panel included several FDA-approved anticancer drugs, such as Rucaparib. None of the compound in the panel significantly inhibited the NAD+-consumption activity of PtxS1 in the presence of Gαi (arbitrary inhibitory threshold = 50%). Would one

of these have worked, it could have provided a fast track to drug development via a drug repositioning strategy, greatly benefiting from the knowledge and existing clinical data of an approved drug compound that have already undergone clinical trials. This panel also included compounds PJ34 and 3-AB, that were further investigated in study II, where they showed inhibition at millimolar levels that were not tested in study I. The screened compound library contained 1,695 molecules with high scaffold diversity from NCI Developmental Therapeutics program repository, being a rather small library for high-throughput screen. However, nine compound hits were identified to effectively inhibit the NAD+-consumption activity of recombinant PtxS1 in the presence of recombinant Gαi. However, further analysis with the independent NAD+-biotin western blot-assay measuring the PtxS1-catalyzed conjugation of biotinylated ADP-ribose onto Gαi revealed that only five out of the nine primary compound hits showed strong inhibition of PtxS1-catalyzed Gαi ADP-ribosylation. In addition, the assay revealed that two of these five compounds, NSC119875 (Cisplatin, DNA alkylating agent used in cancer treatments) and NSC44750, which showed inhibition in the primary screen measuring NAD+-consumption and lack of ADP-ribosylation of Gαi in the secondary assay, did so by influencing to the integrity the recombinant Gαi and/or PtxS1 proteins. This highlights the importance of an alternative and independent *in vitro* assay to validate the primary screening hits obtained from the used primary screening method. The remaining compounds NSC228155, NSC29193 and NSC149286 had IC_{50}-values of 3.0, 6.8 μM and 20 μM respectively in a dose response study utilizing the NAD+ consumption assay. As NSC149286 was less potent than the other two compounds, it was excluded from further analyses. In an additional *in vitro* ADP-ribose conjugation assay using nickel-coated plates, NSC228155 and NSC29193 were seen to inhibit the auto-ADP-ribosylation activity of recombinant PtxS1, indicating that these two compounds interact directly with recombinant PtxS1.

In order to learn more about the interaction between the compounds NSC228155 and NSC29193 with PtxS1, efforts to crystallize them in complex with PtxS1 were undertaken but were unsuccessful. Hence, docking, and molecular dynamic simulations were utilized to study the putative binding poses for both ligands NSC228155 and NSC29193 with a model structure of PtxS1, generated from the structure of S1-like protein from *E. coli* bound with NAD+ (Littler et al. 2017).

NSC29193, which is a purine-2,8-dithiol, a rather rigid purine analogue, mimics the structure of the adenine base of NAD+. In the most plausible, top ranked poses, NSC29193 is bound either where the nicotinamide ring of NAD+ would be bound in PtxS1, or it is seen bound near the location where the adenine ring of NAD+ would be bound. NSC228155 on the other hand contains two ring structures linked together with a sulfur containing rotatable linker, with the benzoxadiazole ring compound

mimicking the adenine base of NAD+ and the pyridine ring compound mimicking the nicotinamide of NAD+. Due to this rotatable bond, the compound can adopt various conformations, which resulted in various binding modes in the simulation. Nonetheless, the top ranked poses of NSC228155 exhibited similar features in the positioning of the aromatic pyridine ring of NSC228155 in a confined area where the nicotinamide ring of NAD+ would bind to PtxS1, with the double benzoxadiazole ring positioned near the center of the NAD+-binding pocket.

Molecular modelling of the inhibitors revealed interaction with various set of PtxS1 amino acids that can be seen in the study II to be involved in the NAD+ binding based on the crystal structure of PtxS1 in complex with NAD+ ($S1_{NAD}$), which is expected, as these compounds share structural similarities to NAD+ and can be seen binding partly to the NAD+ binding site. In pose 1 for NSC228155, the pyridine ring forms hydrogen bond with Y10, π-π stacking interactions with Y59, benzoxadiazole ring forms π-π stacking interactions with Y63. In pose 2, the pyridine ring makes π-π interactions with both Y63 and Y10 and ionic interactions with R9 and R67. In pose 1 for NSC29193, the compound is hydrogen bonding with Y10 and S52, and forms π-cation interactions with R9, π-π stacking with Y63. In pose 2, NSC29193 stacks against the aromatic ring of W26 and hydrogen bonds T24, as well as forms ionic interactions with R9 and R13. The nicotinic ring of NAD+, on the other hand, was shown to have β-sheet–like interaction with Y10 and hydrogen bond with R9 and Y63 of PtxS1. Based on the structure, also D11, T24, H35, C41, S52 and Y59 form hydrogen bonds with NAD+. R13 and W26 form π-cation interaction and W26 also π-π-stacking with NAD+. While the various binding poses from the docking simulations suggest that these two compounds have multiple types of interactions within the active site pocket, which might imply a lack of selectivity, it is also noteworthy that NAD+ is a larger compound compared to the inhibitors. Therefore, the inhibitors only partially occupy the NAD+ binding pocket. It is likely that there is only one true binding mode, but the modeling cannot definitively determine which one is the most likely. Crystal structures of PtxS1 in complex with the compounds would have likely provided valuable information regarding the binding and potential improvements for the compounds. However, in the absence of such crystal structures, the modeling offers potential binding modes for the compounds.

6.4 Inhibitors of pertussis toxin in living human cells

The inhibitory action of the compounds NSC228155 and NSC29193 was tested with HEK293T cells. Of the compounds only NSC228155 was shown to inhibit PtxS1-mediated ADP-ribosylation of Gαi in HEK293T cells with near complete inhibition

at 2.5 hours with 5 μM concentration. No inhibition was detected with NSC29193 even with multiple different experimental set-ups, including concentrations up to 50 μM that did not cause visible alterations or cell detachment of HEK293T cell monolayers, unlike with NSC228155. The non-activity of NSC29193 might be due to poor bioavailability, but the cell permeability of this compound is not known and was not tested in the course of this study. On the other hand, NSC228155 is known to be cell permeable (Sakanyan et al., 2016). NSC228155 displayed cytotoxicity in mammalian cells at 20 μM and higher concentrations after only a short incubation of 3.5 hours, which is somewhat worrisome and might imply poor selectivity and off-target effects. NSC228155 is a nitro-benzoxadiazole compound, which are known to rapidly bind to multiple proteins in cells, leading to impairment different cellular functions that may lead to unpredictable side effects (Ricci et al., 2005). They are also potent producers of hydrogen peroxide and generate reactive oxygen species (Ricci et al., 2005; Sakanyan et al., 2016), which might be the cause of the cytotoxicity. However, in recent studies NSC228155 has been shown to correct energy metabolism, oxidative and ER stress, prevent apoptosis, inhibit inflammation, and protect mitochondria in cell cultures and in kidney injury and septic cardiomyopathy models (Y. Jiang et al., 2023; Y. Li et al., 2022). NSC228155 is also known to promote transactivation of several receptor tyrosine kinases, activate epidermal growth factor receptor and trigger protein phosphorylation in its downstream signaling pathways, while also potently inhibiting cyclic-AMP response element binding protein-dependent gene transcription in living cells (Sakanyan et al., 2014; Xie et al., 2013). Considering these points, and the relatively rapidly manifesting cytotoxic effects, it is possible that NSC228155 is not selective to PtxS1 alone and might have off-target effects in the cells. However, computational analysis of the studied compounds did not identify them, not even NSC228155, as pan-assay interference compounds or aggregators (zinc15.docking.org) containing molecular structures or substructures known to interfere and have non-specific interaction in biological assays. In addition, in respect of the cytotoxic effects, it is noteworthy that upon incubation of cells with inhibitory concentration of 5 μM of NSC228155 for 2.5 h, no auto-ADP-ribosylation of PARP1/ARTD1, known to be induced by reactive oxygen species-induced DNA damage (Miettinen et al., 2019), was detected. Additionally, no caspase mediated proteolytic PARP1/ARTD1 cleavage was detected, which is a robust readout for the onset of programmed cell death (Chaitanya et al., 2010). The conventional assay for apoptosis of cells with Annexin V staining could not be used due to the intrinsic fluorescence of NSC228155 that interferes with Annexin V staining.

The MTT assay was employed to determine the IC_{50} of cytotoxicity for inhibitor NSC228155, which was found to be 15.33 μM. This colorimetric assay assessing cell metabolic activity (Mosmann, 1983) is widely and almost ubiquitously used to

study cell toxicity, but is actually a metabolic assay, where the metabolically active cells NAD(P)H-dependent cellular oxidoreductase enzymes reduce the tetrazolium salt into formazan, which has a purple colour that can be measured (Berridge et al., 2005). This metabolic activity can reflect cytotoxicity (the number of viable cells present), but it can also reflect cytostatic activity (a shift from proliferation to quiescence) or reduction in mitochondrial efficiency. It is also worthwhile to keep in mind the structure of NSC228155 that mimics the adenine base of NAD+ (and NADP+) and might thus interfere with the cellular NAD(P)H-dependent oxidoreductase enzymes that reduce the tetrazolium salt into formazan, and subsequently interfere with the MTT assay results. In future studies, it might be wise to utilize different or complementary cytotoxicity assays. Additionally, more thorough dose response and time course curves should be performed, as this short incubation does not reveal the metabolic fate (*i.e.,* the stability towards metabolic degradation) of the NSC228155 inside the cell nor how long the inhibitory effect and protection against the PTS1 activity can last. Clearly, given the cell-based IC_{50} and toxicity IC_{50} values, the therapeutic index of the compound needs to be substantially increased. As it is now, NSC228155 is a potential hit for a lead series that would benefit from SAR analysis with the S1 subunit. SAR analysis could also be utilized to screen the compound with other ART toxins (*e.g.*, cholera toxin, diphtheria toxin) and other ARTs (PARPS, Sirtuins), NAD-binding or even adenine or nicotinamide binding proteins, in order to gain more information in regards of the selectivity. Pan-bacterial ART toxin inhibition would be desired effect, unlike the inhibition of the host ARTs or other NAD+ interacting enzymes. In addition, the binding properties of the hit compounds should be more fully characterized, as now the study gives indirect indication of the compound binding to PtxS1 from the nickel plate readout, and molecular modelling, but a more definite results remain to be shown. Medicinal chemistry efforts, such as molecular modelling and crystallography should be used to design less toxic analogs with increased potency and specificity to inhibit PtxS1. Analogs to NSC228155 that have nitrogen atom in place of the central sulfur linker atom were tested with the goal of seeing if the lack of reactive sulfur would reduce the toxic effects. However, these compounds proved to be much less effective in the *in vitro* assays (data not shown) and were not taken further to cell-based assays.

It is also worthwhile to keep in mind that the library screened was extremely small and focused on cancer compounds. By selecting a larger, more diverse set of compounds (*e.g.,* other sets from NCI Developmental Therapeutics program repository, ChemBridge or Institute for Molecular Medicine Finland), more and better hits might be found. Nonetheless, this study serves as a proof-of-concept for the *in vitro* high-throughput-compatible screening assay with a recombinant enzyme-substrate pair that can be used to screen inhibitors for bacterial ART toxins and the study provides novel information by describing the identification of the first

small molecular weight compounds inhibiting the ADP-ribosyltransferase activity of pertussis toxin *in vitro* and in living cells. As no previous small molecules inhibiting PT have been identified, this work serves as a starting point for discovery of small molecules against PT despite the limitations of the compounds and the study itself.

6.5 Novel NAD+ analog biocatalysis by ADP-ribosyltransferases

The focus of drug development efforts towards the NAD+ cleaving non-redox enzymes strongly center on compounds that bind to the NAD+ binding site, mimicking NAD+ itself (Wahlberg et al., 2012). However, this presents challenges due to the abundance of proteins that bind to NAD+, both homologous and non-homologous. To enhance the precision and effectiveness of inhibitors, a deeper understanding of NAD+ binding mechanisms is needed. Crystal structures of the enzymes in complex with NAD+ and with compounds mimicking NAD+ provide information that can be used to screen and modify the compounds with enhanced selectivity. With the goal of learning more about the binding of NAD+ mimicking inhibitors to the pertussis toxin active site, efforts to crystallize these inhibitors in complex with PtxS1 were undertaken. A crystal structure was obtained for PJ34 in complex with S1. The inherent flexibility of S1 allows the binding, even though PJ34 does not fully occupy the nucleotide-binding site. The benzamide backbone binds to the nicotinamide site, as expected, with the second aromatic ring base of the tricyclic ring system stacking against R9 instead of NAD+ phosphates. The subsites for adenine moiety and ribose sugars of NAD+ are unoccupied and the dimethylamino acetamide group of PJ34 extends outside the standard NAD+-binding groove. Conversely, no crystals were obtained for the S1 in complex with 3-AB. This might also be explained by the inherent flexibility of S1, which in addition to allowing the above-mentioned induced fit-binding, may result in constant assembly and disassembly of its nicotinamide-binding site. However, a co-complex of PtxS1 together with 3-AB and NAD+ was obtained, where 3-AB was seen to displace nicotinamide-binding location in S1 and the aniline nitrogen of 3-AB was seen to form a covalent bond with the anomeric carbon of *N*-ribose, indicating formation of a novel NAD+ analog (termed BaAD) at the catalytic center of S1.

The formation of BaAD by the catalytic activity of pertussis toxin ADP-ribosyltransferase subunit, and the subsequent release into solution, was confirmed in study III by the use of an orthogonal assay using HPLC coupled to mass spectrometry. The crystal structure obtained, along with molecular modeling, indicate that only α-BaAD is formed in the active site. Thus, the formation of α-BaAD would follow the canonical ADP-ribosyltransferase-catalyzed reaction scheme that produces α-ADP-ribosyl linkages from β-NAD+. First, PtxS1/β-NAD+-

complex undergoes activation of β-NAD+ leading to formation of the short-lived and reactive oxocarbenium cation (Franconetti et al., 2021), with E129 having a major catalytic role. Next, stereospecific nucleophilic attack of the electrophilic ribose 1'-carbon takes place by the nitrogen atom of the 3-AB amine group, instead of the oxygen atom of water molecule or cysteine sulfur atom of the PtxS1 substrate Gαi (Scheuring et al, 1998; Scheuring & Schramm, 1997a, b), at the formation binding pose of the oxocarbenium cation yielding α-BaAD, but not β-BaAD. Lastly, the formed α-BaAD is released into solution, or also partially occupy the active site, as highlighted by the obtained 1.0-Å resolution C41S-PtxS1/BaAD co-complex structure. It might also be possible the BaAD could be formed after the oxocarbenium cation has moved out of its initial formation binding pose, either with a nicotinamide pocket-bound or free solution form of 3-AB. Based on the molecular modeling, oxocarbenium cation has a lower affinity as compared to NAD+ at the NAD+ binding site and thereby potential to move from its initial formation binding pose. PtxS1 could also create a cloud of diffusible oxocarbenium cations, which would react with any suitable nucleophile even across long distances, supported by the finding that three nucleophilic amino acids (C41, Y126, T125) of PtxS1 catalytic site that are relatively far from the electrophilic ribose 1'-carbon, were experimentally detected to be auto-ADP-ribosylated. However, this mechanistic scenario is somewhat unlikely, as the lifetime of the oxocarbenium ion is very short (Franconetti et al., 2021) and as there is no indication, that the active site of S1 would be able to exclude water, which would quickly react with oxocarbenium ion yielding ADP-ribose in this scenario.

α-BaAD is a novel non-hydrolyzable NAD+ analog. These analogs are modified versions of NAD+ that mimic the structure and function of NAD+ while being resistant to enzymatic degradation (hydrolysis), allowing these analogs to be used to investigate NAD+ metabolism, enzyme mechanisms, and cellular processes dependent on NAD+ without the interference of NAD+ degradation. They are, along with catalytically compromised mutants or wild-type forms under catalytically non-permissive conditions (such as the iodide ion utilized in this thesis), important tools for crystallization studies, studying NAD+ binding enzymes and developing inhibitors.

Other NAD+ analogs that do not undergo nicotinamide displacement are *e.g.*, carba-NAD+ and benzamide adenine dinucleotide (BAD). Carba-NAD is a synthetic compound identical to NAD except for one substitution, where an oxygen atom adjacent to the anomeric linkage bearing nicotinamide is replaced with a methylene group, making it inert in nicotinamide displacement reactions (Slama & Simmons, 1988). BAD, on the other hand, the nitrogen atom of the nicotinamide ring is replaced with a carbon atom converting the benzamide moiety into a poor leaving group (Gharehbaghi et al., 1994; Zatorski et al., 1996). Carba-NAD and BAD bind

to NAD+ consuming enzymes in a manner similar to NAD+ but are not hydrolysed and they have been useful in obtaining NAD+ binding mode information of NAD+ consuming non-redox enzymes sirtuins (Szczepankiewicz et al., 2012) and PARP1 (Langelier et al., 2018), respectively.

The synthesis of non-hydrolyzable NAD+ analogs can be challenging and technically demanding, as NAD+ is a structurally complex molecule with multiple functional groups requiring introduction and removal of protecting groups during the synthesis. In addition, maintaining the correct stereochemistry, purifying the desired product from the multiple reaction intermediates and byproducts are just some of the additional challenges associated with the synthesis. Identification of a biocatalytic process to produce non-hydrolyzable NAD+ analogs would be highly advantageous as opposed to the current highly complex and expensive chemical processes. Therein lies the importance of the observation that α-BaAD is formed by the catalytic activity of PtxS1 and released into solution. However, the HPLC results indicate that even in the most optimized reaction condition, which uses a concentration of recombinant PtxS1 at the upper limit of its solubility, along with a 3-AB concentration (20 mM) near its maximum, which, based on the inhibition assay with the NAD+-biotin western blot approach, begins to inhibit the enzyme, a relatively low amount of α-BaAD is formed as compared to the reaction components β-NAD+ and 3-AB. In addition, during the reaction, nicotinamide and ADP-ribose are also getting formed, which have the capacity to occupy the NAD+ binding site, and thereby to interfere with α-BaAD formation. Thus, it is likely that this reaction platform cannot be significantly optimized further as such. It might be possible to improve the yield of α-BaAD by utilizing covalent or non-covalent immobilization of recombinant PtxS1 to a solid carrier particle or surface (Bolivar et al., 2022), which would allow more control with cyclical spiking of reaction components and product retrieval.

Another option to achieve higher yields could involve using other ADP-ribosyltransferases and NAD+ consuming enzymes. Based on preliminary findings (data not shown), the phenomena witnessed here might be more universally applicable to other ADP-ribosyltransferases as well. These enzymes rely on the production of an oxocarbenium cation intermediate in their catalytic process, and it might be that whenever there is an enzyme capable of forming the oxocarbenium ion from β-NAD+ in sufficient quantities, while simultaneously being able to accommodate and to concentrate 3-AB into the catalytic pocket close to the electrophilic ribose 1'-carbon, there is a possibility for α-BaAD formation. Further studies need to be conducted in order to gain more information on this and whether the structural flexibility of PtxS1 has a role to play in this. However, the data acquired in this thesis demonstrate that an ADP-ribosyltransferase catalytically produces a new kind of a non-hydrolyzable NAD+ analog α-BaAD from β-NAD+ and 3-AB, and releases it into solution, paving a way to develop a biocatalytic

process to produce α-BaAD for downstream applications, where it might act as a valuable tool to the enzymology of NAD+ binding enzymes, including high resolution structure-driven development of small molecular weight inhibitory compounds. In addition to α-BaAD being a potential tool to further characterize the NAD+ binding, the inhibitory potential towards ARTs or other NAD+ consuming enzymes should be tested. Biocatalysis-based production of α-BaAD has promise to complement the currently used complex chemical platforms to synthesize non-hydrolyzable NAD+ analogs.

Additionally, in regards of this phenomenon witnessed, when analyzing the binding modes of ART inhibitors, it is important to consider the possibility that this is a general characteristic of ARTs (or limited to those that possess sufficient flexibility), as failing to do so may result in a disconnection between affinity and structural data from the actual inhibition mechanism, and while actual mechanism of inhibition is not a necessary information for a compound to reach clinical trials or clinical use, the information may help in the lead optimization phase and might be valuable information in drug repositioning strategies. The current focus of ART inhibitor design revolves around developing molecules that exhibit affinity for the NAD+ cleft itself. However, if the mechanism described here proves to be more widespread, it may be feasible to explore the use of small "prodrug"-like compounds. These compounds could initially bind within the nicotinamide pocket and potentially extend to the protein substrate-binding site. Subsequent ADP-ribosylation *in vivo* could then serve as a means to generate transition-state analogs with enhanced affinity.

7 Summary and conclusions

The resurgence of pertussis, coupled with the limitations of antibiotic treatment and the understanding of the beneficial role the bacterial microbiota, destroyed by antibiotics, highlight the need for alternative therapeutic approaches for whooping cough treatment. Detailed understanding of the virulence factor involved aids in discovering and designing targeted inhibitors. Collectively, this thesis study increases the mechanistic and structural understanding of the pertussis toxin S1-catalyzed ART-reaction and provides insights into targeted inhibition of the activity.

The first study identified small molecules NSC228155 and NSC29193 that inhibit the ADP-ribosyltransferase activity of pertussis toxin *in vitro*. NSC228155 is also a potent cell permeable hit compound inhibiting pertussis holotoxin-mediated ADP-ribosylation of Gαi in living cells in low micromolar concentrations. To conclude, both NSC228155 and NSC29193 are useful templates for hit development to specifically inhibit pertussis toxin ADP-ribosyltransferase activity in whooping cough. Pertussis toxin inhibitors, administered systemically or via inhalation, could benefit young children without vaccine-induced protection against whooping cough. As young patients are usually diagnosed early, it could provide a therapeutic window for interfering with pertussis toxin-induced pathology. Exposed family members could also receive prophylactic pertussis toxin inhibitors, possibly in-combination with macrolide antibiotics.

The second study describes the structural analysis of pertussis toxin and its mechanism of action in ADP-ribosylation. Crystal structures of pertussis toxin in complex with NAD+ and analogs provide insights into the molecular mechanism and interactions involved in the pre- and post-NAD+ hydrolysis steps of the ADP-ribosyltransferase activity of PT. The study also reports a novel NAD+ analog α-BaAD forming in the catalytic site of PT with co-incubation of β-NAD+ and 3-AB.

The third study experimentally confirms the formation of α-BaAD in the active site of S1. The production of α-BaAD is dependent of the catalytic activity of PtxS1, as it is not formed by a mutant lacking enzymatic activity. After the formation, the compound is released into solution. Data indicate that the α-BaAD formation follows the canonical stereospecific ADP-ribosyltransferase-catalyzed reaction producing α-ADP-ribosyl linkages from β-NAD+, which involves the activation of β-NAD+ to

create an oxocarbenium cation, followed by a nucleophilic attack by 3-AB, resulting in α-BaAD formation. The results collectively contribute to the understanding of the binding, formation, and catalytic activity related to α-BaAD and PtxS1.The discovery of α-BaAD formation opens the possibility of developing a biocatalytic process to produce α-BaAD, a novel non-hydrolyzable NAD+ analog, that could be a valuable tool for studying NAD+ binding and hydrolysing enzymes and developing small molecular weight inhibitors.

The data provided by this thesis study may aid in rational drug design approaches and further development of PT-specific small-molecule inhibitors. Additionally, these findings may have broader implications for understanding the mechanism of ADP-ribosylation in other biological processes, as ART enzymes share common features and reaction mechanisms.

Acknowledgements

The work described in this thesis was carried out at Turku Cellular Microbiology Laboratory (TCML) at the Institute of Biomedicine, Faculty of Medicine, University of Turku, and Turku Doctoral Programme of Molecular Medicine (TuDMM). Financial support from TuDMM, Turku University Foundation, Finnish Cultural Foundation, Research Council of Finland, Sigrid Juselius Foundation, Novo Nordisk Foundation, Jane and Aatos Erkko Foundation, and Finnish Society of Sciences and Letters is gratefully acknowledged.

First and foremost, I would like to sincerely thank my supervisor and the head of TCML, Docent Arto Pulliainen for giving me the opportunity to carry out this thesis work in his group. Arto, your commitment to scientific excellence and pursuit of high-quality discoveries is remarkable and inspiring. Thank you for your guidance and for all the lengthy scientific conversations related and non-related to this thesis. I have learned a lot about science, research, and scientific thinking during my time under your mentorship. Your ability to always find a way forward has been essential during these years and for this thesis to see the day of light.

Next, I offer my gratitude to the members of my follow-up committee, Dr. Anne Rokka and Professor Lari Lehtiö, whose expertise and guidance have been valuable to this project. I am also grateful for Emeritus Professor Mikael Skurnik and Professor Herwig Schüler for their meticulous review of my thesis and their generous feedback. Special thanks to Professor Christian Hedberg for graciously accepting the role of the opponent in the disputation.

My sincere gratitude also belongs to all my co-authors and collaborators for their contribution to this work: Professors Michael Hottiger, Mark Johnson, Lari Lehtiö, Jamie Rossjohn and Travis Beddoe, and Doctors Yashwanth Ashok, Mahlet Tamirat, Katja Näreoja, Dene Littler, Rajendra Bhadane, Rita Azevedo, Morteza Malakoutikhah, Harri Härmä and Kari Kopra, and Danilo de Oliveira, Avlokita Tiwari, Mai Tran, and Ahmadreza Masoumi.

I would like to thank all the past and present members of the TCML, whom I have had the pleasure to work with, for their expertise, help and company during the years: Rajendra Bhadane, Anbu Poosakkannu, Madhukar Vedantham, Sujit Kumar, Olli Laaksoaho, Abdula Habib, Chiara Catalano Vinyals, Mika Savisalo, Avlokita

Tiwari, Rita Azevedo, Katja Näreoja, Rita Pinto, Alaa Benkherouf, Sakina Begum, Vili Niiniskoski, Arttu Laisi, Antti Kaatiala and Sami Lehto. A special thanks to Madhukar for sharing the lab with me the longest. (You'll be next, good luck for the final crunch!). Also, a big thank you to Mika for his assistance with day-to-day lab tasks, allowing me to focus on essential experiments.

I want to offer heartfelt thanks to all the members of Medisiina D 7th floor for creating a warm and enjoyable working environment. It has been a pleasure to work with you all. Thank you for all your help, expertise and (peer-)support. Thanks for the company, all the scientific, non-scientific. interesting, fun and sometimes absurd discussions during lunch and coffee breaks and fun times at the Christmas parties and game nights. Thank you also to Medisiina C4 people for the early years of my thesis work and to all other Medisiina and medical faculty people that I have had the pleasure to meet, work and spend time with during the years.

I want to express gratitude to my friends for providing support and also much-needed respite from academic pursuits. Special thanks to you, Krista, for your constant support and sharing big (and small) life moments with me. Tiina, thank you for all the lunch dates and peer-support and fun times in the (Turku) PhD life. I also want to thank Jenna L., Kaisa, Anniina, Marika, Eerika, Terhi, Jenna T., Annis, Suski, Sami and others (in addition to Krista and Tiina) for bringing so much joy and enriching experiences in my life in the form of travelling, eating, partying, concerts, movies and sports. You really have kept me sane during the years!

I wish to thank my parents Virpi and Jyrki for their endless support and love (and worrying over my late hours and busy weekends). Thank you for providing me with every opportunity to get where I am today. I thank my twin sister Milla for all her support and for being my oldest friend, and my little sister Iina for cheering me up with all the cakes and other goodies.

Finally, with all my heart, I wish to thank my husband, Leo. Thank you for being so patient, loving and encouraging through the many years this has taken to finish. It has not been an easy journey for either of us, but now it is finally (almost) over, and we can continue to face together the new and exciting adventures life is about to give us. Special thanks for all the dinners you have cooked and sandwiches you have made. I owe you, probably like a thousand sandwiches. You can start claiming those now.

Turku, April 11th, 2024
Moona Sakari

References

Acquaye-Seedah, E., Huang, Y., Sutherland, J. N., DiVenere, A. M., & Maynard, J. A. (2018). Humanised monoclonal antibodies neutralise pertussis toxin by receptor blockade and reduced retrograde trafficking. *Cell Microbiol*, *20*(12), e12948. https://doi.org/10.1111/CMI.12948

Aktories, K., Braun, U., Rösener, S., Just, I., & Hall, A. (1989). The rho gene product expressed in E. coli is a substrate of botulinum ADP-ribosyltransferase C3. *Biochem Biophys Res Commun*, *158*, 209–213. https://doi.org/10.1016/S0006-291X(89)80199-8

Allured, V. S., Collier, R. J., Carroll, S. F., & McKay, D. B. (1986). Structure of exotoxin A of Pseudomonas aeruginosa at 3.0-Angstrom resolution. *Proc Natl Acad Sci U S A*, *83*, 1320–1324. https://doi.org/10.1073/PNAS.83.5.1320

Altunaiji, S., Kukuruzovic, R., Curtis, N., & Massie, J. (2007). Antibiotics for whooping cough (pertussis). *Cochrane Database Syst Rev*, *18*, CD004404. https://doi.org/10.1002/14651858.CD004404.pub3

Andreasen, C., & Carbonetti, N. H. (2008). Pertussis toxin inhibits early chemokine production to delay neutrophil recruitment in response to Bordetella pertussis respiratory tract infection in mice. *Infect Immun*, *76*, 5139–5148. https://doi.org/10.1128/IAI.00895-08

Antoine, R., & Locht, C. (1994). The NAD-glycohydrolase activity of the pertussis toxin S1 subunit. Involvement of the catalytic His-35 residue. *J Biol Chem*, *269*, 6450–6457. https://doi.org/10.1016/s0021-9258(17)37393-3

Antoine, R., Tallett, A., Van Heyningen, S., & Locht, C. (1993). Evidence for a catalytic role of glutamic acid 129 in the NAD-glycohydrolase activity of the pertussis toxin S1 subunit. *J Biol Chem, 268*, 24149–24155. https://doi.org/10.1016/S0021-9258(20)80504-3

Aravind, L., Zhang, D., De Souza, R. F., & Iyer, L. M. (2015). The Natural History of ADP-Ribosyltransferases and the ADP-Ribosylation System. *Curr Top Microbiol Immunol*, *384*, 3–32. https://doi.org/10.1007/82_2014_414

Armstrong, G. D., Howard, L. A., & Peppler, M. S. (1988). Use of glycosyltransferases to restore pertussis toxin receptor activity to asialoagalactofetuin. *J Biol Chem, 263*, 8677–8684.

Baell, J. B., & Holloway, G. A. (2010). New substructure filters for removal of pan assay interference compounds (PAINS) from screening libraries and for their exclusion in bioassays. *J Med Chem*, *53*, 2719–2740. https://doi.org/10.1021/JM901137J

Banasik, M., Komura, H., Shimoyama, M., & Ueda, K. (1992). Specific inhibitors of poly(ADP-ribose) synthetase and mono(ADP-ribosyl)transferase . *J Biol Chem*, *267*, 1569–1575.

Banerjee, T., Cilenti, L., Taylor, M., Showman, A., Tatulian, S. A., & Teter, K. (2016). Thermal unfolding of the pertussis toxin S1 subunit facilitates toxin translocation to the cytosol by the mechanism of endoplasmic reticulum-associated degradation. *Infect Immun*, *84*, 3388–3398. https://doi.org/10.1128/IAI.00732-16

Banga, H., Walker, R., Winberry, L., & Rittenhouse, S. (1987). Pertussis toxin can activate human platelets. Comparative effects of holotoxin and its ADP-ribosylating S1 subunit. *J Biol Chem, 262*, 14871–14874.

Barbieri, J. T., & Cortina, G. (1988). ADP-ribosyltransferase mutations in the catalytic S-1 subunit of pertussis toxin. *Infect Immun*, *56*, 1934–1941. https://doi.org/10.1128/IAI.56.8.1934-1941.1988

Barbieri, J. T., Mende-Mueller, L. M., Rappuoli, R., Collier, A. R. J., Cieplak, W., Burnette, W. N., Locht, C., & Keith, J. (1989). Photolabeling of Glu-129 of the S-1 subunit of pertusis toxin with NAD. *Infect Immun*, *57*, 3549–3554. https://doi.org/10.1128/IAI.57.11.3549-3554.1989

Barbieri, J. T., & Sun, J. (2004). Pseudomonas aeruginosa ExoS and ExoT. *Rev Physiol Biochem Pharmacol, 152*, 79–92. https://doi.org/10.1007/S10254-004-0031-7

Barkoff, A. M., Gröndahl-Yli-Hannuksela, K., & He, Q. (2015). Seroprevalence studies of pertussis: what have we learned from different immunized populations. *Pathog Dis*, *73*, ftv050. https://doi.org/10.1093/FEMSPD/FTV050

Barkoff, A. M., & He, Q. (2019). Molecular Epidemiology of Bordetella pertussis. *Adv Exp Med Biol*, *1183*, 19–33. https://doi.org/10.1007/5584_2019_402

Bartlett, A., Padfield, D., Lear, L., Bendall, R., & Vos, M. (2022). A comprehensive list of bacterial pathogens infecting humans. *Microbiology (Reading)*, *168*. https://doi.org/10.1099/mic.0.001269

Baysarowich, J., Koteva, K., Hughes, D. W., Ejim, L., Griffiths, E., Zhang, K., Junop, M., & Wright, G. D. (2008). Rifamycin antibiotic resistance by ADP-ribosylation: Structure and diversity of Arr. *Proc Natl Acad Sci U S A.*, *105*, 4886–4891. https://doi.org/10.1073/PNAS.0711939105

Beattie, B. K., Prentice, G. A., & Merrill, A. R. (1996). Investigation into the Catalytic Role for the Tryptophan Residues within Domain III of Pseudomonas aeruginosa Exotoxin A. *Biochemistry, 35*, 15134–15142. https://pubs.acs.org/sharingguidelines

Bell, C. E., & Eisenberg, D. (1996). Crystal structure of diphtheria toxin bound to nicotinamide adenine dinucleotide. *Biochemistry, 35*, 1137–1149. https://doi.org/10.1021/BI9520848/ASSET/IMAGES/LARGE/BI9520848F00009.JPEG

Berendsen, H. J. C., Postma, J. P. M., Van Gunsteren, W. F., Dinola, A., & Haak, J. R. (1984). Molecular dynamics with coupling to an external bath. *The Journal of Chemical Physics*, *81*(8), 3684–3690. https://doi.org/10.1063/1.448118

Bokoch, G. M., Katada, T., Northup, J. K., Hewlett, E. L., & Gilman, A. G. (1983). Identification of the Predominant Substrate for ADP-Ribosylation by Islet Activating Protein. *J Biol Chem, 258*, 2072–2075.

Bolivar, J. M., Woodley, J. M., & Fernandez-Lafuente, R. (2022). Is enzyme immobilization a mature discipline? Some critical considerations to capitalize on the benefits of immobilization. *Chem Soc Rev*, *51*, 6251–6290. https://doi.org/10.1039/D2CS00083K

Bouchez, V., Brun, D., Cantinelli, T., Dore, G., Njamkepo, E., & Guiso, N. (2009). First report and detailed characterization of B. pertussis isolates not expressing pertussis toxin or pertactin. *Vaccine*, *27*, 6034–6041. https://doi.org/10.1016/j.vaccine.2009.07.074

Bowers, K. J., Chow, E., Xu, H., Dror, R. O., Eastwood, M. P., Gregersen, B. A., Klepeis, J. L., Kolossvary, I., Moraes, M. A., Sacerdoti, F. D., Salmon, J. K., Shan, Y., & Shaw, D. E. (2006). Scalable algorithms for molecular dynamics simulations on commodity clusters. *Proceedings of the 2006 ACM/IEEE Conference on Supercomputing, SC'06*. https://doi.org/10.1145/1188455.1188544

Bradford, M. M. (1976). A Rapid and Sensitive Method for the Quantitation of Microgram Quantities of Protein Utilizing the Principle of Protein-Dye Binding. *Anal Biochem*, *72*, 248–254.

Bradford WL, Scherp HW, & Tinker MR. (1956). Effect of extracts of Hemophilus pertussis on leukocyte counts in normal and sensitized mice. *Pediatrics*, *18*, 64–71.

Brown, D. R., Keith J. M., Sato H., & Sato Y. (1991). Construction and characterization of genetically inactivated pertussis toxin. *Dev Biol Stand*, *73*, 63–73.

Burnette, W. N., Cieplak, W., Mar, V. L., Kaljot, K. T., Sato, H., & Keith, J. M. (1988). Pertussis Toxin S1 Mutant with Reduced Enzyme Activity and a Conserved Protective Epitope. *Science*, *242*, 72–74. https://doi.org/10.1126/SCIENCE.2459776

Burns DL, Hausman, S., Lindner, W., Robey, F., & Manclark, C. (1987). Structural characterization of pertussis toxin A subunit. *J Biol Chem*, *262*, 17677–17682.

Campbell, P., McIntyre, P., Quinn, H., Hueston, L., Gilbert, G. L., & McVernon, J. (2012). Increased population prevalence of low pertussis toxin antibody levels in young children preceding a record

pertussis epidemic in Australia. *PloS One*, *7*, e35874. https://doi.org/10.1371/JOURNAL.PONE.0035874

Carbonetti, N. H. (2015). Contribution of pertussis toxin to the pathogenesis of pertussis disease. In *Pathog Dis.* (Vol. 73, p. ftv073). https://doi.org/10.1093/femspd/ftv073

Carbonetti, N. H. (2016). Bordetella pertussis: new concepts in pathogenesis and treatment. *Curr Opin Infect Dis*, *29*, 287–294. https://doi.org/10.1097/QCO.0000000000000264

Carbonetti, N. H., Artamonova, G. V., Andreasen, C., Dudley, E., Mays, R. M., & Worthington, Z. E. V. (2004). Suppression of serum antibody responses by pertussis toxin after respiratory tract colonization by Bordetella pertussis and identification of an immunodominant lipoprotein. *Infect Immun*, *72*, 3350–3358. https://doi.org/10.1128/IAI.72.6.3350-3358.2004

Carbonetti, N. H., Artamonova, G. V., Mays, R. M., & Worthington, Z. E. V. (2003). Pertussis toxin plays an early role in respiratory tract colonization by Bordetella pertussis. *Infect Immun*, *71*, 6358–6366. https://doi.org/10.1128/IAI.71.11.6358-6366.2003

Carbonetti, N. H., Artamonova, G. V., Van Rooijen, N., & Ayala, V. I. (2007). Pertussis toxin targets airway macrophages to promote Bordetella pertussis infection of the respiratory tract. *Infect Immun*, *75*, 1713–1720. https://doi.org/10.1128/IAI.01578-06

Casey, P. J., Graziano, M. P., & Gilman, A. G. (1989). G protein beta gamma subunits from bovine brain and retina: equivalent catalytic support of ADP-ribosylation of alpha subunits by pertussis toxin but differential interactions with Gs alpha. *Biochemistry*, *28*, 611–616.

Chaitanya, G. V., Alexander, J. S., & Babu, P. P. (2010). PARP-1 cleavage fragments: signatures of cell-death proteases in neurodegeneration. *Cell Commun Signal*, *8*, 31. https://doi.org/10.1186/1478-811X-8-31

Cherry, J. D. (2016). Pertussis in young infants throughout the world. *Clinical Infectious Diseases*, *63*, S119–S122. https://doi.org/10.1093/cid/ciw550

Choe, S., Bennett, M. J., Fujii, G., Curmi, P. M. G., Kantardjieff, K. A., Collier, R. J., & Eisenberg, D. (1992). The crystal structure of diphtheria toxin. *Nature*, *357*, 216–222. https://doi.org/10.1038/357216A0

Chung, D. W., & Collier, J. (1977). Enzymatically active peptide from the adenosine diphosphate-ribosylating toxin of Pseudomonas aeruginosa. *Infect Immun*, *16*, 832–841. https://doi.org/10.1128/IAI.16.3.832-841.1977

Cieplak, W., Locht, C., Mar, V. L., Burnette$, W. N., Keith, J. M., & Biologicals, K. (1990). Photolabelling of mutant forms of the S1 subunit of pertussis toxin with NAD+. *Biochem. J*, *268*, 547–551.

Clark, M. J., Harrison, C., Zhong, H., Neubig, R. R., & Traynor, J. R. (2003). Endogenous RGS protein action modulates mu-opioid signaling through Galphao. Effects on adenylyl cyclase, extracellular signal-regulated kinases, and intracellular calcium pathways. *J Biol Chem*, *278*, 9418–9425. https://doi.org/10.1074/JBC.M208885200

Cockle, S. A. (1989). Identification of an active-site residue in subunit S1 of pertussis toxin by photocrosslinking to NAD. *FEBS Lett, 249*, 329–332. https://doi.org/10.1016/0014-5793(89)80652-0

Cockle, S., Loosmore, S., Radika, K., Zealey, G., Boux, H., Phillips, K., & Klein, M. (1989). Detoxification of pertussis toxin by site-directed mutagenesis. *Advances in Experimental Medicine and Biology*, *251*, 209–214. https://doi.org/10.1007/978-1-4757-2046-4_20

Cohen, M. S. and Chang, P. (2018). Insights into the biogenesis, function, and regulation of ADP-ribosylation. *Nat Chem Biol*, *14*, 236–243. https://doi.org/10.1038/nchembio.2568

Coleman, D. E., Berghuis, A. M., Lee, E., Linder, M. E., Gilman, A. G., & Sprang, S. R. (1994). Structures of active conformations of Giα1 and the mechanism of GTP hydrolysis. *Science*, *265*, 1405–1412. https://doi.org/10.1126/science.8073283

Connelly, C. E., Sun, Y., & Carbonetti, N. H. (2012). Pertussis toxin exacerbates and prolongs airway inflammatory responses during Bordetella pertussis infection. *Infect Immun*, *80*, 4317–4332. https://doi.org/10.1128/IAI.00808-12

Cortina, G., & Barbieri, J. T. (1989). Role of Tryptophan 26 in the NAD Glycohydrolase Reaction of the S-1 Subunit of Pertussis Toxin. *J Biol Chem*, *264*, 17322–17328. https://doi.org/10.1016/S0021-9258(18)71495-6

Cortina, G., Krueger, K. M., & Barbieri, J. T. (1991). The carboxyl terminus of the S1 subunit of pertussis toxin confers high affinity binding to transducin. *J Biol Chem*, *266*, 23810–23814. https://doi.org/10.1016/S0021-9258(18)54355-6

Croston, G. E. (2017). The utility of target-based discovery. *Expert Opin Drug Discov*, *12*, 427–429. https://doi.org/10.1080/17460441.2017.1308351

Davies, A. H., McGlashan, J., Posner, M. G., Roberts, A. K., Shone, C. C., & Acharya, K. R. (2016). Functional significance of active site residues in the enzymatic component of the Clostridium difficile binary toxin. *Biochem Biophys Rep, 8*, 55–61. https://doi.org/10.1016/j.bbrep.2016.08.011

de Gouw, D., Diavatopoulos, D. A., Bootsma, H. J., Hermans, P. W. M., & Mooi, F. R. (2011). Pertussis: a matter of immune modulation. *FEMS Microbiol Rev*, *35*, 441–474. https://doi.org/10.1111/J.1574-6976.2010.00257.X

De Greeff, S. C., Mooi, F. R., Westerhof, A., Verbakel, J. M. M., Peeters, M. F., Heuvelman, C. J., Notermans, D. W., Elvers, L. H., Schellekens, J. F. P., & De Melker, H. E. (2010). Pertussis disease burden in the household: how to protect young infants. *Clin Infect Dis, 50*, 1339–1345. https://doi.org/10.1086/652281

Decker, M. D., & Edwards, K. M. (2021). Pertussis (Whooping Cough). *Journal of Infectious Diseases*, *224*, S310–S320. https://doi.org/10.1093/infdis/jiaa469

Diard, M., & Hardt, W. D. (2017). Evolution of bacterial virulence. *FEMS Microbiol Rev*, *41*, 679–697. https://doi.org/10.1093/FEMSRE/FUX023

Diavatopoulos, D. A., Cummings, C. A., Schouls, L. M., Brinig, M. M., Relman, D. A., & Mooi, F. R. (2005). Bordetella pertussis, the causative agent of whooping cough, evolved from a distinct, human-associated lineage of B. bronchiseptica. *PLoS Pathog, 1*, e45. https://doi.org/10.1371/journal.ppat.0010045

Domenighini, M., & Rappuoli, R. (1996). Three conserved consensus sequences identify the NAD-binding site of ADP-ribosylating enzymes, expressed by eukaryotes, bacteria and T-even bacteriophages. *Mol Microbiol*, *21*, 667–674. https://doi.org/10.1046/j.1365-2958.1996.321396.x

Duan, Q., Xia, P., Nandre, R., Zhang, W., & Zhu, G. (2019). Review of Newly Identified Functions Associated With the Heat-Labile Toxin of Enterotoxigenic Escherichia coli. *Front Cell Infect Microbiol., 9*, 292. https://doi.org/10.3389/FCIMB.2019.00292

Elahi, S., Brownlie, R., Korzeniowski, J., Buchanan, R., O'Connor, B., Peppler, M. S., Halperin, S. A., Lee, S. F., Babiuk, L. A., & Gerdts, V. (2005). Infection of newborn piglets with Bordetella pertussis: a new model for pertussis. *Infect Immun*, *73*, 3636–3645. https://doi.org/10.1128/IAI.73.6.3636-3645.2005

Ernst, K. (2022). Novel Strategies to Inhibit Pertussis Toxin. *Toxins (Basel)*, *14*, 187. https://doi.org/10.3390/toxins14030187

Ernst, K., Eberhardt, N., Mittler, A.-K., Sonnabend, M., Anastasia, A., Freisinger, S., Schiene-Fischer, C., Maleševi´c, M. M., & Barth, H. (2018a). Pharmacological Cyclophilin Inhibitors Prevent Intoxication of Mammalian Cells with Bordetella pertussis Toxin. *Toxins (Basel)*, *10*, 181. https://doi.org/10.3390/toxins10050181

Ernst, K., Kling, C., Landenberger, M., & Barth, H. (2018b). Combined Pharmacological Inhibition of Cyclophilins, FK506-Binding Proteins, Hsp90, and Hsp70 Protects Cells From Clostridium botulinum C2 Toxin. *Front Pharmacol, 9*, 1287. https://doi.org/10.3389/fphar.2018.01287

Ernst, K., Langer, S., Kaiser, E., Osseforth, C., Michaelis, J., Popoff, M. R., Schwan, C., Aktories, K., Kahlert, V., Malesevic, M., Schiene-Fischer, C., & Barth, H. (2015). Cyclophilin-facilitated membrane translocation as pharmacological target to prevent intoxication of mammalian cells by binary clostridial actin ADP-ribosylated toxins. *J Mol Biol, 427*, 1224–1238. https://doi.org/10.1016/J.JMB.2014.07.013

Ernst, K., Liebscher, M., Mathea, S., Granzhan, A., Schmid, J., Popoff, M. R., Ihmels, H., Barth, H., & Schiene-Fischer, C. (2016). A novel Hsp70 inhibitor prevents cell intoxication with the actin ADP-ribosylating Clostridium perfringens iota toxin. *Sci Rep, 6*, 20301. https://doi.org/10.1038/srep20301

Ernst, K., Mittler, A. K., Winkelmann, V., Kling, C., Eberhardt, N., Anastasia, A., Sonnabend, M., Lochbaum, R., Wirsching, J., Sakari, M., Pulliainen, A. T., Skerry, C., Carbonetti, N. H., Frick, M., & Barth, H. (2021). Pharmacological targeting of host chaperones protects from pertussis toxin in vitro and in vivo. *Sci Rep, 11*, 5429. https://doi.org/10.1038/s41598-021-84817-2

Ernst, K., Schmid, J., Beck, M., Hägele, M., Hohwieler, M., Hauff, P., Ückert, A. K., Anastasia, A., Fauler, M., Jank, T., Aktories, K., Popoff, M. R., Schiene-Fischer, C., Kleger, A., Müller, M., Frick, M., & Barth, H. (2017a). Hsp70 facilitates trans-membrane transport of bacterial ADP-ribosylating toxins into the cytosol of mammalian cells. *Sci Rep*, *7*, 2724. https://doi.org/10.1038/s41598-017-02882-y

Ernst, K., Schnell, L., & Barth, H. (2017b). Host cell chaperones Hsp70/Hsp90 and peptidyl-prolyl cis/trans isomerases are required for the membrane translocation of bacterial ADP-ribosylating toxins. *Curr Top Microbiol Immunol, 406*, 163–198. https://doi.org/10.1007/82_2016_14/COVER

Evans, H. R., Sutton, J. M., Holloway, D. E., Ayriss, J., Shone, C. C., & Acharya, K. R. (2003). The crystal structure of C3stau2 from Staphylococcus aureus and its complex with NAD. *J Biol Chem*, *278*, 45924–45930. https://doi.org/10.1074/JBC.M307719200

Ferro, A. M., & Oppenheimer, N. J. (1978). Structure of a poly(adenosine diphosphoribose) monomer: 2'-(5"-Phosphoribosyl)-5'-adenosine monophosphate. *Proc Natl Acad Sci U S A*, *75*, 809–813.

Fieldhouse, R. J., & Merrill, A. R. (2008). Needle in the haystack: structure-based toxin discovery. *Trends Biochem Sci*, *33*, 546–556. https://doi.org/10.1016/j.tibs.2008.08.003

Fieldhouse, R. J., Turgeon, Z., White, D., & Rod Merrill, A. (2010). Cholera- and anthrax-like toxins are among several new ADP-Ribosyltransferases. *PLoS Comput Biol, 6*, e1001029. https://doi.org/10.1371/journal.pcbi.1001029

Finck-Barbançon, V., & Barbieri, J. T. (1996). Preferential processing of the S1 subunit of pertussis toxin that is bound to eukaryotic cells. *Mol Microbiol*, *22*(1), 87–95. https://doi.org/10.1111/J.1365-2958.1996.TB02658.X

Fischer, S., Ückert, A. K., Landenberger, M., Papatheodorou, P., Hoffmann-Richter, C., Mittler, A. K., Ziener, U., Hägele, M., Schwan, C., Müller, M., Kleger, A., Benz, R., Popoff, M. R., Aktories, K., & Barth, H. (2020). Human peptide α-defensin-1 interferes with Clostridioides difficile toxins TcdA, TcdB, and CDT. *FASEB J*, *34*, 6244–6261. https://doi.org/10.1096/FJ.201902816R

Franconetti, A., Ardá, A., Asensio, J. L., Blériot, Y., Thibaudeau, S., & Jiménez-Barbero, J. (2021). Glycosyl Oxocarbenium Ions: Structure, Conformation, Reactivity, and Interactions. *Acc Chem Res*, *54*, 2552–2564. https://doi.org/10.1021/acs.accounts.1c00021

Friesner, R. A., Banks, J. L., Murphy, R. B., Halgren, T. A., Klicic, J. J., Mainz, D. T., Repasky, M. P., Knoll, E. H., Shelley, M., Perry, J. K., Shaw, D. E., Francis, P., & Shenkin, P. S. (2004). Glide: A New Approach for Rapid, Accurate Docking and Scoring. 1. Method and Assessment of Docking Accuracy. *J Med Chem*, *47*, 1739–1749. https://doi.org/10.1021/JM0306430/SUPPL_FILE/JM0306430_S.PDF

Garcia, J. G. N., Wang, P., Liu, F., Hershenson, M. B., Borbiev, T., & Verin, A. D. (2001). Pertussis toxin directly activates endothelial cell p42/p44 MAP kinases via a novel signaling pathway. *Am J Physiol Cell Physiol*, *280*. https://doi.org/10.1152/AJPCELL.2001.280.5.C1233

Gehrig, P. M., Nowak, K., Panse, C., Leutert, M., Grossmann, J., Schlapbach, R., & Hottiger, M. O. (2021). Gas-Phase Fragmentation of ADP-Ribosylated Peptides: Arginine-Specific Side-Chain Losses and Their Implication in Database Searches. *Journal of the American Society for Mass Spectrometry*, *32*(1), 157–168. https://doi.org/10.1021/JASMS.0C00040

Gharehbaghi, K., Paull, K. D., Kelley, J. A., Barchi, J. J., Marquez, V. E., Cooney, D. A., Monks, A., Scudiero, D., Krohn, K., & Jayaram, H. N. (1994). Cytotoxicity and characterization of an active metabolite of benzamide riboside, a novel inhibitor of IMP dehydrogenase. *Int J Cancer*, *56*, 892–899. https://doi.org/10.1002/IJC.2910560623

Giesemann, T., Guttenberg, G., & Aktories, K. (2008). Human alpha-defensins inhibit Clostridium difficile toxin B. *Gastroenterology*, *134*, 2049–2058. https://doi.org/10.1053/J.GASTRO.2008.03.008

Gillespie, E. J., Ho, C. L. C., Balaji, K., Clemens, D. L., Deng, G., Wang, Y. E., Elsaesser, H. J., Tamilselvam, B., Gargi, A., Dixon, S. D., France, B., Chamberlain, B. T., Blanke, S. R., Cheng, G., De La Torre, J. C., Brooks, D. G., Jung, M. E., Colicelli, J., Damoiseaux, R., & Bradley, K. A. (2013). Selective inhibitor of endosomal trafficking pathways exploited by multiple toxins and viruses. *Proc Natl Acad Sci U S A*, *110*. https://doi.org/10.1073/PNAS.1302334110/-/DCSUPPLEMENTAL/PNAS.201302334SI.PDF

Gillet, D., & Barbier, J. (2015). Diphtheria Toxin. In *The Comprehensive Sourcebook of Bacterial Protein Toxins.* (pp. 111–132).

Gray, L., Huber, K., Gray, M., Hewlett, E., & Engelhard, V. (1989). Pertussis toxin effects on T lymphocytes are mediated through CD3 and not by pertussis toxin catalyzed modification of a G protein. *J Immunol, 142*, 1631–1638.

Greenberg, M., Kuo, D., Jankowsky, E., Long, L., Hager, C., Bandi, K., Ma, D., Manoharan, D., Shoham, Y., Harte, W., Ghannoum, M. A., & Shoham, M. (2018). Small-molecule AgrA inhibitors F12 and F19 act as antivirulence agents against Gram-positive pathogens. *Sci Rep*, *8*. https://doi.org/10.1038/S41598-018-32829-W

Guillot, S., Descours, G., Gillet, Y., Etienne, J., Floret, D., & Guiso, N. (2012). Macrolide-resistant Bordetella pertussis infection in newborn girl, France. *Emerg Infect Dis*, *18*, 966–968. https://doi.org/10.3201/EID1806.120091

Gupta, P. K., Liu, S., Batavia, M. P., & Leppla, S. H. (2008). The diphthamide modification on elongation factor-2 renders mammalian cells resistant to ricin. *Cell Microbiol, 10*, 1687–1694. https://doi.org/10.1111/J.1462-5822.2008.01159.X

Hall, E., Parton, R., & Wardlaw, A. C. (1994). Cough production, leucocytosis and serology of rats infected intrabronchially with Bordetella pertussis. *J Med Microbiol, 40*, 205–213.

Hall E, Wodi AP, Hamborsky J, Morelli V, & Schillie S. (2021). Centers for Disease Control and Prevention. Epidemiology and Prevention of Vaccine-Preventable Diseases. In *Pinkbook* (14th ed.). Public Health Foundation. http://bookstore.phf.org/.http://www.cdc.gov/vaccines/pubs/pinkbook/index.html.

Han, S., & Tainer, J. A. (2002). The ARTT motif and a unified structural understanding of substrate recognition in ADP-ribosylating bacterial toxins and eukaryotic ADP-ribosyltransferases. *Int. J. Med. Microbiol*, *291*, 523–529. http://www.urbanfischer.de/journals/ijmm

Harder, E., Damm, W., Maple, J., Wu, C., Reboul, M., Xiang, J. Y., Wang, L., Lupyan, D., Dahlgren, M. K., Knight, J. L., Kaus, J. W., Cerutti, D. S., Krilov, G., Jorgensen, W. L., Abel, R., & Friesner, R. A. (2016). OPLS3: A Force Field Providing Broad Coverage of Drug-like Small Molecules and Proteins. *J Chem Theory Comput*, *12*, 281–296. https://doi.org/10.1021/ACS.JCTC.5B00864

Hartmann, S., Lopez Cruz, R., Alameh, S., Ho, C. L. C., Rabideau, A., Pentelute, B. L., Bradley, K. A., & Martchenko, M. (2018). Characterization of Novel Piperidine-Based Inhibitor of Cathepsin B-Dependent Bacterial Toxins and Viruses. *ACS Infect Dis*, *4*, 1235–1245. https://doi.org/10.1021/ACSINFECDIS.8B00053

Hausman, S. Z., & Burns, D. L. (1993). Binding of Pertussis Toxin to Lipid Vesicles Containing Glycolipids. *Infect Immun*, *61*, 335–337.

Hazes, B., Boodhoo, A., Cockle, S. A., & Read, R. J. (1996). Crystal Structure of the Pertussis Toxin-ATP Complex: A Molecular Sensor. *J. Mol. Biol*, *258*, 661–671.

Hedge, D. D., Strain, J. D., Heins, J. R., & Farver, D. K. (2008). New advances in the treatment of Clostridium difficile infection (CDI). *Ther Clin Risk Manag*, *4*, 949–964. https://doi.org/10.2147/TCRM.S3145

Hewitt, M., & Canning, B. J. (2010). Coughing precipitated by Bordetella pertussis infection. *Lung*, *188 Suppl 1*, S73-9. https://doi.org/10.1007/S00408-009-9196-9

Hinds, P. 2nd, Yin, C., Salvato, M., & Pauza, C. (1996). Pertussis toxin induces lymphocytosis in rhesus macaques. *J Med Primatol*, *25*, 375–381. https://doi.org/10.1111/J.1600-0684.1996.TB00032.X

Holbourn, K. P., Shone, C. C., & Acharya, K. R. (2006). A family of killer toxins. Exploring the mechanism of ADP-ribosylating toxins. *FEBS J*, *273*, 4579–4593. https://doi.org/10.1111/j.1742-4658.2006.05442.x

Hottiger, M. O., Hassa, P. O., Lüscher, B., Schüler, H., & Koch-Nolte, F. (2010b). Toward a unified nomenclature for mammalian ADP-ribosyltransferases. *Trends Biochem Sci., 35*, 208–219. https://doi.org/10.1016/j.tibs.2009.12.003

Hsia, J. A., Tsai, S.-C., Adamik, R., Yost, D. A., Hewlett, E. L., & Moss, J. (1985). Amino acid-specific ADP-ribosylation. Sensitivity to hydroxylamine of [cysteine(ADP-ribose)]protein and [arginine(ADP-ribose)]protein linkages. *J Biol Chem, 260*, 16187–16191.

Jiang, W., Wei, C., Mou, D., Zuo, W., Liang, J., Ma, X., Wang, L., Gao, N., Gu, Q., Luo, P., Ma, Y., Li, J., Liu, S., Shi, L., & Sun, M. (2021). Infant rhesus macaques as a non-human primate model of Bordetella pertussis infection. *BMC Infect Dis*, *21*. https://doi.org/10.1186/s12879-021-06090-y

Jiang, Y., Li, Y., Zhang, Y., Hu, D., Zhang, S., Wang, C., Huang, S., Zhang, A., Jia, Z., & You, R. (2023). NSC228155 alleviates septic cardiomyopathy via protecting mitochondria and inhibiting inflammation. *Int Immunopharmacol*, *116*, 109847. https://doi.org/10.1016/J.INTIMP.2023.109847

Jin, J., Hsieh, Y. H., Cui, J., Damera, K., Dai, C., Chaudhary, A. S., Zhang, H., Yang, H., Cao, N., Jiang, C., Vaara, M., Wang, B., & Tai, P. C. (2016). Using Chemical Probes to Assess the Feasibility of Targeting SecA for Developing Antimicrobial Agents against Gram-Negative Bacteria. *ChemMedChem*, *11*, 2511–2521. https://doi.org/10.1002/CMDC.201600421

Jørgensen, R., Merrill, A. R., & Andersen, G. R. (2006). The life and death of translation elongation factor 2. *Biochem Soc Trans*, *34*, 1–6. https://doi.org/10.1042/BST20060001

Jørgensen, R., Merrill, A. R., Yates, S. P., Marquez, V. E., Schwan, A. L., Boesen, T., & Andersen, G. R. (2005). Exotoxin A-eEF2 complex structure indicates ADP ribosylation by ribosome mimicry. *Nature*, *436*, 979–984. https://doi.org/10.1038/nature03871

Jørgensen, R., Purdy, A. E., Fieldhouse, R. J., Kimber, M. S., Bartlett, D. H., & Merrill, A. R. (2008). Cholix toxin, a novel ADP-ribosylating factor from Vibrio cholerae. *J Biol Chem*, *283*(16), 10671–10678. https://doi.org/10.1074/jbc.M710008200

Jørgensen, R., Wang, Y., Visschedyk, D., & Merrill, A. R. (2008). The nature and character of the transition state for the ADP-ribosyltransferase reaction. *EMBO Rep*, *9*, 802–809. https://doi.org/10.1038/embor.2008.90

Jumper, J., Evans, R., Pritzel, A., Green, T., Figurnov, M., Ronneberger, O., Tunyasuvunakool, K., Bates, R., Žídek, A., Potapenko, A., Bridgland, A., Meyer, C., Kohl, S. A. A., Ballard, A. J., Cowie, A., Romera-Paredes, B., Nikolov, S., Jain, R., Adler, J., … Hassabis, D. (2021). Highly accurate protein structure prediction with AlphaFold. *Nature*, *596*(7873), 583–589. https://doi.org/10.1038/S41586-021-03819-2

Kaiser, E., Böhm, N., Ernst, K., Langer, S., Schwan, C., Aktories, K., Popoff, M., Fischer, G., & Barth, H. (2012). FK506-binding protein 51 interacts with Clostridium botulinum C2 toxin and FK506 inhibits membrane translocation of the toxin in mammalian cells. *Cell Microbiol*, *14*, 1193–1205. https://doi.org/10.1111/j.1462-5822.2012.01788.x

Kaiser, E., Kroll, C., Ernst, K., Schwan, C., Popoff, M., Fischer, G., Buchner, J., Aktories, K., & Barth, H. (2011). Membrane translocation of binary actin-ADP-ribosylating toxins from Clostridium difficile and Clostridium perfringens Is facilitated by Cyclophilin A and Hsp90. *Infect Immun*, *79*(10), 3913–3921. https://doi.org/10.1128/IAI.05372-11

Kandel, J., Collier, R. J., & Chung, D. W. (1974). Interaction of Fragment A from Diphtheria Toxin with Nicotinamide Adenine Dinucleotide. *J Biol Chem*, *249*, 2088–2097.

Kashyap, A., Singh, P. K., & Silakari, O. (2018). Counting on Fragment Based Drug Design Approach for Drug Discovery. *Curr Top Med Chem*, *18*, 2284–2293. https://doi.org/10.2174/1568026619666181130134250

Katada, T., Oinuma, M., & Ui, M. (1986). Two guanine nucleotide-binding proteins in rat brain serving as the specific substrate of islet-activating protein, pertussis toxin. Interaction of the α-subunits

with βγ-subunits in development of their biological activities. *J Biol Chem*, *261*, 8182–8191. https://doi.org/10.1016/s0021-9258(19)83894-2

Katada, T., & Ui, M. (1980). Slow interaction of islet-activating protein with pancreatic islets during primary culture to cause reversal of alpha-adrenergic inhibition of insulin secretion. *J Biol Chem, 255*, 9580–9588.

Katada, T., & Ui, M. (1982). Direct modification of the membrane adenylate cyclase system by islet-activating protein due to ADP-ribosylation of a membrane protein. *Proc Natl Acad Sci U S A, 79*, 3129–3133. https://doi.org/10.1073/PNAS.79.10.3129

Kellner, A., Taylor, M., Banerjee, T., Christopher, |, Britt, B. T., Teter, K., & Address, P. (2019). A binding motif for Hsp90 in the A chains of ADP-ribosylating toxins that move from the endoplasmic reticulum to the cytosol. *Cell Microbiol, 21*, e13074. https://doi.org/10.1111/cmi.13074

Kilgore, P. E., Salim, A. M., Zervos, M. J., & Schmitt, H. J. (2016). Pertussis: Microbiology, disease, treatment, and prevention. *Clin Microbiol Rev, 29*, 449–486. https://doi.org/10.1128/CMR.00083-15

Kim, C., Gajendran, N., Mittrücker, H. W., Weiwad, M., Song, Y. H., Hurwitz, R., Wilmanns, M., Fischer, G., & Kaufmann, S. H. E. (2005). Human α-defensins neutralize anthrax lethal toxin and protect against its fatal consequences. *Proc Natl Acad Sci U S A*, *102*(13), 4830–4835. https://doi.org/10.1073/PNAS.0500508102

Kirimanjeswara, G. S., Agosto, L. M., Kennett, M. J., Bjornstad, O. N., & Harvill, E. T. (2005). Pertussis toxin inhibits neutrophil recruitment to delay antibody-mediated clearance of Bordetella pertussis. *J Clin Invest*, *115*, 3594–3601. https://doi.org/10.1172/JCI24609

Klimova, N., Holubova, J., Streparola, G., Tomala, J., Brazdilova, L., Stanek, O., Bumba, L., & Sebo, P. (2022). Pertussis toxin suppresses dendritic cell-mediated delivery of B. pertussis into lung-draining lymph nodes. *PLoS Pathog*, *18*, e1010577. https://doi.org/10.1371/JOURNAL.PPAT.1010577

Kling, C., Pulliainen, A. T., Barth, H., & Ernst, K. (2021). Human Peptides α-Defensin-1 and -5 Inhibit Pertussis Toxin. *Toxins (Basel)*, *13*(7), 480. https://doi.org/10.3390/toxins13070480

Korbmacher, M., Fischer, S., Landenberger, M., Papatheodorou, P., Aktories, K., & Barth, H. (2020). Human α-Defensin-5 Efficiently Neutralizes Clostridioides difficile Toxins TcdA, TcdB, and CDT. *Front Pharmacol*, *11*, 1204. https://doi.org/10.3389/FPHAR.2020.01204/BIBTEX

Krueger, K. M., & Barbieri, J. T. (1994). Assignment of Functional Domains Involved in ADP-Ribosylation and B-Oligomer Binding within the Carboxyl Terminus of the SI Subunit of Pertussis Toxin. *Infect Immun*, *62*, 2071–2078.

Krueger, K. M., & Barbieri, J. T. (1995). The Family of Bacterial ADP-Ribosylating Exotoxins. *Clin Microbiol Rev.*, *8*, 34–47. http://cmr.asm.org/

Kudryashova, E., Quintyn, R., Seveau, S., Lu, W., Wysocki, V. H., & Kudryashov, D. S. (2014). Human defensins facilitate local unfolding of thermodynamically unstable regions of bacterial protein toxins. *Immunity*, *41*, 709–721. https://doi.org/10.1016/J.IMMUNI.2014.10.018

Kudryashova, E., Seveau, S. M., & Kudryashov, D. S. (2017). Targeting and inactivation of bacterial toxins by human defensins. *Biol Chem*, *398*, 1069–1085. https://doi.org/10.1515/HSZ-2017-0106

Lang, A. E., Schmidt, G., Schlosser, A., Hey, T. D., Larrinua, I. M., Sheets, J. J., Mannherz, H. G., & Aktories, K. (2010). Photorhabdus luminescens toxins ADP-ribosylate actin and RhoA to force actin clustering. *Science*, *327*, 1139–1142. https://doi.org/10.1126/SCIENCE.1184557

Langelier, M. F., Zandarashvili, L., Aguiar, P. M., Black, B. E., & Pascal, J. M. (2018). NAD+ analog reveals PARP-1 substrate-blocking mechanism and allosteric communication from catalytic center to DNA-binding domains. *Nat Commun*, *9*, 844. https://doi.org/10.1038/s41467-018-03234-8

Leaney, J. L., & Tinker, A. (2000). The role of members of the pertussis toxin-sensitive family of G proteins in coupling receptors to the activation of the G protein-gated inwardly rectifying potassium channel. *Proc Natl Acad Sci U S A*, *97*, 5651–5656. https://doi.org/10.1073/PNAS.080572297

Lee, H. Y., Kim, S. D., Shim, J. W., Kim, H. J., Yun, J., Baek, S. H., Kim, K., & Bae, Y. S. (2010). A pertussis toxin sensitive G-protein-independent pathway is involved in serum amyloid A-induced formyl peptide receptor 2-mediated CCL2 production. *Exp Mol Med, 42*, 302–309. https://doi.org/10.3858/EMM.2010.42.4.029

Li, H., & Wong, W. S. F. (2001). Pertussis toxin activates tyrosine kinase signaling cascade in myelomonocytic cells: a mechanism for cell adhesion. *Biochem Biophys Res Commun, 283*, 1077–1082. https://doi.org/10.1006/BBRC.2001.4910

Li, Y., Jiang, Y., Zhou, W., Wu, Y., Zhang, S., Ding, G., Zhang, Y., Zhang, A., Huang, S., Jia, Z., & You, R. (2022). Maintaining homeostasis of mitochondria and endoplasmic reticulum with NSC228155 alleviates cisplatin-induced acute kidney injury. *Free Radic Biol Med*, *181*, 270–287. https://doi.org/10.1016/J.FREERADBIOMED.2022.02.003

Littler, D. R., Ang, S. Y., Moriel, D. G., Kocan, M., Kleifeld, O., Johnson, M. D., Tran, M. T., Paton, A. W., Paton, J. C., Summers, R. J., Schembri, M. A., Rossjohn, J., & Beddoe, T. (2017). Structure-function analyses of a pertussis-like toxin from pathogenic Escherichia coli reveal a distinct mechanism of inhibition of trimeric G-proteins. *J Biol Chem*, *292*, 15143–15158. https://doi.org/10.1074/JBC.M117.796094

Llosa, M., Roy, C., & Dehio, C. (2009). Bacterial type IV secretion systems in human disease. *Mol Microbiol, 73*, 141–151. https://doi.org/10.1111/j.1365-2958.2009.06751.x

Lobban, M. D., Irons, L. I., & van Heyningen, S. (1991). Binding of NAD+ to pertussis toxin. *Biochim Biophys Acta*, *1078*, 155–160. https://doi.org/10.1016/0167-4838(91)99004-C

Lobet, Y., Feron, C., Dequesne, G., Sirnoen, E., Hauser, P., & Locht, C. (1993). Site-specific alterations in the B oligomer that affect receptor-binding activities and mitogenicity of pertussis toxin. *J Exp Med*, *177*, 79–87. https://doi.org/10.1084/JEM.177.1.79

Locht, C. (2023). Pasteurian Contributions to the Study of Bordetella pertussis Toxins. *Toxins (Basel)*, *15*, 176. https://doi.org/10.3390/toxins15030176

Locht, C., & Antoine, R. (1995). A proposed mechanism of ADP-ribosylation catalyzed by the pertussis toxin S1 subunit NAD-glycohydrolase / enzyme mechanism. *Biochimie*, *77*, 333–340.

Locht, C., & Antoine, R. (2021). The History of Pertussis Toxin. *Toxins (Basel)*. *13*, 623. doi: 10.3390/toxins13090623.

Locht, C., Antoine, R., & Jacob-Dubuisson, F. (2001). Bordetella pertussis, molecular pathogenesis under multiple aspects. *Curr Opin Microbiol, 4*, 82–89. https://doi.org/10.1016/S1369-5274(00)00169-7

Locht, C., Capiau, C., & Feron, C. (1989). Identification of amino acid residues essential for the enzymatic activities of pertussis toxin. *Proc Natl Acad Sci U S A*, *86*, 3075. https://doi.org/10.1073/PNAS.86.9.3075

Locht, C., Cieplak, W., Marchito, K. S., Sato, H., & Keith, J. M. (1987). Activities of complete and truncated forms of pertussis toxin subunits S1 and S2 synthesized by Escherichia coli. *Infect Immun*, *55*(11), 2546–2553. https://doi.org/10.1128/IAI.55.11.2546-2553.1987

Locht C, Coutte L, Mielcarek N (2011). The ins and outs of pertussis toxin. *FEBS J*, *278*, 4668-82. doi: 10.1111/j.1742-4658.2011.08237.x.

Locht, C., Lobet, Y., Feron, C., Cieplak, W., & Keith, J. M. (1990). The role of cysteine 41 in the enzymatic activities of the pertussis toxin S1 subunit as investigated by site-directed mutagenesis. *J Biol Chem, 265*, 4552–4559. https://doi.org/10.1016/S0021-9258(19)39598-5

Loosmore, S., Zealey, G., Cockle, S., Boux, H., Chong, P., Yacoob, R., & Klein, M. (1993). Characterization of pertussis toxin analogs containing mutations in B-oligomer subunits. *Infect Immun*, *61*, 2316–2324. https://doi.org/10.1128/IAI.61.6.2316-2324.1993

Lu, C., Wu, C., Ghoreishi, D., Chen, W., Wang, L., Damm, W., Ross, G. A., Dahlgren, M. K., Russell, E., Von Bargen, C. D., Abel, R., Friesner, R. A., & Harder, E. D. (2021). OPLS4: Improving Force Field Accuracy on Challenging Regimes of Chemical Space. *J Chem Theory Comput*, *17*, 4291–4300. https://doi.org/10.1021/ACS.JCTC.1C00302

Lüscher, B., Bütepage, M., Eckei, L., Krieg, S., Verheugd, P., & Shilton, B. H. (2018). ADP-Ribosylation, a Multifaceted Posttranslational Modification Involved in the Control of Cell Physiology in Health and Disease. *Chem Rev*, *118*, 1092–1136. https://doi.org/10.1021/ACS.CHEMREV.7B00122

Lyons, B., Ravulapalli, R., Lanoue, J., Lugo, M. R., Dutta, D., Carlin, S., & Merrill, A. R. (2016). Scabin, a Novel DNA-acting ADP-ribosyltransferase from Streptomyces scabies. *J Biol Chem*, *291*(21), 11198–11215. https://doi.org/10.1074/JBC.M115.707653

Markossian, S., Ang, K. K., Wilson, C. G., & Arkin, M. R. (2018). Small-Molecule Screening for Genetic Diseases. *Annu Rev Genomics Hum Genet*, *19*, 263–288. https://doi.org/10.1146/annurev-genom-083117

Martyna, G. J., Klein, M. L., & Tuckerman, M. (1992). Nosé–Hoover chains: The canonical ensemble via continuous dynamics. *J Chem Phys*, *97*, 2635–2643. https://doi.org/10.1063/1.463940

Martyna, G. J., Tobias, D. J., & Klein, M. L. (1994). Constant pressure molecular dynamics algorithms. *J Chem Phys*, *101*, 4177–4189. https://doi.org/10.1063/1.467468

Mateyak, M. K., & Kinzy, T. G. (2013). ADP-ribosylation of translation elongation factor 2 by diphtheria toxin in yeast inhibits translation and cell separation. *J Biol Chem*, *288*, 24647–24655. https://doi.org/10.1074/JBC.M113.488783

McCarthy, M., Goncalves, M., Powell, H., Morey, B., Turner, M., & Merrill, A. R. (2021). A Structural Approach to Anti-Virulence: A Discovery Pipeline. *Microorganisms*, *9*, 2514. https://doi.org/10.3390/MICROORGANISMS9122514

Melvin, J. A., Scheller, E. V., Miller, J. F., & Cotter, P. A. (2014). Bordetella pertussis pathogenesis: Current and future challenges. *Nat Rev Microbiol*. 12(4), 274-88. doi: 10.1038/nrmicro3235.

Ménétrey, J., Flatau, G., Boquet, P., Ménez, A., & Stura, E. A. (2008). Structural basis for the NAD-hydrolysis mechanism and the ARTT-loop plasticity of C3 exoenzymes. *Protein Sci, 17*, 878–886. https://doi.org/10.1110/PS.073398508

Miettinen, M., Vedantham, M., & Pulliainen, A. T. (2019). Host poly(ADP-ribose) polymerases (PARPs) in acute and chronic bacterial infections. *Microbes Infect*, *21*(10), 423–431. https://doi.org/10.1016/J.MICINF.2019.06.002

Mikolčević, P., Hloušek-Kasun, A., Ahel, I., & Mikoč, A. (2021). ADP-ribosylation systems in bacteria and viruses. *Comput Struct Biotechnol J,19*, 2366-2383.

doi: 10.1016/j.csbj.2021.04.023.

Mixon, M. B., Lee, E., Coleman, D. E., Berghuis, A. M., Gilman, A. G., & Sprang, S. R. (1995). Tertiary and quaternary structural changes in Gi alpha 1 induced by GTP hydrolysis. *Science*, *270*, 954–960. https://doi.org/10.1126/SCIENCE.270.5238.954

Moayeri, M., Leppla, S. H., Vrentas, C., Pomerantsev, A. P., & Liu, S. (2015). Anthrax Pathogenesis. *Annu Rev Microbiol*, *69*, 185–208. https://doi.org/10.1146/ANNUREV-MICRO-091014-104523

Moffat, J. G., Vincent, F., Lee, J. A., Eder, J., & Prunotto, M. (2017). Opportunities and challenges in phenotypic drug discovery: an industry perspective. *Nat Rev Drug Discov*, *16*, 531–543. https://doi.org/10.1038/NRD.2017.111

Mooi, F. R., Hallander, H., Wirsing Von König, C. H., Hoet, B., & Guiso, N. (2000). Epidemiological typing of Bordetella pertussis isolates: recommendations for a standard methodology. *Eur J Clin Microbiol Infect Dis*, *19*, 174–181. https://doi.org/10.1007/S100960050455

Morse, S., & Morse, J. (1976). Isolation and properties of the leukocytosis- and lymphocytosis-promoting factor of Bordetella pertussis. *J Exp Med, 143*, 1483–1502.

Mosmann, T. (1983). Rapid colorimetric assay for cellular growth and survival: application to proliferation and cytotoxicity assays. *J Immunol Methods*, *65*(1–2), 55–63. https://doi.org/10.1016/0022-1759(83)90303-4

Moss, J., Garrison, S., Oppenheimer, N. J., & Richardson, S. H. (1979). NAD-dependent ADP-ribosylation of arginine and proteins by Escherichia coli heat-labile enterotoxin. *J Biol Chem*, *254*(14), 6270–6272. https://doi.org/10.1016/s0021-9258(18)50358-6

Moss, J., Stanley, S. J., Burns, D. L., Hsia, J. A., Yost, D. A., Myers, G. A., & Hewlett, E. L. (1983). Activation by thiol of the latent NAD glycohydrolase and ADP-ribosyltransferase activities of Bordetella pertussis toxin (islet-activating protein). *J Biol Chem*, *258*, 11879–11882. https://doi.org/10.1016/s0021-9258(17)44314-6

Müller-Wieland, D., White, M. F., Behnke, B., Gebhardt, A., Neumann, S., Krone, W., & Kahn, C. R. (1991). Pertussis toxin inhibits autophosphorylation and activation of the insulin receptor kinase. *Biochem Biophys Res Commun, 181*, 1479–1485. https://doi.org/10.1016/0006-291X(91)92106-T

Munoz, J. J., Arai, H., Bergman, R. K., & Sadowski, P. L. (1981). Biological activities of crystalline pertussigen from Bordetella pertussis. *Infect Immunol*, *33*, 820–826. https://doi.org/10.1128/IAI.33.3.820-826.1981

Nakano, T., Matsushima-Hibiya, Y., Yamamoto, M., Takahashi-Nakaguchi, A., Fukuda, H., Ono, M., Takamura-Enya, T., Kinashi, H., & Totsuka, Y. (2013). ADP-ribosylation of guanosine by SCO5461 protein secreted from Streptomyces coelicolor. *Toxicon*, *63*(1), 55–63. https://doi.org/10.1016/J.TOXICON.2012.11.019

Narwal, M., Fallarero, A., Vuorela, P., & Lehtiö, L. (2012). Homogeneous screening assay for human tankyrase. *J Biomol Screen*, *17*(5), 593–604. https://doi.org/10.1177/1087057112436558

Nguyen, A. W., DiVenere, A. M., Papin, J. F., Connelly, S., Kaleko, M., & Maynard, J. A. (2020). Neutralization of pertussis toxin by a single antibody prevents clinical pertussis in neonatal baboons. *Sci Adv*, *6*, eaay9258. https://doi.org/10.1126/SCIADV.AAY9258

Nguyen, A. W., Wagner, E. K., Laber, J. R., Goodfield, L. L., Smallridge, W. E., Harvill, E. T., Papin, J. F., Wolf, R. F., Padlan, E. A., Bristol, A., Kaleko, M., & Maynard, J. A. (2015a). A cocktail of humanized anti-pertussis toxin antibodies limits disease in murine and baboon models of whooping cough. *Sci Transl Med*, *7*, 316ra195. https://doi.org/10.1126/SCITRANSLMED.AAD0966

Nguyen, A. W., Wagner, E. K., Laber, J. R., Goodfield, L. L., Smallridge, W. E., Harvill, E. T., Papin, J. F., Wolf, R. F., Padlan, E. A., Bristol, A., Kaleko, M., & Maynard, J. A. (2015b). A cocktail of humanized anti-pertussis toxin antibodies limits disease in murine and baboon models of whooping cough. *Science Translational Medicine*, *7*(316), 316ra195. https://doi.org/10.1126/SCITRANSLMED.AAD0966

Nishida, M., Suda, R., Nagamatsu, Y., Tanabe, S., Onohara, N., Nakaya, M., Kanaho, Y., Shibata, T., Uchida, K., Sumimoto, H., Sato, Y., & Kurose, H. (2010). Pertussis toxin up-regulates angiotensin type 1 receptors through Toll-like receptor 4-mediated Rac activation. *J Biol Chem*, *285*, 15268–15277. https://doi.org/10.1074/JBC.M109.076232

O'Brien, A. D., Gentry, M. K., Thompson, M. R., Doctor, B. P., Gemski, P., & Formal, S. B. (1979). Shigellosis and Escherichia coli diarrhea: relative importance of invasive and toxigenic mechanisms. *Am J Clin Nutr*, *32*, 229–233. https://doi.org/10.1093/AJCN/32.1.229

Oliveira, D., Borges, A., & Simões, M. (2018). Staphylococcus aureus Toxins and Their Molecular Activity in Infectious Diseases. *Toxins (Basel)*, *19*, 252. https://doi.org/10.3390/toxins10060252

Oppenheimer, N. J. (1978). Structural determination and stereospecificity of the Choleragen-catalyzed reaction of NAD+ with guanidines. *J Biol Chem*, *253*, 4907–4910. https://doi.org/10.1016/s0021-9258(17)34632-x

Pande, A. H., Moe, D., Jamnadas, M., Tatulian, S. A., & Teter, K. (2006). The Pertussis Toxin S1 Subunit Is a Thermally Unstable Protein Susceptible to Degradation by the 20S Proteasome. *Biochemistry, 45*, 13734–13740. https://doi.org/10.1021/bi061175

Paramonov, V. M., Sahlgren, C., Rivero-Müller, A., & Pulliainen, A. T. (2020). IGIST - A Kinetic Bioassay for Pertussis Toxin Based on Its Effect on Inhibitory GPCR Signaling. *ACS Sens*, *5*(11), 3438–3448. https://doi.org/10.1021/ACSSENSORS.0C01340/ASSET/IMAGES/LARGE/SE0C01340_0006.JPEG

Parton, R., Hall, E., & Wardlaw, A. C. (1994). Responses to Bordetela pertussis mutant strains and to vaccination in the coughing rat model of pertussis. *J. Med. Microbiol*, *40*, 307–312.

Pauza, C., Hinds PW 2nd, Yin, C., McKechnie, TiS., Hinds, SB., & Salvato, MS. (1997). The lymphocytosis-promoting agent pertussis toxin affects virus burden and lymphocyte distribution

in the SIV-infected rhesus macaque. *AIDS Res Hum Retroviruses*, *13*, 87–95. https://doi.org/10.1089/AID.1997.13.87

Phadke, V. K., Bednarczyk, R. A., Salmon, D. A., & Omer, S. B. (2016). Association Between Vaccine Refusal and Vaccine-Preventable Diseases in the United States: A Review of Measles and Pertussis. *JAMA*, *315*, 1149–1158. https://doi.org/10.1001/JAMA.2016.1353

Pizza, M., Bartoloni, A., Prugnola, A., Silvestri, S., & Rappuoli, R. (1988). Subunit S1 of pertussis toxin: mapping of the regions essential for ADP-ribosyltransferase activity. *Proc NatI Acad Sci U S A*, *85*, 7521–7525.

Plaut, R. D., & Carbonetti, N. H. (2008). Retrograde transport of pertussis toxin in the mammalian cell. *Cell Microbiol, 10*, 1130–1139. https://doi.org/10.1111/J.1462-5822.2007.01115.X

Plaut, R. D., Scanlon, K. M., Taylor, M., Teter, K., & Carbonetti, N. H. (2016). Intracellular disassembly and activity of pertussis toxin require interaction with ATP. *Pathog Dis*, *74*, ftw065. https://doi.org/10.1093/femspd/ftw065

Pollard, D. J., Berger, C. N., So, E. C., Yu, L., Hadavizadeh, K., Jennings, P., Tate, E. W., Choudhary, J. S., & Frankel, G. (2018). Broad-Spectrum Regulation of Nonreceptor Tyrosine Kinases by the Bacterial ADP-Ribosyltransferase EspJ. *MBio*, *9*, e00170-18. https://doi.org/10.1128/mBio

Poltorak, A., He, X., Smirnova, I., Liu, M. Y., Van Huffel, C., Du, X., Birdwell, D., Alejos, E., Silva, M., Galanos, C., Freudenberg, M., Ricciardi-Castagnoli, P., Layton, B., & Beutler, B. (1998). Defective LPS signaling in C3H/HeJ and C57BL/10ScCr mice: mutations in Tlr4 gene. *Science*, *282*, 2085–2088. https://doi.org/10.1126/SCIENCE.282.5396.2085

Pulliainen, A. T., Pieles, K., Brand, C. S., Hauert, B., Böhm, A., Quebatte, M., Wepf, A., Gstaiger, M., Aebersold, R., Dessauer, C. W., & Dehio, C. (2012). Bacterial effector binds host cell adenylyl cyclase to potentiate Gαs-dependent cAMP production. *Proc Natl Acad Sci U S A, 109*, 9581–9586. https://doi.org/10.1073/PNAS.1117651109/-/DCSUPPLEMENTAL

Putt, K. S., & Hergenrother, P. J. (2004). An enzymatic assay for poly(ADP-ribose) polymerase-1 (PARP-1) via the chemical quantitation of NAD+: Application to the high-throughput screening of small molecules as potential inhibitors. *Anal Biochem*, *326*, 78–86. https://doi.org/10.1016/j.ab.2003.11.015

Ricci, G., De Maria, F., Antonini, G., Turella, P., Bullo, A., Stella, L., Filomeni, G., Federici, G., & Caccuri, A. M. (2005). 7-Nitro-2,1,3-benzoxadiazole derivatives, a new class of suicide inhibitors for glutathione S-transferases. Mechanism of action of potential anticancer drugs. *J Biol Chem*, *280*, 26397–26405. https://doi.org/10.1074/JBC.M503295200

Rominski, A., Roditscheff, A., Selchow, P., Böttger, E. C., & Sander, P. (2017). Intrinsic rifamycin resistance of Mycobacterium abscessus is mediated by ADP-ribosyltransferase MAB_0591. *J Antimicrob Chemother*, *72*, 376–384. https://doi.org/10.1093/JAC/DKW466

Sakanyan, V., Angelini, M., Le Béchec, M., Lecocq, M. F., Benaiteau, F., Rousseau, B., Gyulkhandanyan, A., Gyulkhandanyan, L., Logé, C., Reiter, E., Roussakis, C., & Fleury, F. (2014). Screening and discovery of nitro-benzoxadiazole compounds activating epidermal growth factor receptor (EGFR) in cancer cells. *Sci Rep*, *4*, 3977. https://doi.org/10.1038/SREP03977

Sakanyan, V., Hulin, P., Alves De Sousa, R., Silva, V. A. O., Hambardzumyan, A., Nedellec, S., Tomasoni, C., Logé, C., Pineau, C., Roussakis, C., Fleury, F., & Artaud, I. (2016). Activation of EGFR by small compounds through coupling the generation of hydrogen peroxide to stable dimerization of Cu/Zn SOD1. *Sci Rep*, *6*, 21088. https://doi.org/10.1038/SREP21088

Sakari, M., Laisi, A., & Pulliainen, A. T. (2022). Exotoxin-Targeted Drug Modalities as Antibiotic Alternatives. In *ACS Infect Dis* (Vol. 8, pp. 433–456). American Chemical Society. https://doi.org/10.1021/acsinfecdis.1c00296

Sakurai, J., Nagahama, M., Oda, M., Tsuge, H., & Kobayashi, K. (2009). Clostridium perfringens iota-toxin: structure and function. *Toxins (Basel)*, *1*, 208–228. https://doi.org/10.3390/TOXINS1020208

Samore, M. H., & Siber, G. R. (1992). Effect of pertussis toxin on susceptibility of infant rats to Haemophilus influenzae type b. *J Infect Dis*, *165*, 945–948. https://doi.org/10.1093/INFDIS/165.5.945

Sato, H., & Sato, Y. (1990). Protective activities in mice of monoclonal antibodies against pertussis toxin. *Infect Immun*, *58*, 3369–3374. https://doi.org/10.1128/IAI.58.10.3369-3374.1990

Sato, H., Sato, Y., Ito, A., & Ohishi, I. (1987). Effect of monoclonal antibody to pertussis toxin on toxin activity. *Infect Immun*, *55*, 909–915. https://doi.org/10.1128/IAI.55.4.909-915.1987

Scanlon, K. M., Chen, L., & Carbonetti, N. H. (2022). The Journal of Infectious Diseases Pertussis Toxin Promotes Pulmonary Hypertension in an Infant Mouse Model of Bordetella pertussis Infection. *J Infect Dis, 225*, 172–178. https://doi.org/10.1093/infdis/jiab325

Scanlon, K., Skerry, C., & Carbonetti, N. (2019). Association of pertussis toxin with severe pertussis disease. *Toxins (Basel), 11*, 373. https://doi.org/10.3390/toxins11070373

Scanlon, K., Snyder, Y., Skerry, C., & Carbonetti, N. (2017). Fatal pertussis in the neonatal mouse model is associated with pertussis toxin-mediated pathology beyond the airways. *Infect Immun*, *85*(11), e00355-17. https://doi.org/10.1128/IAI.00355-17

Scheuring, J., Berti, P. J., & Schramm, V. L. (1998). Transition-state structure for the ADP-ribosylation of recombinant Gialpha1 subunits by pertussis toxin. *Biochemistry, 37*, 2748–2758. https://pubs.acs.org/sharingguidelines

Scheuring, J., & Schramm, V. L. (1997a). Kinetic isotope effect characterization of the transition state for oxidized nicotinamide adenine dinucleotide hydrolysis by pertussis toxin. *Biochemistry*, *36*, 4526–4534. https://pubs.acs.org/sharingguidelines

Scheuring, J., & Schramm, V. L. (1997b). Pertussis toxin: transition state analysis for ADP-ribosylation of G-protein peptide alphai3C20. *Biochemistry, 36*, 8215–8223. https://pubs.acs.org/sharingguidelines

Schlander, M., Hernandez-Villafuerte, K., Cheng, C. Y., Mestre-Ferrandiz, J., & Baumann, M. (2021). How Much Does It Cost to Research and Develop a New Drug? A Systematic Review and Assessment. *Pharmacoeconomics*, *39*, 1243–1269. https://doi.org/10.1007/S40273-021-01065-Y

Schneider, O. D., Weiss, A. A., & Miller, W. E. (2007). Pertussis toxin utilizes proximal components of the T-cell receptor complex to initiate signal transduction events in T cells. *Infect Immun*, *75*, 4040–4049. https://doi.org/10.1128/IAI.00414-07

Sealey, K. L., Harris, S. R., Fry, N. K., Hurst, L. D., Gorringe, A. R., Parkhill, J., & Preston, A. (2015). Genomic analysis of isolates from the United Kingdom 2012 pertussis outbreak reveals that vaccine antigen genes are unusually fast evolving. *J Infec Dis*, *212*, 294–301. https://doi.org/10.1093/INFDIS/JIU665

Secher, T., Shima, A., Hinsinger, K., Cintrat, J. C., Johannes, L., Barbier, J., Gillet, D., & Oswald, E. (2015). Retrograde Trafficking Inhibitor of Shiga Toxins Reduces Morbidity and Mortality of Mice Infected with Enterohemorrhagic Escherichia coli. *Antimicrob Agents Chemother*, *59*, 5010–5013. https://doi.org/10.1128/AAC.00455-15

Sheridan, S. L., Ware, R. S., Grimwood, K., & Lambert, S. B. (2012). Number and order of whole cell pertussis vaccines in infancy and disease protection. *JAMA*, *308*, 454–456. https://doi.org/10.1001/JAMA.2012.6364

Simon, N. C., Aktories, K., & Barbieri, J. T. (2014). Novel bacterial ADP-ribosylating toxins: Structure and function. In *Nat Rev Microbiol* (Vol. 12, pp. 599–611). Nature Publishing Group. https://doi.org/10.1038/nrmicro3310

Sindt, K. A., Hewlett, E. L., Redpath, G. T., Rappuoli, R., Gray, L. S., & Vandenberg, S. R. (1994). Pertussis toxin activates platelets through an interaction with platelet glycoprotein Ib. *Infect Immun*, *62*, 3108–3114. https://doi.org/10.1128/IAI.62.8.3108-3114.1994

Sixma, T. K., Pronk, S. E., Kalk, K. H., Wartna, E. S., van Zanten, B. A. M., Witholt, B., & Hoi, W. G. J. (1991). Crystal structure of a cholera toxin-related heat-labile enterotoxin from E. coli. *Nature*, *351*, 371–377.

Slama, J. T., & Simmons, A. M. (1988). Carbanicotinamide adenine dinucleotide: synthesis and enzymological properties of a carbocyclic analogue of oxidized nicotinamide adenine dinucleotide. *Biochemistry*, *27*, 183–193. https://doi.org/10.1021/BI00401A028

Soderberg, Timothy, "Organic Chemistry with a Biological Emphasis Volume I" (2019). Chemistry Publications. 1. https://digitalcommons.morris.umn.edu/chem_facpubs/1

Soman, G., Narayanan, J., Martin, B. L., & Graves, D. J. (1986). Use of substituted (benzylidineamino)guanidines in the study of guanidino group specific ADP-ribosyltransferase. *Biochemistry*, *25*(14), 4113–4119. https://doi.org/10.1021/BI00362A019

Song, J., Gao, X., & Galán, J. E. (2013). Structure and function of the Salmonella Typhi chimaeric A 2 B 5 typhoid toxin. *Nature, 499*, 350–354. https://doi.org/10.1038/nature12377

Spangrude, G., Sacchi, F., Hill, H., Van Epps, D., & Daynes RA. (1985). Inhibition of lymphocyte and neutrophil chemotaxis by pertussis toxin. *J Immunol*, *135*, 4135–4143.

Spaulding, A. R., Salgado-Pabón, W., Kohler, P. L., Horswill, A. R., Leung, D. Y. M., & Schlievert, P. M. (2013). Staphylococcal and Streptococcal Superantigen Exotoxins. *Clin Microbiol Rev*, *26*, 422–447. https://doi.org/10.1128/CMR.00104-12

Stechmann, B., Bai, S. K., Gobbo, E., Lopez, R., Merer, G., Pinchard, S., Panigai, L., Tenza, D., Raposo, G., Beaumelle, B., Sauvaire, D., Gillet, D., Johannes, L., & Barbier, J. (2010). Inhibition of retrograde transport protects mice from lethal ricin challenge. *Cell*, *141*, 231–242. https://doi.org/10.1016/J.CELL.2010.01.043

Stein, P. E., Boodhoo, A., Armstrong, G. D., Cockle, S. A., Klein, M. H., & Read, R. J. (1994a). The crystal structure of pertussis toxin. *Structure*, *2*, 45–57.

Stein P, Boodhoo A, Armstrong G, Heerze L, Cockle S, Klein M, & Read R. (1994b). Structure of a pertussis toxin-sugar complex as a model for receptor binding. *Nat Struct Biol.*, *1*, 591–596. http://www.nature.com/nsmb

Steinmetz, K. L., & Spack, E. G. (2009). The basics of preclinical drug development for neurodegenerative disease indications. *BMC Neurol*, *9 Suppl 1*, S2. https://doi.org/10.1186/1471-2377-9-S1-S2

Strnad, C. F., & Carchman, R. A. (1987). Human T lymphocyte mitogenesis in response to the B oligomer of pertussis toxin is associated with an early elevation in cytosolic calcium concentrations. *FEBS Lett*, *225*, 16–20. https://doi.org/10.1016/0014-5793(87)81123-7

Sun, J., Maresso, A. W., Kim, J. J. P., & Barbieri, J. T. (2004). How bacterial ADP-ribosylating toxins recognize substrates. *Nat Struct Mol Biol, 11*, 868–876. https://doi.org/10.1038/NSMB818

Suskiewicz, M. J., Palazzo, L., Hughes, R., & Ahel, I. (2021). Progress and outlook in studying the substrate specificities of PARPs and related enzymes. *FEBS J, 288*, 2131–2142. https://doi.org/10.1111/febs.15518

Szczepankiewicz, B. G., Dai, H., Koppetsch, K. J., Qian, D., Jiang, F., Mao, C., & Perni, R. B. (2012). Synthesis of carba-NAD and the structures of its ternary complexes with SIRT3 and SIRT5. *J Org Chem*, *77*, 7319–7329. https://doi.org/10.1021/jo301067e

Tam, J., Hamza, T., Ma, B., Chen, K., Beilhartz, G. L., Ravel, J., Feng, H., & Melnyk, R. A. (2018). Host-targeted niclosamide inhibits C. difficile virulence and prevents disease in mice without disrupting the gut microbiota. *Nat Commun*, *9*, 5233. https://doi.org/10.1038/S41467-018-07705-W

Tamamura, Y., Tanaka, K., & Uchida, I. (2017). Characterization of pertussis-like toxin from Salmonella spp. that catalyzes ADP-ribosylation of G proteins. *Scientific Reports*, *7*(1). https://doi.org/10.1038/S41598-017-02517-2

Tamura, M., Nogimori, K., Murai, S., Yajima, M., Ito, K., Katada, T., Ui, M., & Ishii, S. (1982). Subunit structure of islet-activating protein, pertussis toxin, in conformity with the A-B model. *Biochemistry*, *21*, 5516–5522. https://doi.org/10.1021/BI00265A021

Tamura, M., Nogimori, K., Yajima, M., Ase. K, & Ui, M. (1983). A role of the B-oligomer moiety of islet-activating protein, pertussis toxin, in development of the biological effects on intact cells. *J Biol Chem, 258*, 6756–6761.

Tartof, S. Y., Lewis, M., Kenyon, C., White, K., Osborn, A., Liko, J., Zell, E., Martin, S., Messonnier, N. E., Clark, T. A., & Skoff, T. H. (2013). Waning immunity to pertussis following 5 doses of DTaP. *Pediatrics*, *131*, e1047-52. https://doi.org/10.1542/PEDS.2012-1928

Thom, R. E., & Casnellie, J. E. (1989). Pertussis toxin activates protein kinase C and a tyrosine protein kinase in the human T cell line Jurkat. *FEBS Lett*, *244*, 181–184. https://doi.org/10.1016/0014-5793(89)81188-3

Toda, A., Tsurumura, T., Yoshida, T., Tsumori, Y., & Tsuge, H. (2015). Rho GTPase recognition by C3 exoenzyme based on C3-RhoA complex structure. *J Biol Chem, 290*, 19423–19432. https://doi.org/10.1074/jbc.M115.653220

Tomura, H., Itoh, H., Sho, K., Sato, K., Nagao, M., Ui, M., Kondo, Y., & Okajima, F. (1997). Betagamma subunits of pertussis toxin-sensitive G proteins mediate A1 adenosine receptor agonist-induced activation of phospholipase C in collaboration with thyrotropin. A novel stimulatory mechanism through the cross-talk of two types of receptors. *J Biol Chem*, *272*, 23130–23137. https://doi.org/10.1074/JBC.272.37.23130

Toyota, T., Kai, Y., Kakizaki, M., Sakai, A., Goto, Y., Yajima, M., & Ui, M. (1980). Effects of islet-activating protein (IAP) on blood glucose and plasma insulin in healthy volunteers (phase 1 studies). *Tohoku J Exp Med, 130*, 105–116. https://doi.org/10.1620/TJEM.130.105

Tsuge, H., Nagahama, M., Nishimura, H., Hisatsune, J., Sakaguchi, Y., Itogawa, Y., Katunuma, N., & Sakurai, J. (2003). Crystal Structure and Site-directed Mutagenesis of Enzymatic Components from Clostridium perfringens Iota-toxin. *J Mol Biol, 325*, 471–483. https://doi.org/10.1016/S0022-2836(02)01247-0

Tsuge, H., Nagahama, M., Oda, M., Iwamoto, S., Utsunomiya, H., Marquez, V. E., Katunuma, N., Nishizawa, M., & Sakurai, J. (2008). Structural basis of actin recognition and arginine ADP-ribosylation by Clostridium perfringens-toxin. *Proc Natl Acad Sci U S A, 105*, 7399–7404.

Tsuge, H., & Tsurumura, T. (2015). Reaction mechanism of mono-ADP-ribosyltransferase based on structures of the complex of enzyme and substrate protein. *Current Topics in Microbiology and Immunology*, *384*, 69–87. https://doi.org/10.1007/82_2014_415

Tsurumura, T., Tsumori, Y., Qiu, H., Oda, M., Sakurai, J., Nagahama, M., & Tsuge, H. (2013). Arginine ADP-ribosylation mechanism based on structural snapshots of iota-toxin and actin complex. *Proc Natl Acad Sci U S A*, *110*(11), 4267–4272.https://doi.org/10.1073/pnas.1217227110

U.S. Food and Drug Administration (2018). Step 3: Clinical Research. The Drug Development Process; https://www.fda.gov/patients/drug-development-process/step-3-clinical-research.

Vamathevan J, Clark D, Czodrowski P, Dunham I, Ferran E, Lee G, Li B, Madabhushi A, Shah P, Spitzer M, Zhao S (2019). Applications of machine learning in drug discovery and development. *Nat Rev Drug Discov, 18,* 463-477. doi: 10.1038/s41573-019-0024-5.

Van der Maas, N. A. T., Mooi, F. R., de Greeff, S. C., Berbers, G. A. M., Spaendonck, M. A. E. C. van, & de Melker, H. E. (2013). Pertussis in the Netherlands, is the current vaccination strategy sufficient to reduce disease burden in young infants? *Vaccine*, *31*, 4541–4547. https://doi.org/10.1016/J.VACCINE.2013.07.060

Venkannagari, H., Fallarero, A., Feijs, K. L. H., Lüscher, B., & Lehtiö, L. (2013). Activity-based assay for human mono-ADP-ribosyltransferases ARTD7/PARP15 and ARTD10/PARP10 aimed at screening and profiling inhibitors. *Eur J Pharm Sci*, *49*, 148–156. https://doi.org/10.1016/j.ejps.2013.02.012

Visschedyk, D., Rochon, A., Tempel, W., Dimov, S., Park, H. W., & Merrill, A. R. (2012). Certhrax toxin, an anthrax-related ADP-ribosyltransferase from Bacillus cereus. *J Biol Chem.*, *287*, 41089–41102. https://doi.org/10.1074/JBC.M112.412809

Wagner, E. K., Wang, X., Bui, A., & Maynard, J. A. (2016). Synergistic Neutralization of Pertussis Toxin by a Bispecific Antibody In Vitro and In Vivo. *Clin Vaccine Immunol*, *23*, 851–862. https://doi.org/10.1128/CVI.00371-16

Wahlberg, E., Karlberg, T., Kouznetsova, E., Markova, N., Macchiarulo, A., Thorsell, A. G., Pol, E., Frostell, Å., Ekblad, T., Öncü, D., Kull, B., Robertson, G. M., Pellicciari, R., Schüler, H., &

Weigelt, J. (2012). Family-wide chemical profiling and structural analysis of PARP and tankyrase inhibitors. *Nat Biotechnol*, *30*, 283–288. https://doi.org/10.1038/NBT.2121

Wang, Z., Cui, Z., Li, Y., Hou, T., Liu, X., Xi, Y., Liu, Y., Li, H., & He, Q. (2014). High prevalence of erythromycin-resistant Bordetella pertussis in Xi'an, China. *Clin Microbiol Infect*, *20*, O825–O830. https://doi.org/10.1111/1469-0691.12671

Wang, Z. Y., Yang, D., Chen, Q., Leifer, C. A., Segal, D. M., Su, S. B., Caspi, R. R., Howard, Z. O. M., & Oppenheim, J. J. (2006). Induction of dendritic cell maturation by pertussis toxin and its B subunit differentially initiate Toll-like receptor 4-dependent signal transduction pathways. *Exp Hematol*, *34*, 1115–1124. https://doi.org/10.1016/J.EXPHEM.2006.04.025

Warfel, J. M., Beren, J., Kelly, V. K., Lee, G., & Merkel, T. J. (2012). Nonhuman primate model of pertussis. *Infect Immunol*, *80*, 1530–1536. https://doi.org/10.1128/IAI.06310-11

Warfel, J. M., Zimmerman, L. I., & Merkel, T. J. (2014). Acellular pertussis vaccines protect against disease but fail to prevent infection and transmission in a nonhuman primate model. *Proc Natl Acad Sci U S A*, *111*, 787–792. https://doi.org/10.1073/PNAS.1314688110

Weiss, A. A., Johnsont, F. D., & Burnstt, D. L. (1993). Molecular characterization of an operon required for pertussis toxin secretion. In *Proc. Natl. Acad. Sci. USA* (Vol. 90).

West, R. E. J., Moss, J., VaughanS, M., Lius, T., & Liug, T.-Y. (1985). Pertussis toxin-catalyzed ADP-ribosylation of transducin. Cysteine 347 is the ADP-ribose acceptor site. *J Biol Chem*, *260*, 14428–1443.

Wilson, B. A., Blanke, S. R., Reichll, K. A., & John Collier, R. (1994). Active-site mutations of diphtheria toxin. Tryptophan 50 is a major determinant of NAD affinity. *J Biol Chem*, *269*, 23296–23301.

Wilson, B. A., & Collier, R. J. (1992). Diphtheria Toxin and Pseudomonas aeruginosa Exotoxin A: Active-Site Structure and Enzymic Mechanism. *Curr Top Microbiol Immunol*, *175*, 27–41.

Wilson, B. A., Reich, K. A., Weinstein, B. R., & Collier, R. J. (1990). Active-Site Mutations of Diphtheria Toxin: Effects of Replacing Glutamic Acid-148 with Aspartic Acid, Glutamine, or Serine. *Biochemistry*, *29*, 8643–8651.

Winter, K., Glaser, C., Watt, J., Harriman, K., & Centers for Disease Control and Prevention (CDC). (2014). Pertussis Epidemic — California, 2014. *MMWR Morb Mortal Wkly Rep*, *63*, 1129–1132. /pmc/articles/PMC4584602/

Winter, K., Harriman, K., Zipprich, J., Schechter, R., Talarico, J., Watt, J., & Chavez, G. (2012). California pertussis epidemic, 2010. *J Pediatr*, *161*, 1091–1096. https://doi.org/10.1016/J.JPEDS.2012.05.041

Wirsing Von König, C. H., Halperin, S., Riffelmann, M., & Guiso, N. (2002). Pertussis of adults and infants. *Lancet Infect Dis*, *2*, 744–750. https://doi.org/10.1016/S1473-3099(02)00452-8

Witt, M. A., Katz, P. H., & Witt, D. J. (2012). Unexpectedly limited durability of immunity following acellular pertussis vaccination in preadolescents in a North American outbreak. *Clin Infect Dis*, *54*, 1730–1735. https://doi.org/10.1093/CID/CIS287

Witvliet, M. H., Burns, D. L., Brennan, M. J., Poolman, J. T., & Manclark, C. R. (1989). Binding of Pertussis Toxin to Eucaryotic Cells and Glycoproteins. *Infect Immun, 57*, 3324–3330.

Worthington, Z. E. V., & Carbonetti, N. H. (2007). Evading the proteasome: Absence of lysine residues contributes to pertussis toxin activity by evasion of proteasome degradation. *Infect Immun*, *75*, 2946–2953. https://doi.org/10.1128/IAI.02011-06

Wouters, O. J., McKee, M., & Luyten, J. (2020). Estimated Research and Development Investment Needed to Bring a New Medicine to Market, 2009-2018. In *JAMA* (Vol. 323, pp. 844–853). American Medical Association. https://doi.org/10.1001/jama.2020.1166

Wu, E. H. T., & Wong, Y. H. (2005a). Involvement of Gi/o proteins in nerve growth factor-stimulated phosphorylation and degradation of tuberin in PC-12 cells and cortical neurons. *Mol Pharmacol*, *67*, 1195–1205. https://doi.org/10.1124/mol.104.007237

Wu, E. H. T., & Wong, Y. H. (2005b). Pertussis toxin-sensitive Gi/o proteins are involved in nerve growth factor-induced pro-survival Akt signaling cascade in PC12 cells. *Cell Signal*, *17*, 881–890. https://doi.org/10.1016/J.CELLSIG.2004.11.008

Xie, F., Li, B. X., Broussard, C., & Xiao, X. (2013). Identification, Synthesis and Evaluation of Substituted Benzofurazans as Inhibitors of CREB-mediated Gene Transcription. *Bioorg Med Chem Lett*, *23*, 5371–5375. https://doi.org/10.1016/J.BMCL.2013.07.053

Xu, Y., Barbancon-Finck, V., & Barbieri, J. T. (1994). Role of histidine 35 of the S1 subunit of pertussis toxin in the ADP-ribosylation of transducin. *J Biol Chem, 269*, 9993–9999. https://doi.org/10.1016/S0021-9258(17)36980-6

Yang, Y., Yao, K., Ma, X., Shi, W., Yuan, L., & Yang, Y. (2015). Variation in Bordetella pertussis Susceptibility to Erythromycin and Virulence-Related Genotype Changes in China (1970-2014). *PLoS One*, *10*, e0138941. https://doi.org/10.1371/JOURNAL.PONE.0138941

Yates, S. P., Taylor, P. L., Jørgensen, R., Ferraris, D., Zhang, J., Andersen, G. R., & Merrill, A. R. (2005). Structure-function analysis of water-soluble inhibitors of the catalytic domain of exotoxin A from Pseudomonas aeruginosa. *Biochem J*, *385*, 667–675. https://doi.org/10.1042/BJ20041480

Yeung K.H.T., Duclos P., Nelson E.A.S., Hutubessy R.C.W (2017). An update of the global burden of pertussis in children younger than 5 years: a modelling study. *Lancet Infect Dis. 17*: 974-980. doi: 10.1016/S1473-3099(17)30390-0.

Yoshida, T., & Tsuge, H. (2021). Common Mechanism for Target Specificity of Protein-and DNA-Targeting ADP-Ribosyltransferases. *Toxins (Basel)*, *13*, 40. https://doi.org/10.3390/TOXINS13010040

Young, J. C., Clements, A., Lang, A. E., Garnett, J. A., Munera, D., Arbeloa, A., Pearson, J., Hartland, E. L., Matthews, S. J., Mousnier, A., Barry, D. J., Way, M., Schlosser, A., Aktories, K., & Frankel, G. (2014). The Escherichia coli effector EspJ blocks Src kinase activity via amidation and ADP ribosylation. *Nat Commun , 5*, 5887. https://doi.org/10.1038/ncomms6887

Yung, L. Y., Tso, P. H., Wu, E. H. T., Yu, J. C. H., Ip, N. Y., & Wong, Y. H. (2008). Nerve growth factor-induced stimulation of p38 mitogen-activated protein kinase in PC12 cells is partially mediated via G(i/o) proteins. *Cell Signal*, *20*, 1538–1544. https://doi.org/10.1016/J.CELLSIG.2008.04.007

Zatorski, A., Watanabe, K. A., Carr, S. F., Goldstein, B. M., & Pankiewicz, K. W. (1996). Chemical synthesis of benzamide adenine dinucleotide: inhibition of inosine monophosphate dehydrogenase (types I and II). *J Med Chem*, *39*, 2422–2426. https://doi.org/10.1021/JM9601415

Zhang, R. G., Westbrook, M. L., Nance, S., Spangler, B. D., Westbrook, E. M., Scott, D. L., & Shipley, G. G. (1995). The three-dimensional crystal structure of cholera toxin. *J Mol Biol*, *251*, 563–573. https://doi.org/10.1006/JMBI.1995.0456

Zhou, G.-C., Parikh, S. L., Tyler, P. C., Evans, G. B., Furneaux, R. H., Zubkova, O. V, Benjes, P. A., & Schramm, V. L. (2004). Inhibitors of ADP-Ribosylating Bacterial Toxins Based on Oxacarbenium Ion Character at Their Transition States. *J Am Chem Soc, 126*, 5690–5698. https://doi.org/10.1021/ja038159

TURUN
YLIOPISTO
UNIVERSITY
OF TURKU

Painosalama, Turku, Finland 2024

ISBN 978-951-29-9688-9 (PRINT)
ISBN 978-951-29-9689-6 (PDF)
ISSN 0355-9483 (Print)
ISSN 2343-3213 (Online)